DESIGN OF MULTIFUNCTIONAL MICROSTRIP PATCH DIRECTIONAL COUPLERS AND STEPPED-IMPEDANCE SLOTLINE POWER DIVIDERS

LIM SHENG LOKE

MASTER OF ENGINEERING SCIENCE

Faculty of Engineering and Science

Universiti Tunku Abdul Rahman

MAY 2014

ABSTRACT

Microwave couplers are frequently used for designing various microwave components such as filters, power dividers, phase shifters, etc. In the first part of this thesis, several multifunctional power-dividing directional couplers that can generate output signals with multiple levels are studied. Two passive power dividers, working in the in-phase or out-of-phase operation, are first proposed. Three rectangular microstrip patches are cascaded for the excitation of their degenerate modes. By adding two extra output ports to the in-phase power divider, it is interesting to note that the new multifunctional power-dividing directional coupler is able to produce additional 10 and 20 dB coupled signals, both in-phase and out-of-phase. This is the first demonstration, to the best of my knowledge, that a single component can generate half-powered division as well as multiple (10 and 20 dB) coupled signals at the same time, leading to significant cost saving. In the second part, the stepped-impedance slotline resonator has been deployed for designing several passive in-phase and out-of-phase power dividers, which can be made reconfigurable by incorporating RF PIN diodes at the output feedlines. Reasonable agreement is observed between the simulated and measured results.

ACKNOWLEDGEMENT

I would like to thank Dr. Lim Eng Hock and Dr. Lo Fook Loong for their directions, ideas and guidance. Throughout the completion of this research project, invaluable recommendations and suggestions have been shared. In addition, they were always available whenever I have problems.

I also wish to thank Mr. Ho, who taught me the fabrication process. With his guidance, I was able to make all my circuit boards. Besides that, I would also like to extend my gratitude to all my seniors and friends for many useful discussions.

I am thankful to UTAR for supporting all the necessary equipment, facilities, and research materials. The online databases such as IEEE Xplore and Microwave and Optical Technology Letters are very handy and helpful.

APPROVAL SHEET

This thesis entitled **'<u>DESIGN OF MULTIFUNCTIONALMICROSTRIP PATCH DIRECTIONAL COUPLERS AND STEPPED-IMPEDANCESLOTLINE POWER DIVIDERS</u>'** was prepared by LIM SHENG LOKE and submitted as partial fulfillment of the requirement for the degree of Master of Engineering Science at Universiti Tunku Abdul Rahman.

Approved by,

____

(Dr. Lim Eng Hock) Date: ____________
Supervisor
Department of Electrical and Electronic Engineering
Faculty of Engineering Science
Universiti Tunku Abdul Rahman

____

(Dr. Lo Fook Loong) Date: ____________
Co-supervisor
Department of Electrical and Electronic Engineering
Faculty of Engineering Science
Universiti Tunku Abdul Rahman

FACULTY OF ENGINEERING SCIENCE

UNIVERSITI TUNKU ABDUL RAHMAN

Date: ________________

SUBMISSION OF FINAL YEAR PROJECT /DISSERTATION /THESIS

It is hereby certified that **LIM SHENG LOKE** (ID No: **12 UEM 01155**) has completed this dissertation entitled "**DESIGN OF MULTIFUNCTIONAL MICROSTRIP PATCH DIRECTIONAL COUPLERS AND STEPPED-IMPEDANCE SLOTLINE POWER DIVIDERS**" under the supervision of Dr. Lim Eng Hock (Supervisor) from the Department of Electrical and Electronic Engineering, Faculty of Engineering and Science (FES), and Dr. Lo Fook Loong(Co-Supervisor) from the Department of Electrical and Electronic Engineering, Faculty of Engineering and Science (FES).

I understand that University will upload softcopy of my final dissertationinpdf format into UTAR Institutional Repository, which may be made accessible to UTAR community andpublic.

Yours truly,

____

(LIM SHENG LOKE)

DECLARATION

I hereby declare that the thesis is based on my original work except for citations and quotations which have been duly acknowledged. I also declare that it has not been previously and concurrently submitted for any other degree or award at UTAR or other institutions.

Name : LIM SHENG LOKE

Date : ____________________

TABLE OF CONTENTS

LIST OF TABLES

LIST OF FIGURES

CHAPTER 1

INTRODUCTION

1.1 Background

Microwave is defined as an electromagnetic wave with frequency ranging from 300 MHz to 300 GHz, which corresponds to wavelengths from 1 m to 1 mm in free space. Signals with wavelength less than 1 mm are often referred to as millimeter waves (D. M. Pozar, 2011). Most of the microwave technologies are intended for the wireless networking and communication systems. Nowadays, with the rapid growth of the mobile and wireless communications, microwave components are highly sought after. In this thesis, several microwave power dividers and directional couplers will be studied. The background of the components will be briefly introduced here.

In the past, many types of microwave resonators were proposed for designing various power-dividing structures (E. J. Wilkinson, 1960; M. E. Goldfarb, 1991; M. Nakatsugawa, K. Nishikawa, 2001). Among all, the Wilkinson power divider, which makes use of the quarter-wavelength microstrip lines, is the most popular as it has low coupling between the output ports. Later, many other power dividers have been proposed by modifying the Wilkinson in order to achieve different purposes such as dual-band operation (Y. Wu, Y. Liu, et al., 2011; B. Li, X. Wu, et al., 2011; A. S. S. Mohra, 2008), tri-band operation (H. Chen, Y. Pang, 2011; X. Wang, Y. Bai, et al., 2011; B. Li, X. Wu, et al., 2011), ultra wideband operation (X. Ou, Q. Chu, 2008; D. Hawatmeh, N. Dib, et al., 2012), good harmonic suppression (K. Yi, B. Kang., 2003; J. Wang, J. Ni, et al., 2009; D. Woo, T. Lee, 2005), as well as high isolation with an improved bandwidth (J. Kao, Z. Tsai, et al., 2012) etc.

In the 40s, several directional couplers were invented and characterized at the MIT Radiation Laboratory (D. M. Pozar, 2011). These include the Bethe-hole coupler, the multi-hole directional coupler, and others which are designed using the coaxial lines. In the mid-50s to 60s, many of these directional couplers were re-designed using the stripline and microstrip technologies because they are planar and easy to integrate with other microwave systems. Again, bandwidth expansion is a current heat. A wideband composite right/left-handed (CRLH) coplanar waveguide (CPW) coupler, with 3dB coupling value and quadrature phase difference, was proposed by (S. Mao, M. Wu, 2007). The authors have made use of the symmetrical structure, consisting of a gap capacitor, a broadside-coupled capacitor, and a meandering short-circuited stub inductor, to achieve wide operating bandwidth. Microstrip and suspended stripline were combined to design a directional coupler with wide bandwidth and low insertion loss (S. Lin, M. Eron, et al., 2011).

1.2 Research Objectives and Motivation

This thesis encompassed two design projects. The main objective here is to explore the multifunction of the multiport microstrip resonator as either a passive or an active device. In the first part, degenerate modes are deployed to design the multifunctional and multiport power-dividing directional couplers in a microstrip rectangular patch resonator. It is able to provide half-power division as well as the 10 dB and 20 dB coupling outputs at the same time. Next, several multiport microstrip power dividers, which are designed using the stepped-impedance slotline on a ground plane, are proposed. They can provide in-phase or out-of-phase operation in a single module.

1.3 Thesis Organization

Chapters 1 and **2** briefly introduce the background of the microwave power dividers and directional couplers. The recent developments and applications of the two components are analyzed, along with the research objectives and motivation. Some technologies that are used to achieve broad bandwidth, multifunction, and miniaturization are discussed.

In **Chapter 3**, several directional couplers are proposed and discussed. It starts with the discussion of the passive in-phase and out-of-phase power dividers.

Then, the two are combined to form the 10dB and 20dB power-dividing directional couplers. Lastly, a multifunctional power-dividing directional coupler that can produce outputs with multiple levels is demonstrated. Measured and simulated insertion losses, reflection coefficients, amplitude imbalances, and phase differences, and group delays are presented, showing good agreement.

Chapter 4 proposes the stepped-impedance slotline power-dividing structures. To begin, the passive in-phase and out-of-phase power dividers are studied. By incorporating a few RF PIN diodes, the two are combined to form a reconfigurable unit. Again, the insertion losses, reflection coefficients, phase differences, and group delays are investigated. Finally, the design parameters are studied.

Chapter 5 summarizes the research works presented in this thesis.

CHAPTER 2

LITERATURE REVIEW ON MICROWAVE COUPLER

2.1 Background and Introduction

Microstrip couplers are passive microwave components that have been widely used in microwave applications such as antenna feeds, power amplifiers, mixers and others. Couplers can be divided into two categories, first for equal (power divider) power division while second for unequal (directional coupler). Both of these components can perform power division or combining. Recently, most of the microstrip couplers (A. M. Abbosh, M. E. Bialkowski, 2007; N. Yang, C. Caloz, et al., 2010; M. E. Bialkowski, Y. Wang, 2010; C. Lin, S. Chung, 2011) are made multifunctional in order to achieve compact size and low cost. Furthermore, new technologies are also employed to achieve wide passband, good isolation between the output ports as well as high harmonic suppression. Recent development will be discussed for power dividers and directional couplers in the following sections.

2.1.1 Power Dividers and Directional Couplers

In this section, the fundamental operations of the conventional power dividers and directional couplers are briefly introduced. The configuration of a two-output power divider is shown in Figure 2.1, which can provide either in-phase ($|\phi_1-\phi_2| = 0^o$) or out-of-phase ($|\phi_1-\phi_2| = 180^o$) output signals. It can have two or more output ports but the amplitude imbalances in between them must be less than 1 dB. Such dividers are usually designed to have equal power division ratio (3 dB) among all of the outputs. Many (X. Ou, Q. Chu, 2008; Y. Wu, Y. Liu, et al., 2011;J. Li, B. Wang, 2011) are designed based on the Wilkinson power divider (E. J. Wilkinson, 1960).

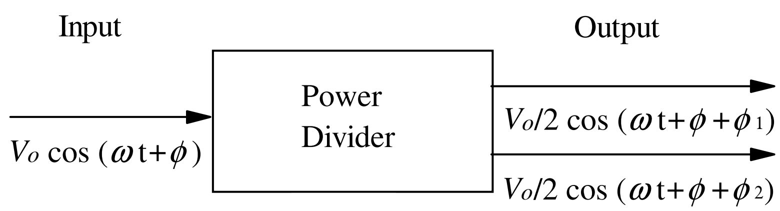

Figure 2.1: The schematic of a conventional power divider.

A directional coupler is a four-port device that let an input power (*Port* 1) couple to *Port* 2 (through port) and to *Port* 3 (coupled port) but not into *Port* 4 (isolation port). Figure 2.2 illustrates the schematic of a conventional directional coupler. For an ideal case, any one of the coupler ports can work as an input with different through port, coupled port, and isolation port. An ideal directional coupler has infinite directivity and isolation. Ideal directional coupler with perfect isolation and matching performances can be realized only if the resonator structure is symmetric (M. Dydyk, 1999).

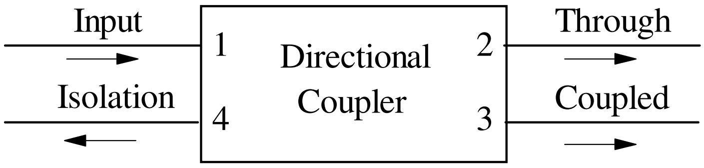

Figure 2.2: The schematic of a conventional directional coupler.

2.1.2 Microwave Resonators

Microwave resonator is used by many applications such as oscillators, mixers, and others. A microwave resonator operates in the way very similar to those made of lumped-elements (D. M. Pozar, 2011). There are several types of microwave resonators such as patch resonators (S. R. Zinka, A. Moham, et al., 2007; J. Xiao, Q. Chu, et al., 2008; J. Li, J. Wang, et al., 2010; R. Zhang, L. Zhu, et al., 2012), slot resonators (A. A. Semenov, P. Yu, et al., 2008; M. Ohira, Z. Ma, et al., 2011; Y. Lu, S. Chen, et al., 2012; C. Lee, C. G. Hsu, et al., 2012), and dielectric resonators (R. Zhang, R. R. Mansour, 2007; A. A. Kishk, W. Huang, 2011; A. Bhardwaj, V. D. Kumar, 2012; K. A. O'Connor, R. D. Curry, 2012). All have been widely used to design various microwave components. Patch resonator is planar but with a higher conduction loss. Having a low Q factor, the slot resonator is able to provide broad bandwidth. But this comes with poorer frequency selectivity. To improve it, the dielectric resonator (DR) can be deployed as it has a higher Q factor.

Power dividers made by slot resonators are popular. In (A. Dadgarpour, G. Dadashzadeh, et al.; 2010), a compact planar UWB in-phase power divider is proposed by joining up three T-shaped microstrip lines in parallel on the top surface of substrate with a H-shaped slot etched on the reverse. The authors in (M. E. Bialkowski, A. M. Abbosh; 2007) employed a T-junction formed by a slotline and a microstrip line to design a compact out-of-phase planar power divider. Later, a similar structure was also proposed by (H. Ma, Q. Chu, et al.; 2008) using a T-shaped microstrip-etched slot to achieve equal power division with high phase stability. Slot resonators can also incorporate multilayered technologies for designing various high-performing power dividers. In (K. Song, Y. Fan, et al.; 2008), a wideband power divider is designed with the use of a five-layered broadside slot-coupled configuration. Another piece of work, (Q. Li, J. Gong, et al.; 2010) proposed a broadband in-phase structure that was achieved by combining the elliptical microstrip patches with a rectangular slot.

2.2 Recent Developments of Power Dividers

2.2.1 Broadband and Dualband Power Dividers

The demand on various wideband power-dividing structures is on the rise because of the emergence of myriads of broadband wireless systems. To extend the frequency passband of a power divider, multiple resonances are usually required. In (W. Liu, F. Wei, et al., 2012), a novel microstrip power divider is proposed by installing three open stubs and two aperture-backed interdigital coupled-lines to excite a couple of resonances, providing ultrawide bandwidth as well as good impedance matching at all of the output ports. Another broadband power divider with good in-band power splitting is proposed in (S. W. Wong, L. Zhu, 2008) by cascading a pair of stepped-impedance open-circuited stubs and parallel-coupled lines, again, for the excitation of multimode. To do this, multistage $\lambda/4$ impedance transformers can also be introduced (F. Xu, G. Guo, et al., 2012; Y. Wu, X. Xie, et al., 2012) to broaden the passband. Multiple frequency channels are strongly needed by the communication systems. Many dual- and multi-band circuits have been proposed to meet this demand. It was found in (X. Li, Y. J. Yang, et al., 2009) that open and short stubs can be used to produce double passbands. Similar technique was also demonstrated by (J. Lee, I. Jeon, et al., 2012).

2.2.2 Multifunctional Power Dividers

Recently, the multifunction concept has been explored for miniaturizing many microwave components (E. H. Lim, K. W. Leung; 2012). It is a trend to make a power divider to provide output signals with different phases in a single piece. In (M. E. Bialkowski, Y. Wang, 2011), the authors have used the microstrip-slot technology to design a Wilkinson power divider that can generate in-phase and out-of-phase (180^o) outputs. Similar technology was again demonstrated by the same authors in (M. E. Bialkowski, Y. Wang, 2010).

Most of the standalone microwave power dividers do not have filtering effect. To improve their frequency selectivity, they are usually cascaded with bandpass filters. This is not desirable as it makes the component bulky. Recently, it has seen the formation of the concept of filtering power divider, which is a multifunctional device that can provide half-powered division as well as remove unwanted signals. Integration of a single-stage coupled line bandpass filter and a conventional Wilkinson power divider was proposed in (P.K. Singh, S. Basu, et al., 2009) to achieve filtering effect. Also, bandpass-filtering response was introduced into the power-dividing structure by using the multilayer microstrip line-slotline coupling structure (K. Song, Q. Xue, 2010). Later, (M. A. Beldi, F. Boone, et al., 2012) showed that filtering effect was also possible by combining several T-junctions into the power divider.

2.3 Recent Developments of Directional Couplers

2.3.1 Broadband Directional Couplers

Broadband directional couplers are a very important category of passive microwave circuits which are used for power dividing/combining, sampling, signal rejection and power monitoring in microwave communication sub-systems. Some of the recent technologies are introduced here. A double-layer and multi-aperture directional coupler was presented in (C. Wang, K. Chang, 2002). It consists of two back-to-back substrates along with 15 small coupling apertures on the central ground plane to greatly increase the operating bandwidth. A broadband 8.34 dB directional coupler was proposed by (S. Gruszczynski, K. Wincza, 2007) using a stripline technique, where a three-section asymmetric coupled-line was used to achieve broadband frequency response. (M. E. Bialkowski, N. Seman, et al., 2009) has proposed a compact ultra-wideband 3 dB directional coupler which consists of two elliptically shaped conducting disks. A low profile broadband directional coupler was demonstrated by combining the microstrip line and the suspended stripline, giving low insertion loss and high power capability in (S. Lin, M. Eron, et al., 2011).

2.3.2 Miniaturized Directional Couplers

Nowadays, increasing attention has been paid to researching various miniaturized microwave components to achieve compact size. By introducing different equivalent inductances for the even and odd modes, (J. Yen, S. Hsu, et al., 2011) showed that the circuit size of a forward-wave directional coupler can be much reduced. The same group of researchers also proposed another miniaturization method by introducing the periodical mushroom-shaped ground plane to the conventional coupled-line directional coupler, which has identical characteristic impedances for the even and odd modes (S. Hsu, C. Tsai, et al., 2010). Besides that, the defected ground structure described in (J. Yen, S. Hsu, et al., 2011) can be used to make a directional coupler compact. In (P. Chi, T. Itoh, 2009), the authors designed a compact dual-band directional coupler using the composite right/left-handed (CRLH) transmission structures.

CHAPTER 3

MULTIFUNCTIONAL POWER-DIVIDING DIRECTIONAL COUPLERS WITH MULTIPLE OUTPUTS

3.1 Introduction

Couplers are widely used in microwave applications such as mixers, phase shifters and antenna arrays. Branch-line (J. Reed, G. J. Wheeler; 1956) was used for providing equal power division and 90^{o} phase shift, but it has a bandwidth (BW) of ~10% only. Although the BW can be broadened by cascading multiple branch lines, it introduces additional coupling between the branches and such structure has very high impedance lines that are difficult to be made. Also, the junctions introduce parasitic reactances. In order to overcome these problems, patch coupler was introduced. In 1980s, a simple 3dB rectangular patch coupler was proposed in (J. W. Burn; 1985; V.F. Fusco, J.A.C. Stewart, 1986; V. F. Fusco, L. N. Merugu; 1990). The design equation was given in (J. W. Burn; 1985) for calculating the resonance frequency of the rectangular microstrip patch coupler. Patch couplers can be easily designed into different shapes such as rectangular, circular (K. C. Gupta, M. Abouzahra, 1985; M. Abouzahra, K. C. Gupta, 1987), and elliptical (M. E. Bialkowski, S. T. Jellett, 1994; K. L. Chan, F. A. Alhargan, et al.; 1997). Open-/shorted stubs and impedance steps are introduced to the periphery of the microstrip resonators (T. Kawai, I. Ohta,et al; 1992; M. E. Bialkowski, S. T. Jellett; 1994) to obtain flat coupling response and broader operational bandwidth. Without using any stub, Chan etal. (K. L. Chan, F. A. Alhargan, et al.; 1997) showed that the quadrature bandwidth of an elliptical patch hybrid can also be improved by inserting impedance transformers into the feedlines. Recently, various methods have been proposed to miniaturize the conventional patch hybrid coupler. Asymmetrically loaded cross slots (S. Sun, L. Zhu, 2009) are added to the conventional 3dB patch hybrid to reduce the overall size due to its inductive loading effect. In (S. Y. Zheng, S. H. Yeung, et al., 2009), the size of patch hybrid is miniaturized by introducing patternedslots behind the patch resonator without increasing circuit complexity.

In modern microwave systems, integration of multiple RF components into a single module has been widely used in order to obtain multi-functionality such as high compactness, low loss, and low cost (E. H. Lim, K. W. Leung, 2012). Recently, patch resonator has also been explored for multifunction. Two cross-slotted patch resonators with an inserted conductor plane (J. X. Chen, C. Y. Cheung, et al., 2007) are sandwiched to make a dual-mode balun bandpass filter. However, the additional conductor plane increases the material cost and design complexity. In order to solve this problem, a dual-mode balun filter with only a single cross-slotted patch resonatorwas proposed (S. Sun, W. Menzel, 2011; C. H. Ng, E. H. Lim, et al., 2011), where two degenerate modes are excited by the etched asymmetrical-cross slots. So far, the dualfunction of the patch as a power divider and a directional coupler has not been found.

In this chapter, a microstrip patch is explored for designing six different power-dividing structures. In the first part, the patch is dividing an input power into two outputs, which can be made to be either in-phase or out-of-phase. By adding in two extra output ports, the proposed patch can function simultaneously as 10dB and 20dB power-dividing directional couplers. Here, the 10dB coupled signals can be made either in- or out-of-phase. It is very interesting to note that the proposed configuration can provide half-power, as well as 10dB and 20dB couplings at the same time. All the simulated results are accomplished using Ansoft HFSS (Ansoft Corporation, HFSS). Experiment was conducted on the R&S®ZVB8 Vector Network Analyzer (VNA). The substrate Duroid RO4003C, with a dielectric constant of $\varepsilon_r = 3.38$ and a thickness of $h = 1.524$ mm, was used throughout the entire project. In this chapter, the design methodology, configurations, results, discussions, and parametric analysis of the proposed multifunctional couplers are presented.

3.2 Design Methodology

In this section, the design methodology will be discussed and analyzed. Figure 3.1(a) shows the configuration of a rectangular microstrip patch, with its electric field distribution depicted in Figure 3.1(b) for the TE_{01} mode. It has one null in the y-direction. The resonant frequency of the TE_{nm} mode can be calculated by using the cavity model describable by eqn. (3.1), where n and m denote the numbers of nulls in the x- and y- directions. Here, c is the speed of light and ε_r is the relative permittivity of substrate. This model holds when the substrate thickness (h) is small, where electric field (E_z) variation in the z-direction is assumed to be constant due to negligible substrate thickness.

$$(f_r)_{nm} = \frac{c}{2\sqrt{\varepsilon_r}}\sqrt{\left(\frac{n}{L}\right)^2 + \left(\frac{m}{W}\right)^2} \tag{3.1}$$

The first higher-order TE_{01} mode of the microstrip long patch is deployed and the resonant frequency can be calculated using $(f_r)_{01} = \frac{c}{2W\sqrt{\varepsilon_r}}$. The simulated $S_{11}$and S_{21} of a simple patch (with width of W = 28 mm and length of L = 22 mm) are shown in Figure 3.2 for different lengths. It can be seen that the resonant frequency decreases with length. With the use of eqn (3.1), the resonant frequencies for W= 24, 28, and 32 mm are calculated to be 3.4, 2.91, and 2.54 GHz, respectively, which are pretty close to the simulated ones of 3.33, 2.89, and 2.57 GHz. This shows that the width of the microstrip patch is inversely proportional to the operating frequency. Longer width gives lower operating bandwidth, and vice versa.

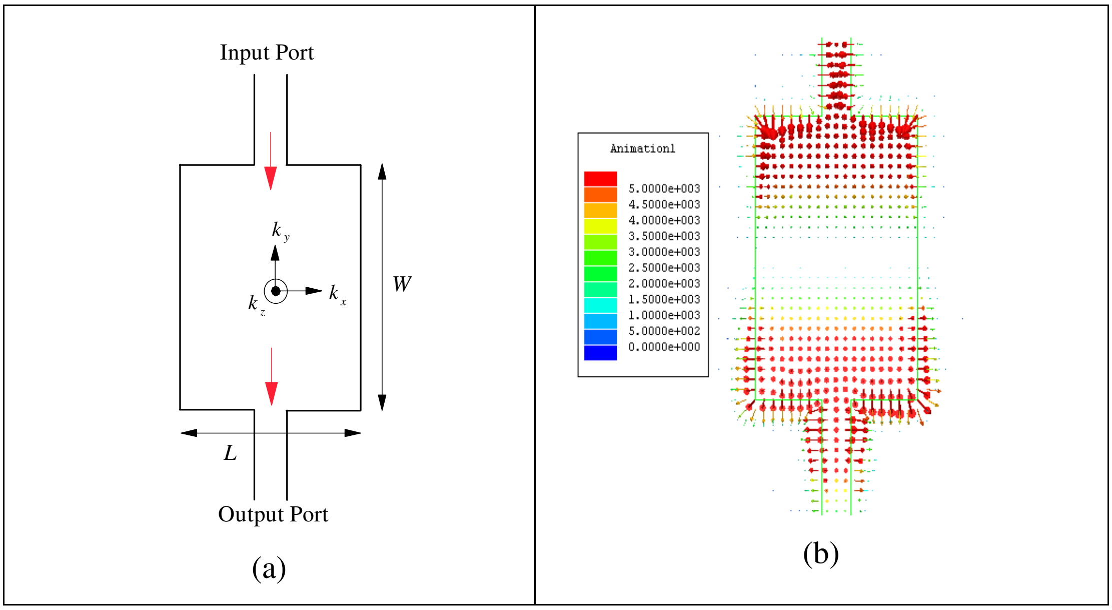

Figure 3.1: (a) Configuration of a rectangular microstrip patch, (b) Electric field distribution at 2.9 GHz.

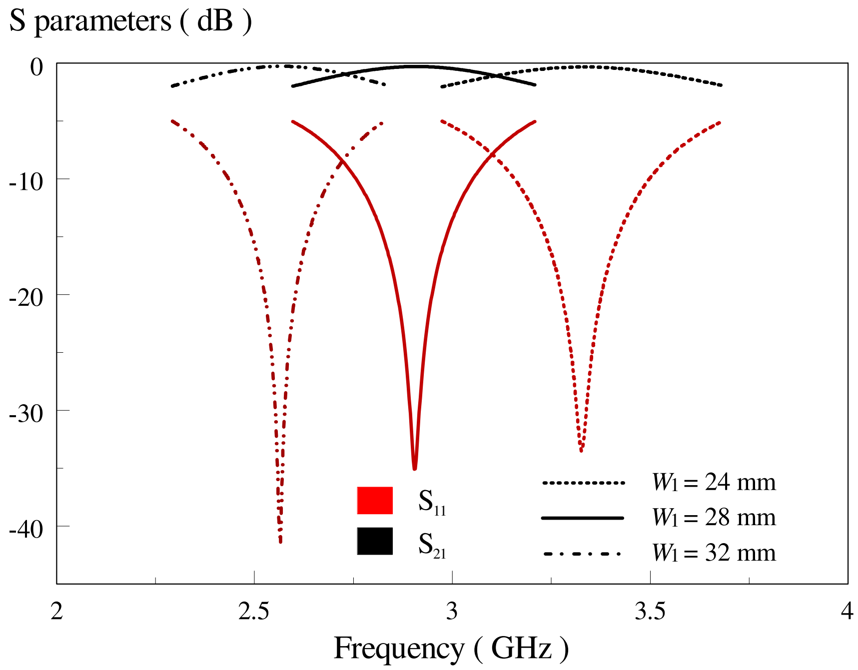

Figure 3.2: Simulated S parameters of the simple rectangular patch shown in Figure 3.1(a).

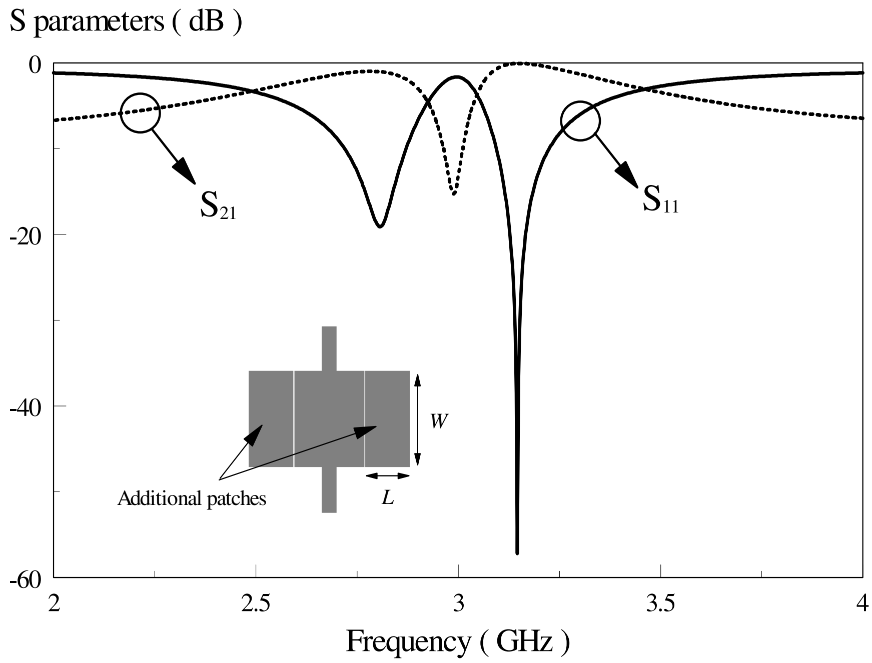

Figure 3.3: Simulated S parameters of the new patch structure (in the inset) with two additional side patches.

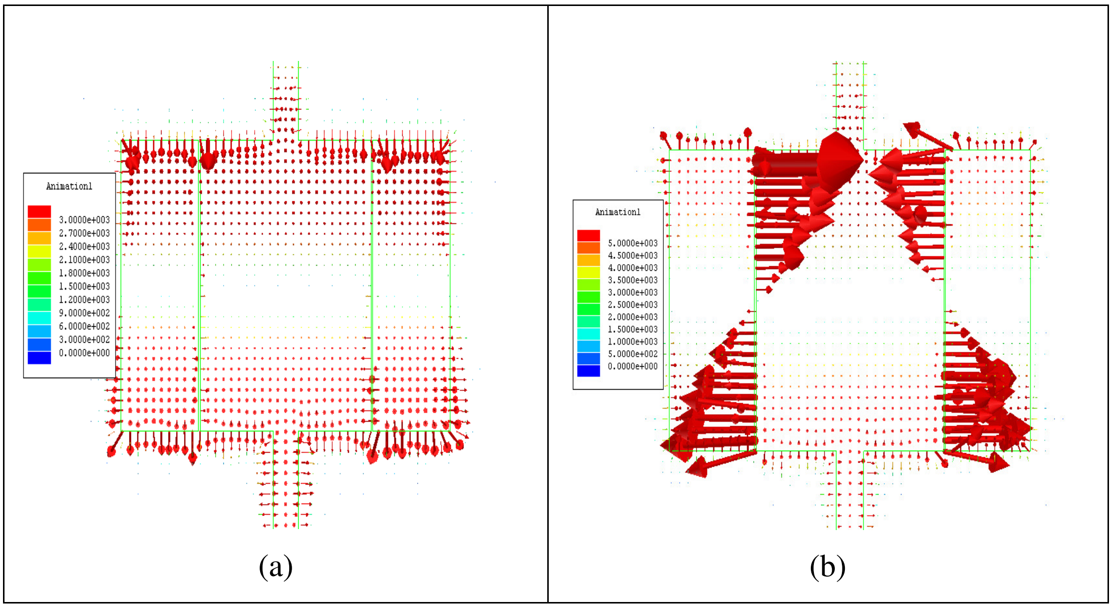

Figure 3.4: The electric field distributions at two modes, (a) 2.83 GHz, and (b) 3.15 GHz.

Figure 3.3 depicts the S parameters of the patch configuration in the inset (Figure 3.3), which is constructed by capacitively attaching two equal rectangular patches (W = 28 mm and L = 10 mm) with a gap of 0.2 mm to that in Figure 3.1. In this case, it has two resonating modes at 2.83 GHz and 3.15 GHz. With reference to Figure 3.4(a) and (b), the electric field distributions in all of the patches are similar with that in Figure 3.1(b). This shows that the two resonances are the degenerate modes, which are introduced by the two side patches, and their resonant frequency can be estimated by eqn. (3.1).

3.3 Power Dividers

3.3.1 In-phase Power Divider

Figure 3.5 shows the top-view schematic of the proposed in-phase power divider. As can be seen from the figure, the proposed structure consists of three microstrip patches on the top surface. The proposed structure is designed with only a single-layered substrate with 50 Ω microstrip feedlines. The central patch has a dimension of W_1 = 28 mm and L_1 = 22 mm. With reference to the figure, the two side patches have identical dimension as they are symmetrically designed to have equal output signals. Other design parameters are L_2 = 9 mm, W_2 = 5mm, W_3 = 19.8 mm, and g_1 = 0.2mm. Figure 3.6 shows the photograph of the fabricated prototype.

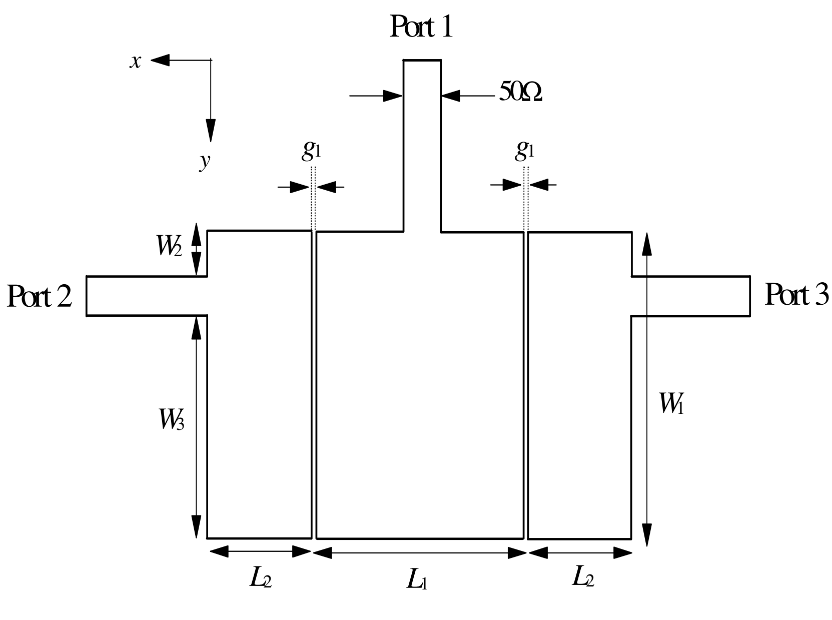

Figure 3.5: Top-view schematic of the proposed in-phase power divider.

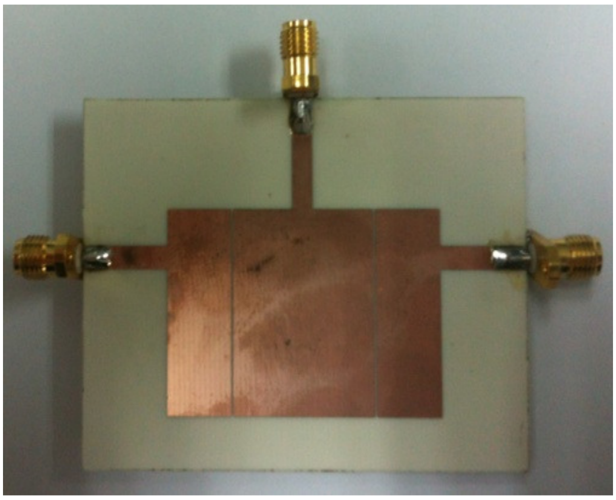

Figure 3.6: Prototype of the proposed in-phase power divider.

3.3.1.1 Simulation and Experimental Results

Figure 3.7(a) shows the simulation and measurement results of the proposed power divider in Figure 3.5. The proposed structure has a measured passband covering frequencies from 2.77 GHz to 3.0 GHz, giving a fractional bandwidth (FBW) of 8.15% (simulation: 2.83 GHz – 3.08 GHz, FBW: 8.53%). In the passband, the measured insertion loss is in the range of -4.5dB to -5.3dB (simulation: -3.8dB - -4.7dB). Because of its conduction loss, the patch resonator usually has higher insertion loss (C. Pedro, T. S. Lv, et al., 2011; S. Sun, W. Menzel; 2011). Additional loss can be introduced by impedance mismatch between the feedlines and connectors in experiment. Both of the simulated and measured $|S_{11}|$ read ~ -15 dB. The measured and simulated center frequencies are 2.89 GHz and 2.96 GHz, respectively, with an error of 2.42%.There is a transmission zero at 2.72 GHz. In general, reasonable agreement is observed between simulated and measured results. The isolation level between the two output ports is illustrated in Figure 3.7(b), with measurement going below ~ -9.6 dB across the passband. The group delay of the proposed structure is shown in Figure 3.8. Reasonable agreement can be observed. The group delay is almost constant across the passband, with the measured maximum delay of 1.38 ns (simulation: 1.10 ns). Figure 3.9 shows the measured amplitude imbalance and phase difference of the proposed in-phase power divider (Figure 3.5). It is observed that the calculated amplitude imbalance and phase difference are within ± 0.18 dB and 2.3^{o}, respectively, across the operating bandwidth.

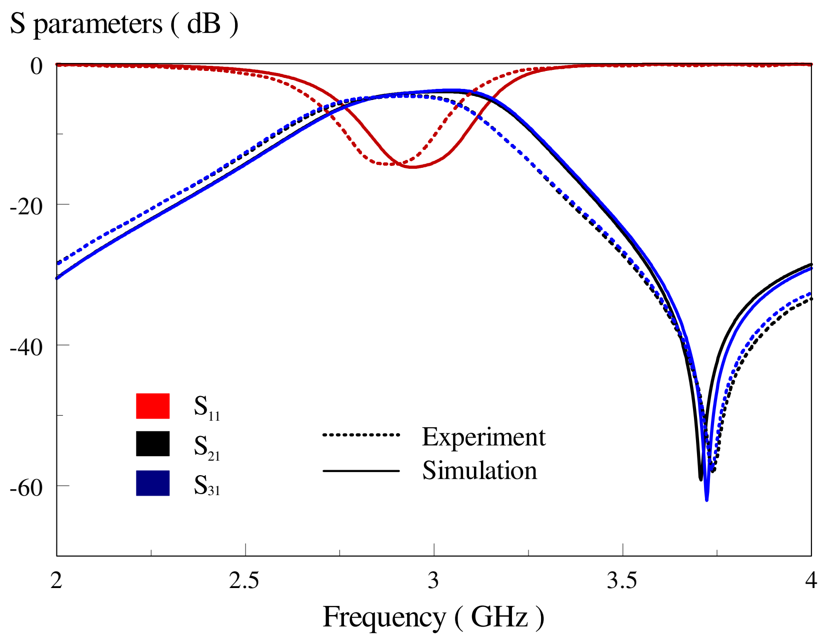

(a)

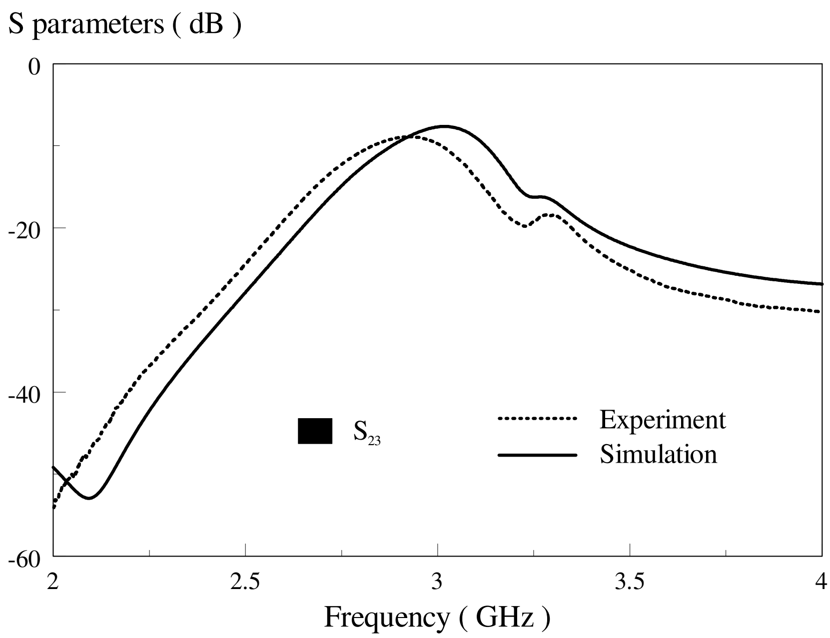

(b)

Figure 3.7: Simulated and measured of the (a) reflection and transmission coefficients, and (b) isolation S_{23} between the output ports.

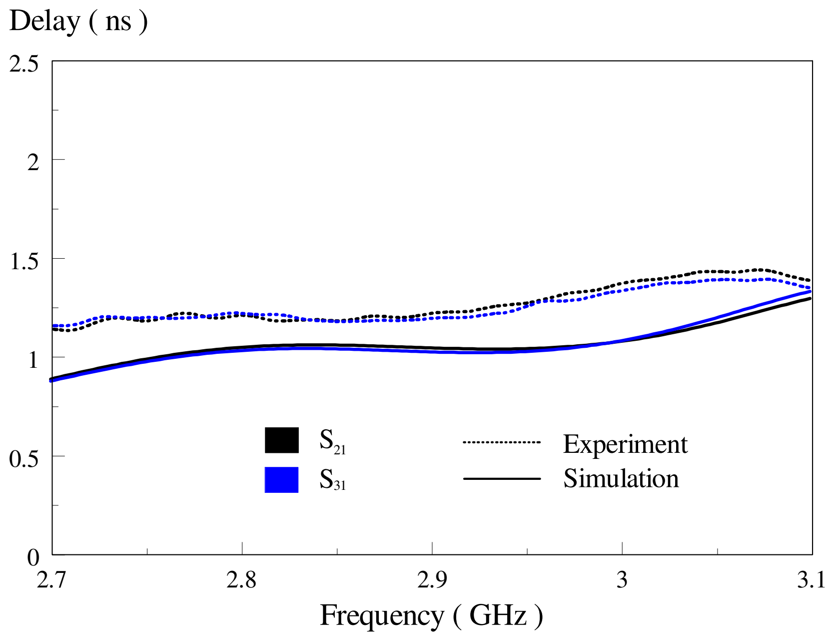

Figure 3.8: Simulated and measured of the group delay of the proposed in-phase power divider.

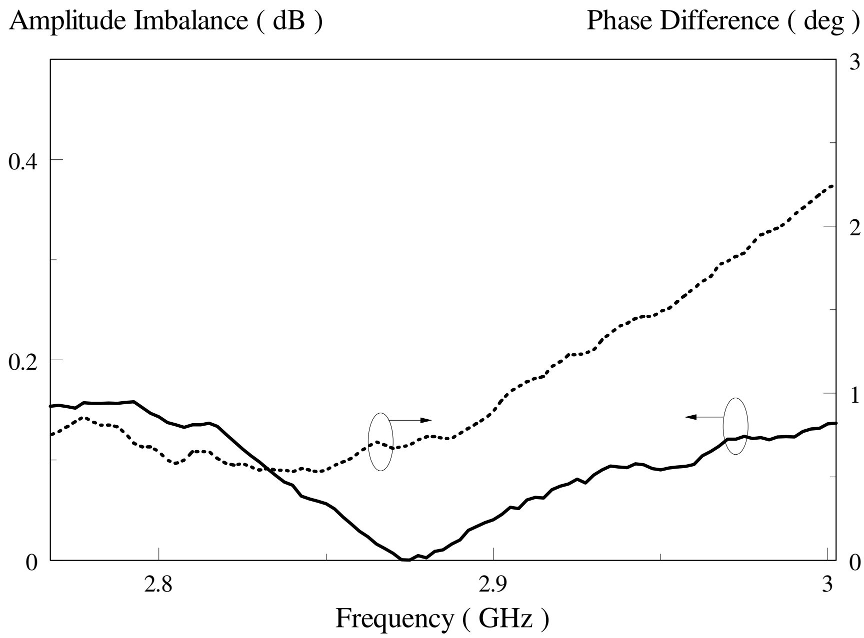

Figure 3.9: Calculated amplitude imbalance and phase difference.

3.3.1.2 Theoretical and Parametric Studies

In this section, the theoretical and parametric studies are analyzed and discussed. All the simulated results are generated from the configuration in Figure 3.5. The simulated electric field distributions of the poles (P_1 = 2.828 and P_2 = 3.081 GHz) are shown in vector form in Figure 3.10. With reference to the figure, the two poles have similar electric field distributions in the central patch but asymmetrical field patterns at the two side patches. As can be seen from the side views of Figure 3.10, it is clear that the output signals at the two ports are tapped symmetrically at two positions which have identical electric vectors, causing them to have the same phase. To obtain a better understanding, the design parameters of the in-phase power divider are analyzed.

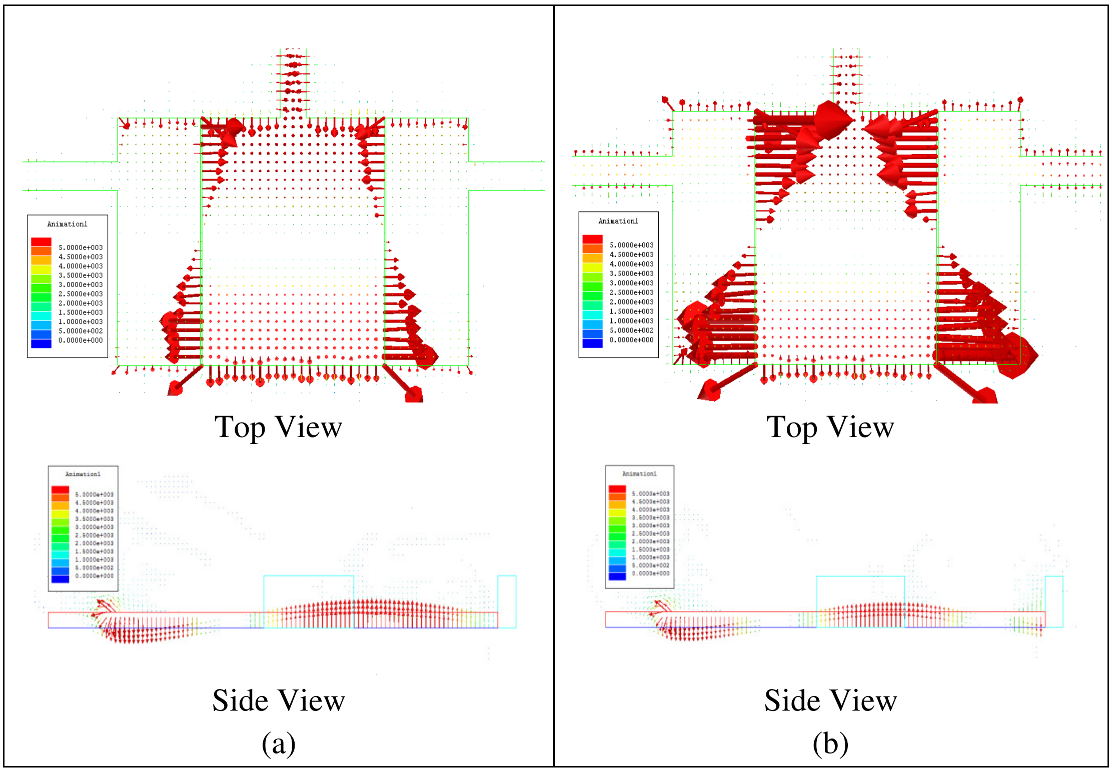

Figure 3.10: The electric field distributions of the proposed in-phase power divider at poles, (a) 2.828 GHz, and (b) 3.081 GHz.

3.3.1.2.1 Widths of Patches W_1

The patch width W_1 is studied in this section. With reference to Figure 3.11, it can be observed that the center frequency of the passband decreases from 3.19 GHz to 2.75 GHz when the patch width W_1 is made larger (26 mm → 30 mm). Also noted is that the resonating frequency of the transmission zero becomes lower with increasing patch width. This shows that this design parameter plays an important role in the calculation of the pole and zero frequencies of the proposed structure.

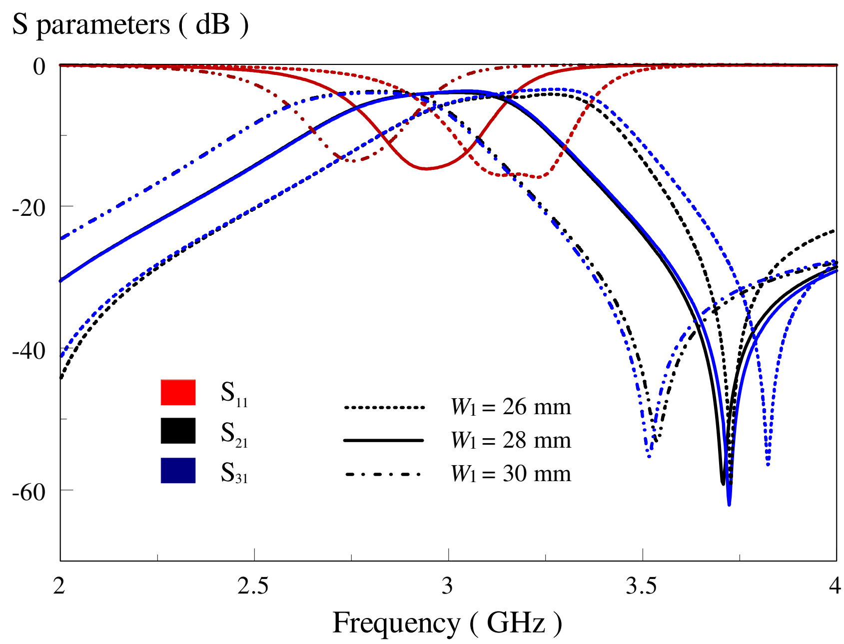

Figure 3.11: Effect of patch width W_1 on the S parameters.

3.3.1.2.2 Feedline Offset W_2

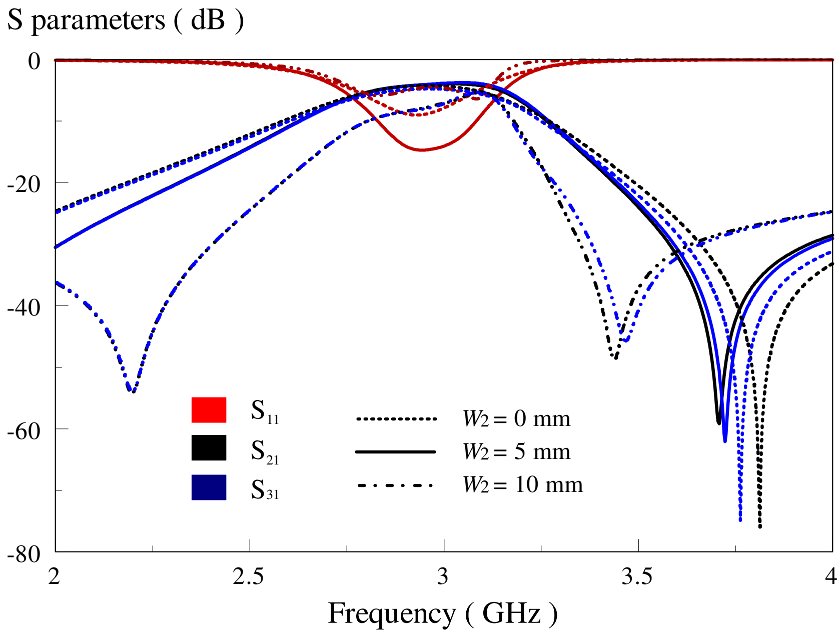

Figure 3.12: Effect of the feedline position W_2 on the S parameters.

The offset position W_2 of the feedlines at *Ports* 2 and 3 is studied here. With reference to Figure 3.12, it is found that W_2 is optimized at 5mm, and the impedance matching ($|S_{11}|$) is made worse for other offset values (-9.02dB at W_2 = 0mm and -4.47dB at W_2 = 10 mm). The transmission zero near to the lower cutoff frequency increases from 1.72GHz to 2.19 GHz when the offset distance is increased from 5 mm to 7 mm. Meanwhile, for the same amount of increment, the transmission zero at the upper cutoff frequency reduces from 3.72GHz to 3.43GHz.

3.3.1.2.3 Gap Distance g_1 between Patches

Figure 3.13 shows the effect of the gap distance g_1 between the patches. It does not affect the simulated S parameters much. When the gap distance is reduced to 0.05 mm, the amplitude imbalance between *Ports* 2 and 3 goes larger than 1 dB, which is undesirable. The impedance matching level worsens (~ -10dB) when the gap distance goes beyond 0.5 mm. For the gap of 0.05mm, the upper transmission zeros is 3.52 GHz at *Port* 2 and 3.38 GHz at *Port* 3. For a larger gap of 0.5 mm, the upper transmission zero moves higher to 3.88GHz.

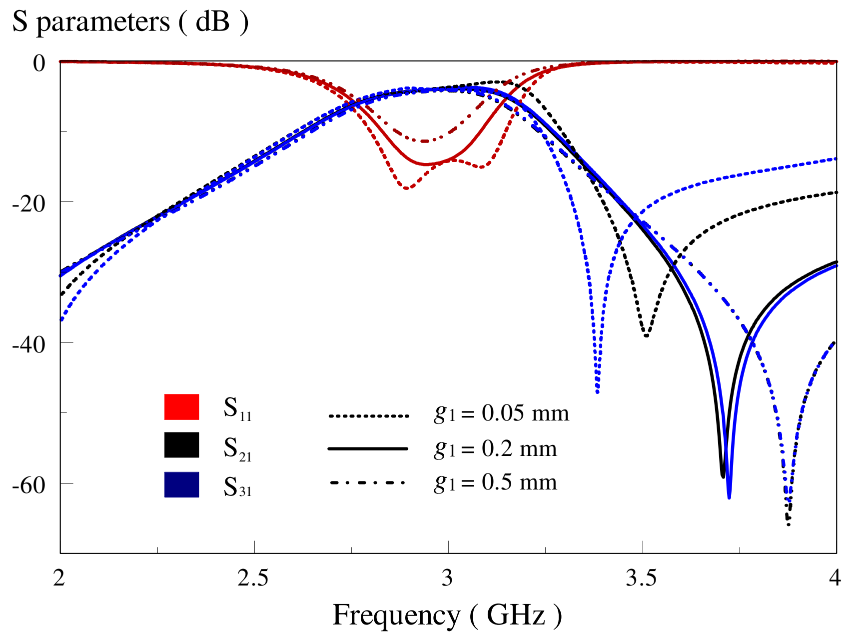

Figure 3.13: Effect of gap distance g_1 between patches on the S parameters.

3.3.2 Out-of-Phase Power Divider

The configuration of the proposed out-of-phase power divider is shown in Figure 3.14, which is quite similar to the in-phase one. The only difference is that, now, the feedline (*Port* 3) is tapping out signal at the lower end of the side patch. It will be shown later that this tapping is possible as the side has almost identical field strength, but with opposite direction, at this position. As can be seen from Figure 3.14, the patch is fed by three 50Ω microstrip feedlines at all of the ports. The detailed design parameters are given by: W_1 = 28 mm, W_2 = 5 mm, W_3= 19.8 mm, L_1 = 22 mm, L_2 = 10 mm, and g_1 = 0.2mm. Figure 3.15 shows the photograph of the fabricated prototype.

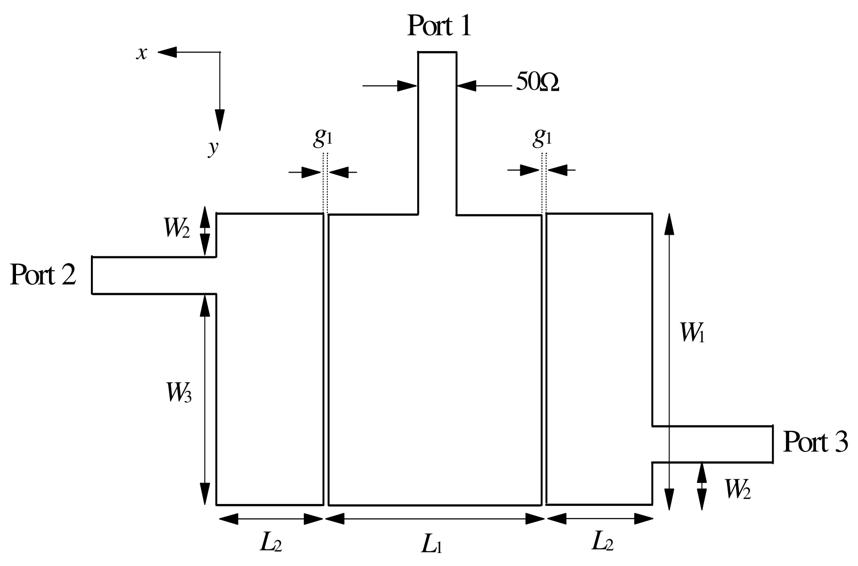

Figure 3.14: Top-view schematic of the proposed out-of-phase power divider.

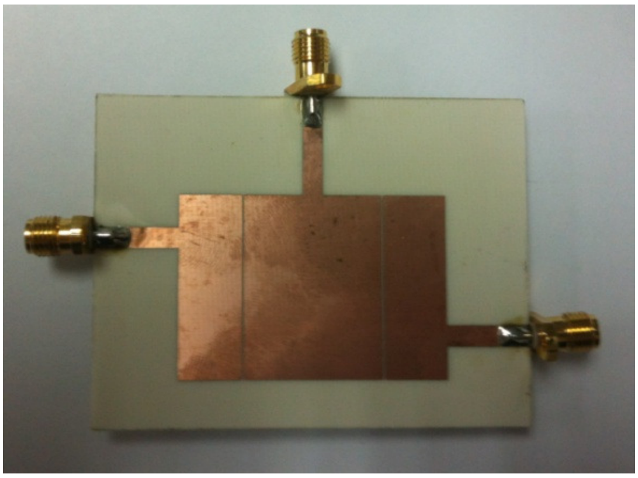

Figure 3.15: Prototype of the proposed out-of-phase power divider.

3.3.2.1 Simulation and Experiment Results

Figure 3.16(a) illustrates the simulation and experimental S parameters of the proposed out-of-phase power divider. The measured and simulated passbands are 2.77 – 3.0 GHz and 2.82 – 3.11 GHz, respectively. With the use of $\frac{f_H - f_L}{f_c} \times 100\,\%$, the measured fractional bandwidth (8.24%) is slight lower than the simulated (9.51%). In the passband, the measured insertion loss is in the range of -4.6dB to -5.4dB (simulation: -3.9dB - -4.8dB), with a matching level of ~ -15dB at the center frequency, which read2.88 GHz in experiment (simulation: 2.97 GHz). Reasonable agreement was observed between the experimental and simulation results, with a slight error of 2.82% in the center frequencies. Figure 3.16(b) shows the isolation between the two output ports. It is lower than -8.5 dB (simulation: -7.2 dB) in measurement. The group delay is shown in Figure 3.17. The group delay is almost constant across the passband, with the measured maximum delay of 1.41 ns (simulation: 1.17 ns). The calculated output amplitude imbalance and phase difference are illustrated in Figure 3.18, and are less than 0.3 dB and1.3^{o} across the entire passband.

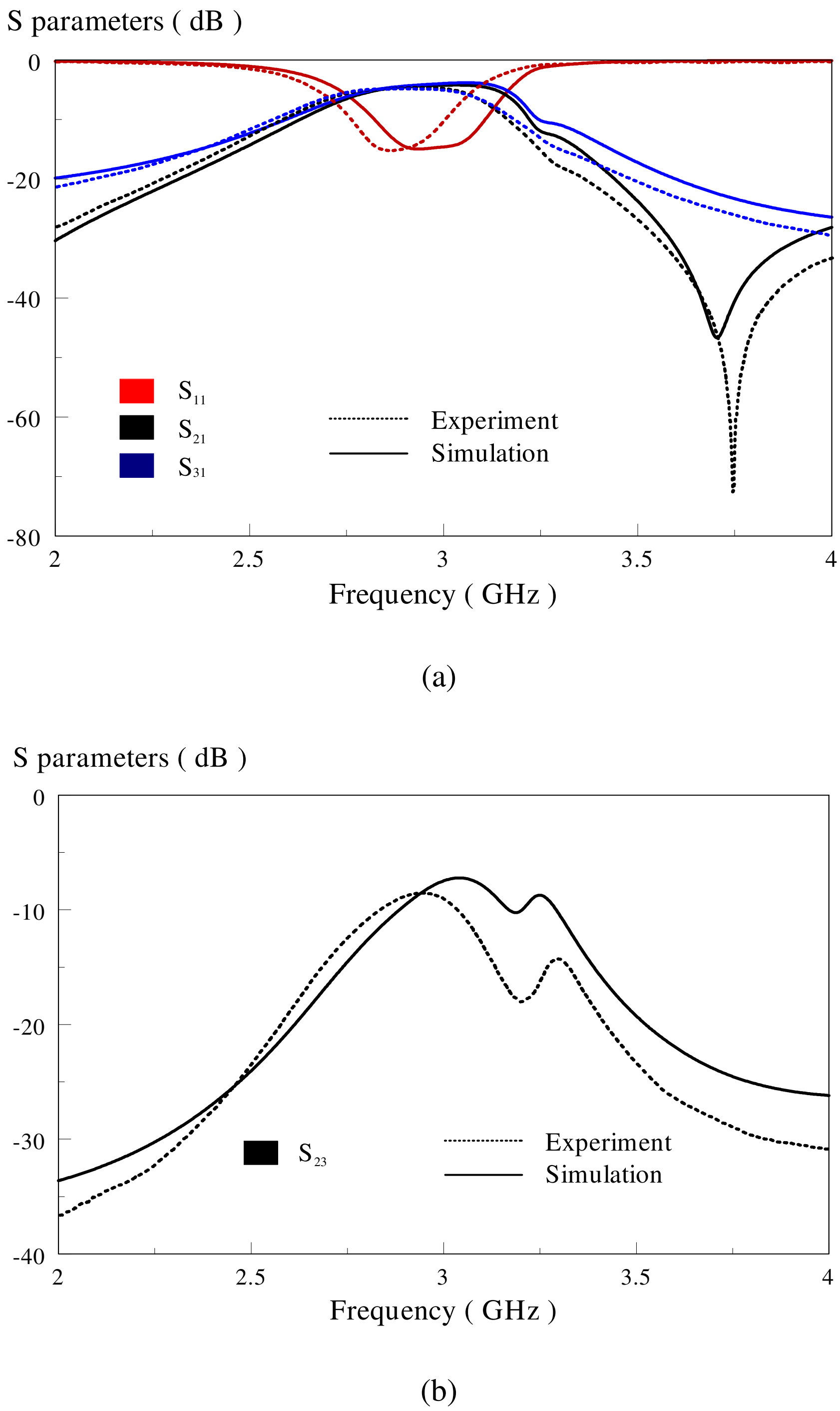

Figure 3.16: Simulated and measured (a) reflection and transmission coefficients, and (b) isolation S_{23} between the output ports.

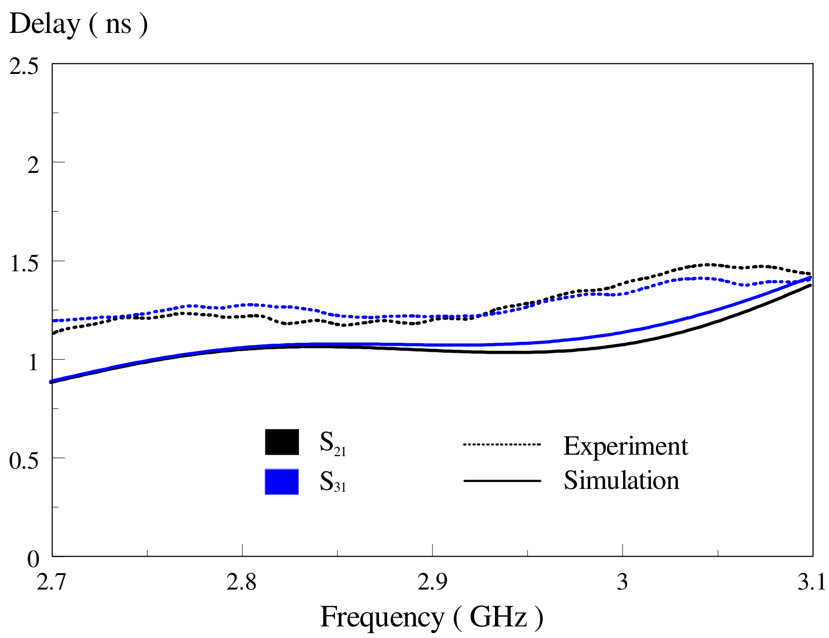

Figure 3.17: Simulated and measured group delay.

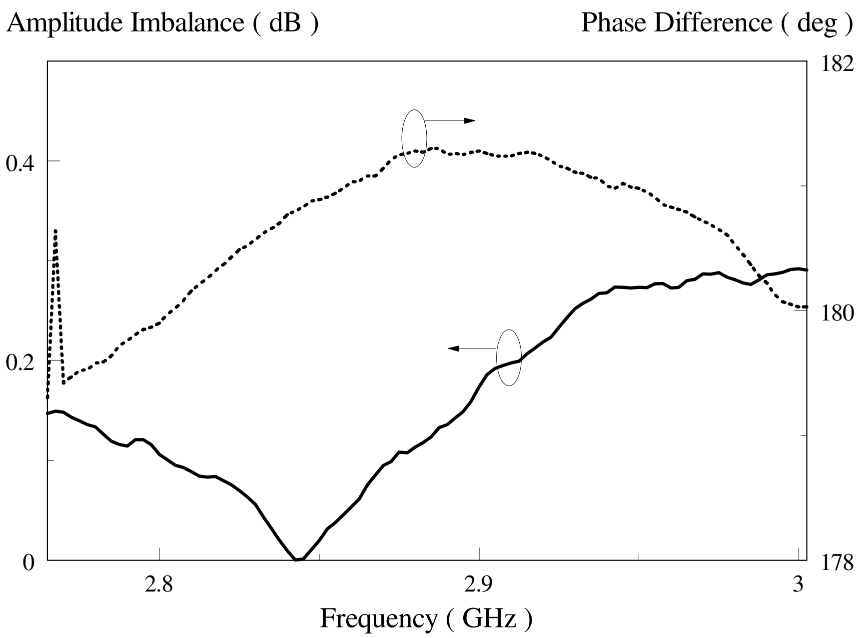

Figure 3.18: Calculated amplitude imbalance and phase difference.

3.3.2.2 Theoretical and Parametric Studies

In this section, the theoretical and parametric analysis of the proposed out-of-phase power divider is discussed. Figure 3.19 illustrates the simulated electric field distributions at pole frequencies, 2.82 GHz and 3.11 GHz. It can be seen from Figure 3.19 that the field strength at the bottom edge of the side patch maximizes, with the field in the opposite directions. Referring to the side views in Figure 3.19, it can be seen that the electric vectors are in the opposite directions at the two output ports, making the output signals out-of-phase. The design parameters are also studied here.

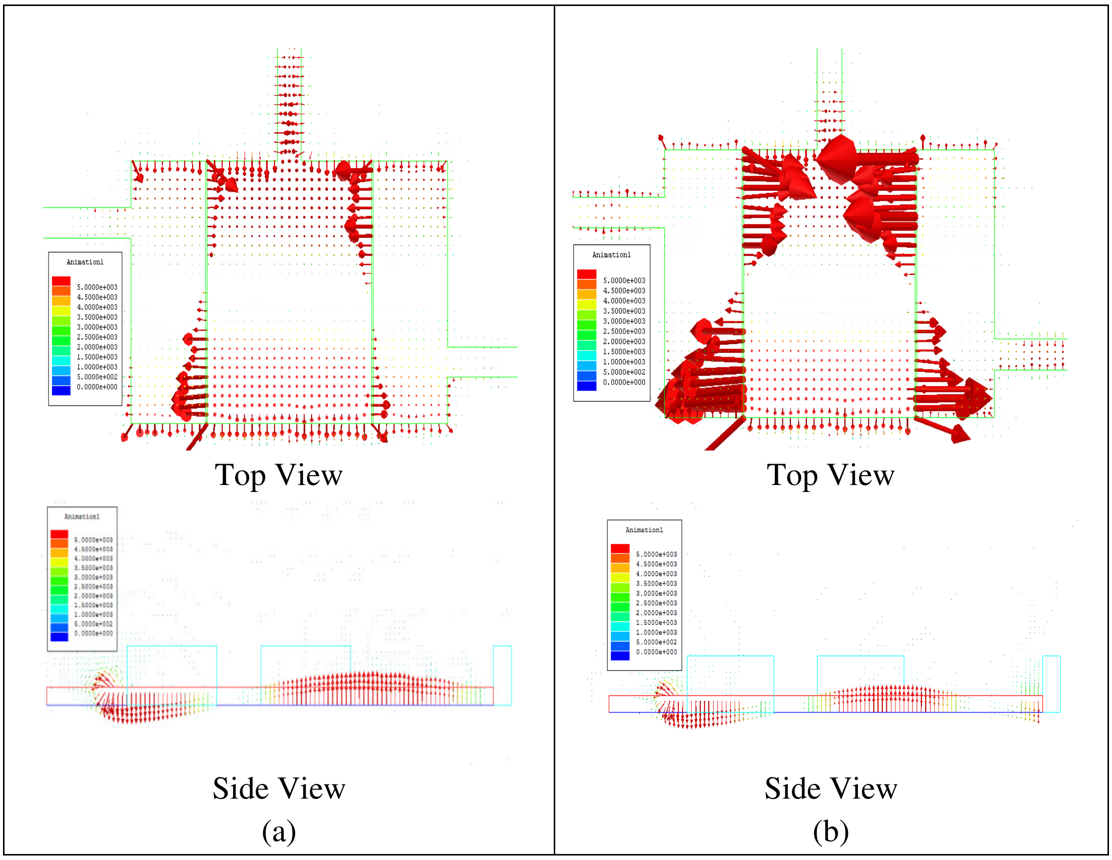

Figure 3.19: The electric field distributions of the proposed out-of-phase power divider at poles, (a) 2.82 GHz, and (b) 3.11 GHz.

3.3.2.2.1 Widths of Patches W_1

Figure 3.20 depicts the simulated S parameters with respect to the change of the width W_1.With reference to the figure, it can be observed that when the patch width is made smaller (30mm to 26 mm), the centre frequency of the passband increases from 2.76 GHz to 3.17 GHz. Besides that, the transmission zero shifts to lower frequency (3.5 GHz) when W_1 is increased. This shows that this design parameter plays an important role in the calculation of the pole and zero frequencies of the proposed structure.

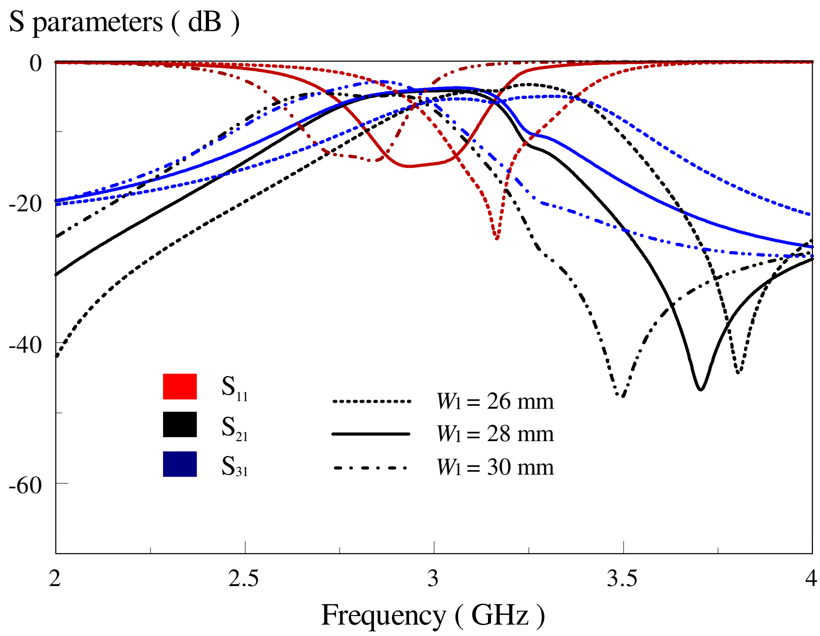

Figure 3.20: Effect of the patch width W_1 on the S parameters.

3.3.2.2.2 Feedline Offset W_2

The offset position of the feedlines at *Port* 2 and *Port* 3 is now studied. With reference to Figure 3.21, W_2 is optimized at 5mm. The matching level ($|S_{11}|$) is affected when offset is changed (-9.6 dB at W_2 = 0mm and -3.95dB at W_2 = 10 mm). The transmission zero near to the higher cutoff frequency increases from 3.72 GHz to 3.88 GHz when the offset distance is decreased from 5 mm to 0 mm. Two transmission zeros are observed at 2.19 GHz and 3.47 GHz when W_2 is set to be 10 mm.

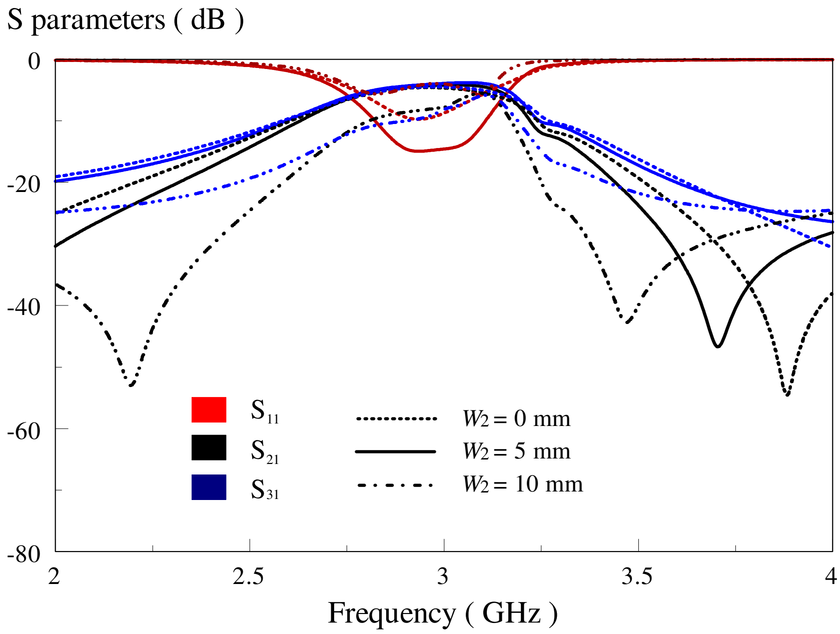

Figure 3.21: Effect of the feedlines position W_2 on the S parameters.

3.3.2.2.3 Length of Patch L_1

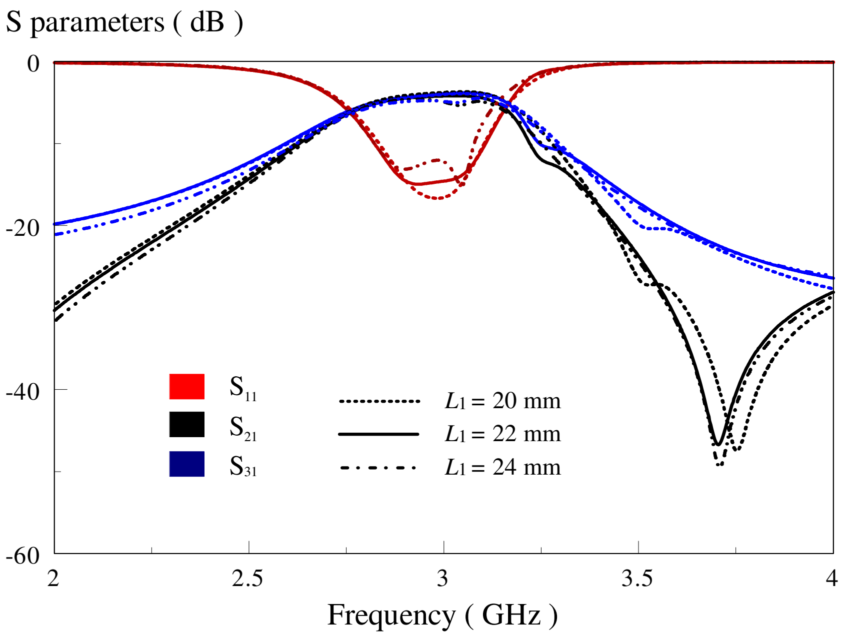

Figure 3.22: Effect of the patch length L_1 on the S parameters.

The length of patch L_1 is now studied. The simulated S parameters with respect to the change of L_1 are shown in Figure 3.22. The L_1 value has only minor effect on S parameters. With reference to the figure, the optimal value for L_1 is 22 mm. Furthermore, no difference is observed in the pole frequencies when the patch width L_1 is varied.

3.4 Power-dividing Directional Coupler

3.4.1 10dB Power-dividing In-phase Directional Coupler

Next, the power-dividing in-phase directional coupler is discussed and analyzed in this section. The proposed structure is created be by adding two extra output ports to the configuration shown in Figure 3.5 to form a new device that can give two half-powered in-phase outputs as well as the 10dB coupled signals. The feedlines have a characteristic impedance of 50Ω for ease of interconnection with other microwave systems. Also, all the unused ports are terminated with the 50Ω loads in experiments. With reference to Figure 3.23, *Port* 2 and *Port* 3 give the half-powered outputs while the two newly added ports (*Port* 4 and *Port* 5) are the coupled ports, which are also producing in-phase signals with a phase difference of ~ $0\pm5^{\circ}$across the operating bandwidth. Figure 3.23 shows the top-down view schematic of the proposed multifunctional power-dividing directional coupler. Like the previous power divider, the proposed directional coupler is composed of three side-coupled microstrip patches on the top surface of the grounded substrate. The detailed design parameters are given by: W_1= 28 mm, L_1 = 22mm, W_2 = 5 mm, W_3= 14.7 mm, L_2= 10mm, and g_1 = 0.2 mm. Figure 3.24 shows a photograph of the fabricated prototype.

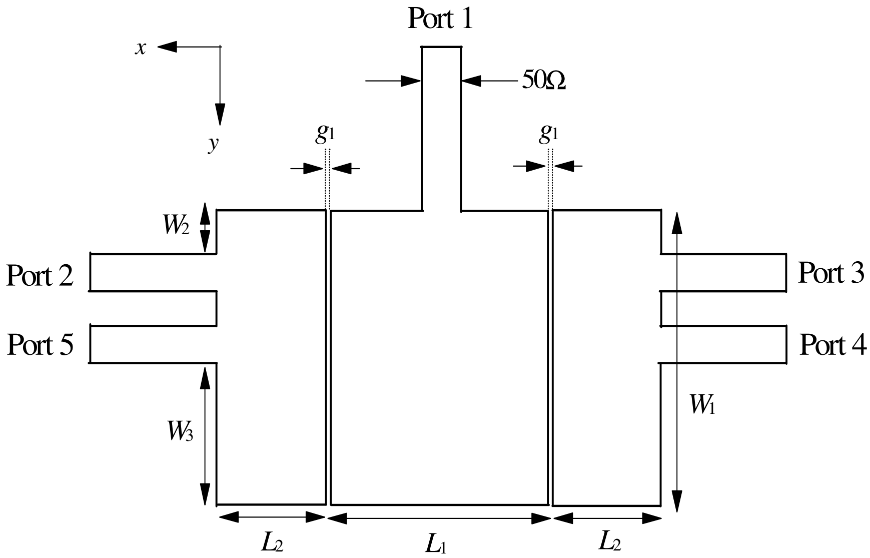

Figure 3.23: Top-view schematic of the proposed 10dB power-dividing in-phase directional coupler.

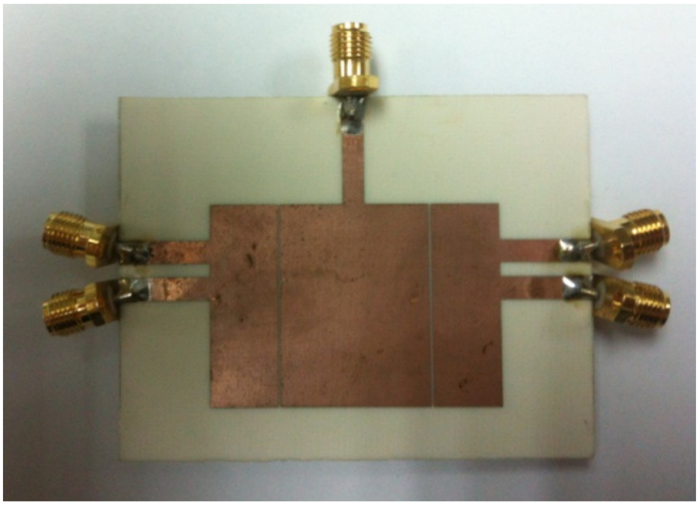

Figure 3.24: Prototype of the proposed 10dB power-dividing in-phase directional coupler.

3.4.1.1 Simulation and Experimental Results

The simulation and experimental results will be illustrated and analyzed in this section. Figure 3.25(a) shows the simulated and measured S parameters of the proposed structure, showing two poles with a measured passband of 2.76 – 3.0 GHz (simulation: 2.84 – 3.09 GHz) and a measured FBW of 8.51% (simulation:8.33%). In the passband, the measured transmission coefficient is in the range of -4.9dB to -5.4dB (simulation: -4.3dB - -5.2dB) at *Ports* 2 and 3, which is quite close to the theoretical value of -3.98dB. It is lower as part (-10dB) of the input power has been directed to *Ports* 4 and 5. The measured and simulated center frequencies are 2.88 GHz and 2.97 GHz, respectively, with an error of 3.13%. Also, three transmission zeros are measured at 2.13 GHz (simulation: 2.21 GHz), 3.42 GHz (3.43 GHz), and 3.75 GHz (3.71 GHz). Figure 3.25(b) shows the measured and simulated coupling coefficients between the output and coupled ports. The calculated amplitude imbalance and phase difference of the proposed configuration is illustrated in Figure 3.26. As can be seen from the figure, the amplitude imbalance and phase difference fall within$|S_{21}$ or $S_{31}|-|S_{41}$ or $S_{51}|=10\pm0.3$ dB, $|\angle S_{21}-\angle S_{31}|\leq\pm1^{o}$, and$|\angle S_{41}-\angle S_{51}|\leq\pm1.5^{o}$, respectively. Both are calculated from the measured results across the passband. Figure 3.27 shows the measured and simulated group delays of both of the half-powered output ports and 10dB coupled ports. Reasonable agreement is observed. It shows that the same piece of resonator can be used to generate power division and coupling signals. This can lead to significant cost saving.

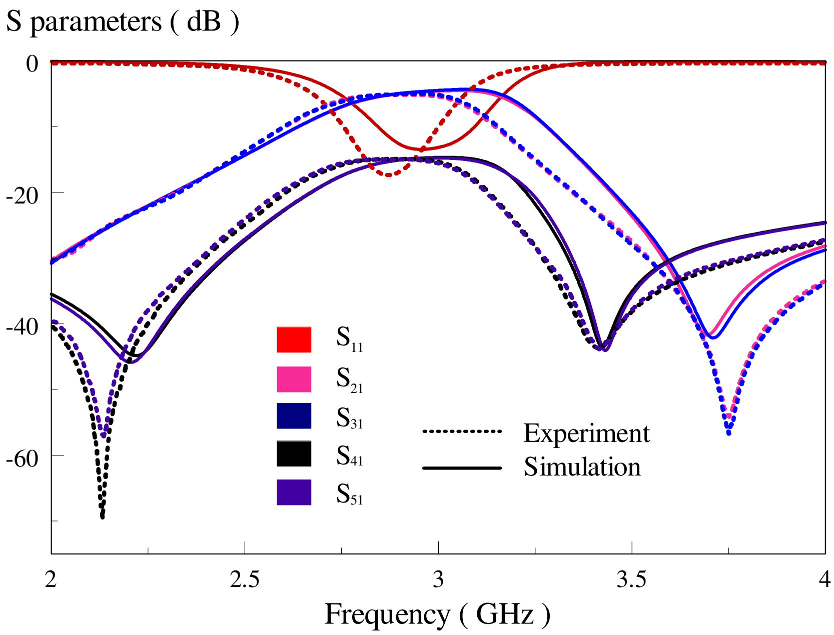

(a)

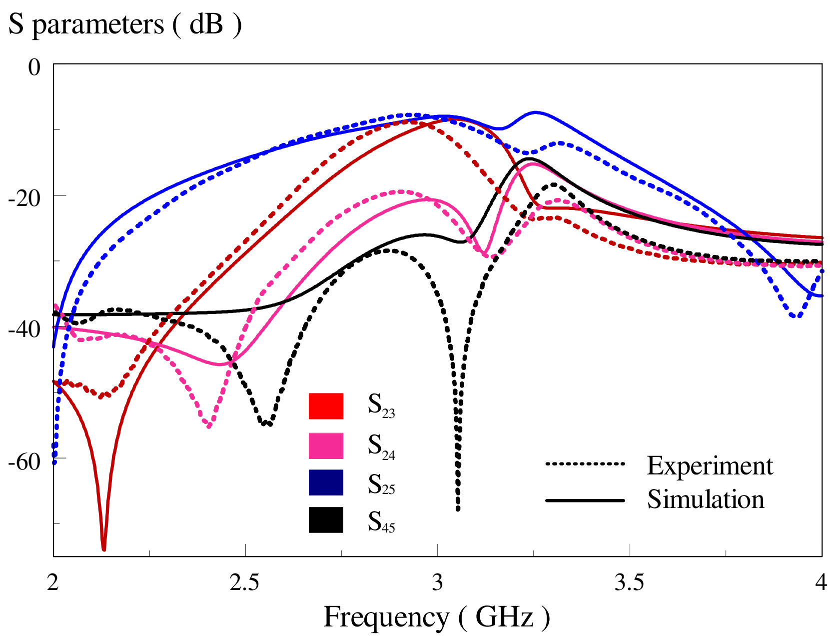

(b)

Figure 3.25: Simulated and measured (a) reflection and transmission coefficients, and (b) isolation levels between the output ports.

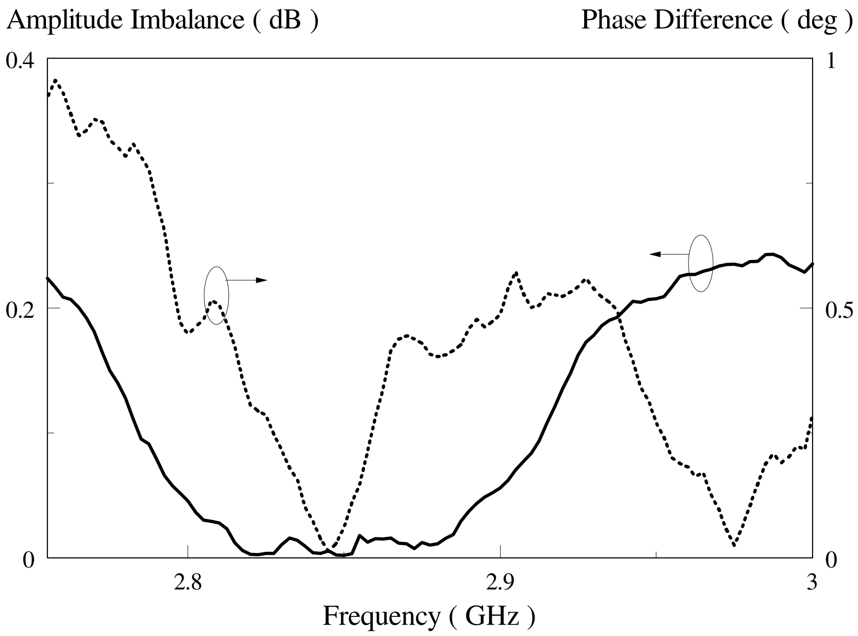

(a)

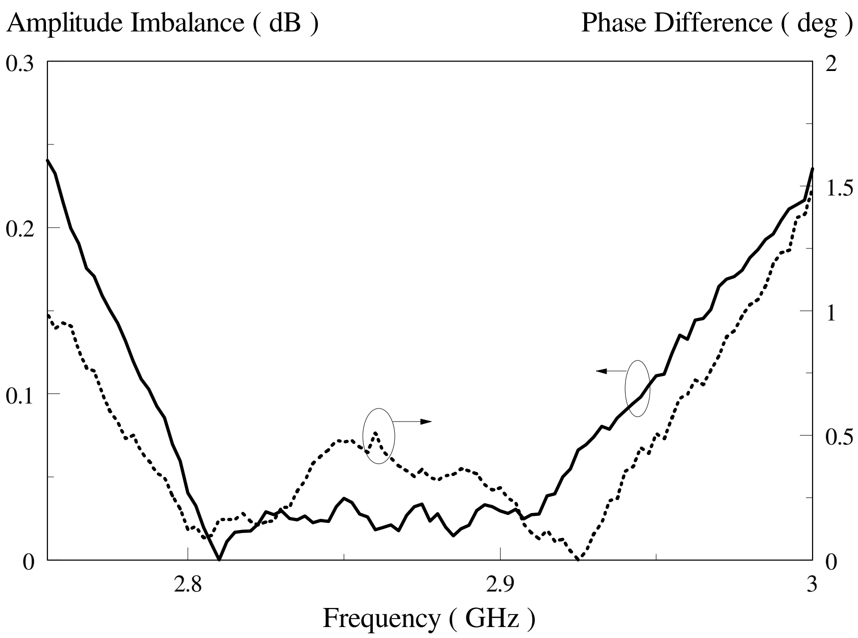

(b)

Figure 3.26: Calculated amplitude imbalance and phase difference of the (a) half-powered outputs, and (b) 10dB coupled ports.

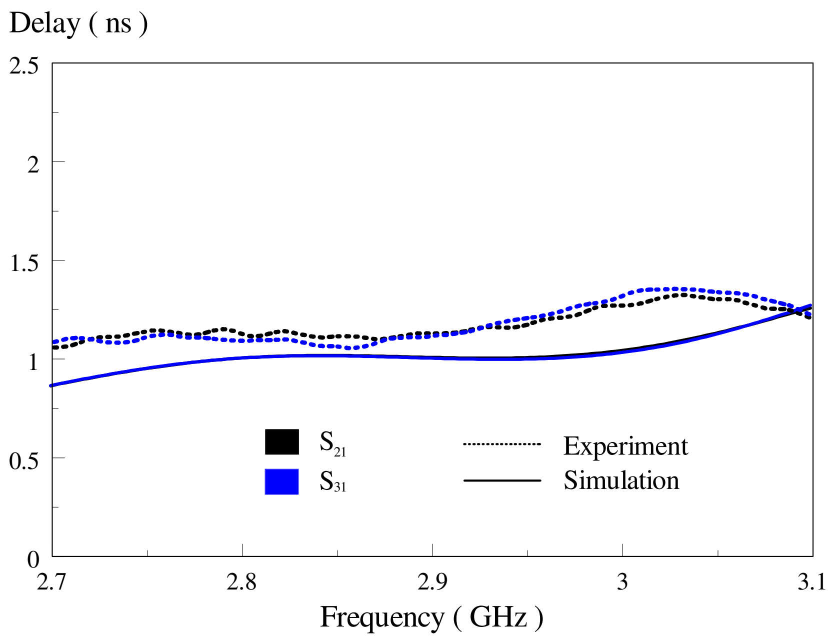

(a)

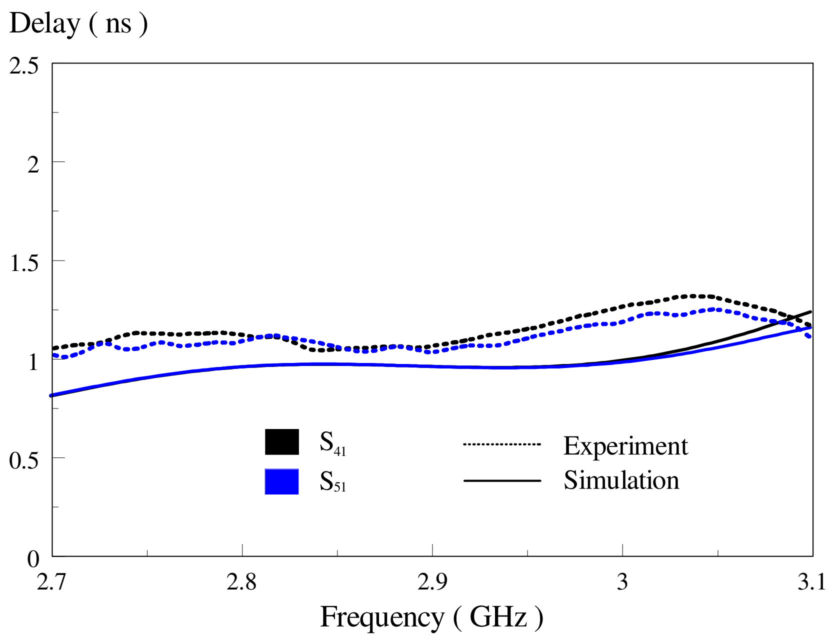

(b)

Figure 3.27: Simulated and measured group delays for the (a) half-powered outputs, and (b) 10dB coupled ports.

3.4.2 10dB Power-dividing Out-of-phase Directional Coupler

In this section, the 10dB power-dividing out-of-phase directional coupler is proposed. It has the same characteristics as the previous one, but provides two half-powered in-phase output signals (*Port* 2 and *Port* 3) as well as another two 180^o out-of-phase coupled outputs (*Port* 4 and *Port* 5), which are 10dB lower. Figure 3.28 shows the top-view schematic of the proposed power-dividing out-of-phase directional coupler, which is quite similar to that in Figure 3.23. The only difference is that the feedline position for *Port* 5is further apart from *Port* 2. This is because such a feeding configuration can make the signals at *Port* 4 and *Port* 5 out-of-phase. The detailed design parameters are given by: W_1 = 28 mm, W_2 = 4.9 mm, W_3= 9.9 mm, W_4 = 14.7 mm, L_1 = 20mm, L_2 = 12 mm, and g_1 = 0.2 mm. Again, all the feedlines are designed with a characteristic impedance of 50 Ω. Figure 3.29 shows the top-view photograph of the fabricated prototype.

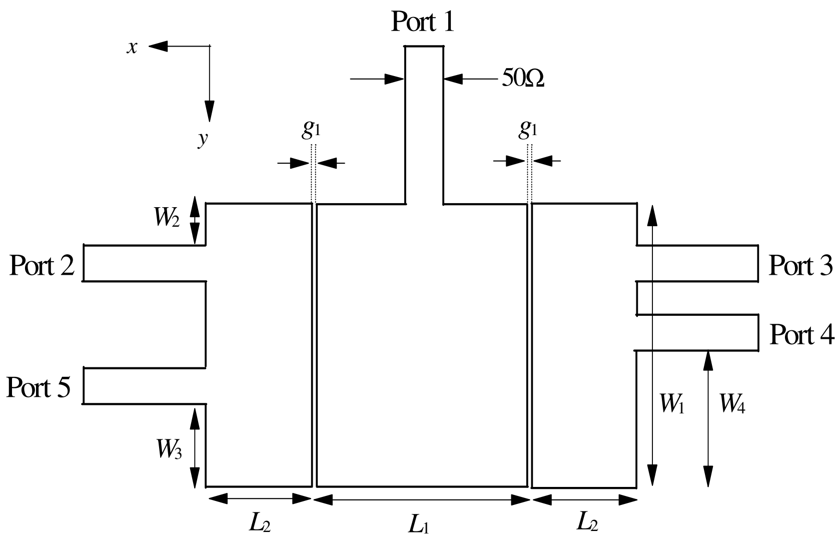

Figure 3.28: Top-view schematic of the proposed 10dB power-dividing out-of-phase directional coupler.

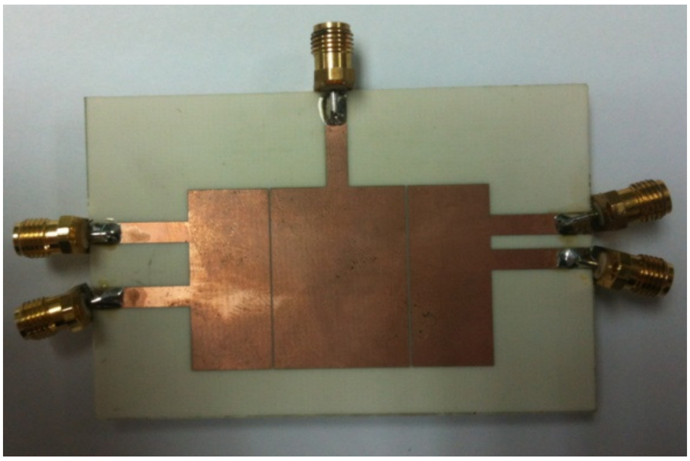

Figure 3.29: Prototype of the proposed 10dB power-dividing out-of-phase directional coupler.

3.4.2.1 Simulation and Experimental Results

Figure 3.30(a) shows the simulated and measured S parameters of the proposed structure. Two resonances are observed in the passband. The proposed structure has a measured passband covering 2.76 – 2.96 GHz (simulation: 2.85 – 3.04 GHz), with a FBW of 7% (simulation: 6.53%). The measured and simulated center frequencies are 2.86 GHz and 2.95 GHz, respectively, with an error of 2.97%. The simulated and measured coupling coefficients between the output and coupled ports are shown in Figure 3.30(b). In general, the measured coupling levels between any two output ports are less than -9.7dB. Good agreement has been observed between simulation and experimental results. Figure 3.31 illustrates the calculated amplitude imbalance and phase difference. The amplitude imbalance and phase difference fall within $|S_{21}$ or $S_{31}| - |S_{41}$ or $S_{51}|=10\pm0.8$ dB, $|\angle S_{21}-\angle S_{31}|\leq\pm4.5^{o}$, and $|\angle S_{41}-\angle S_{51}|\leq180\pm4^{o}$, respectively, in the operating bandwidth. The corresponding group delays of the half-powered and coupled ports are shown in Figure 3.32. Good agreement between measurement and simulation results can be observed.

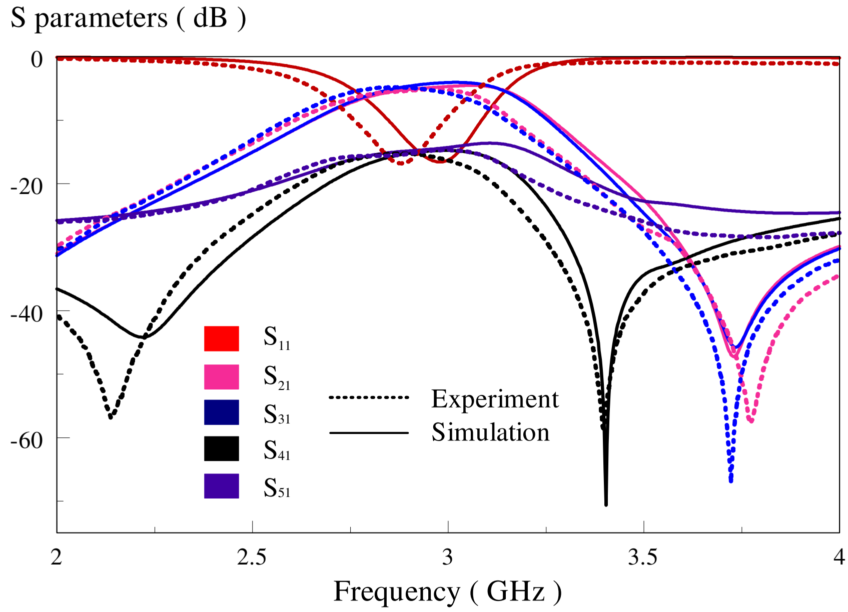

(a)

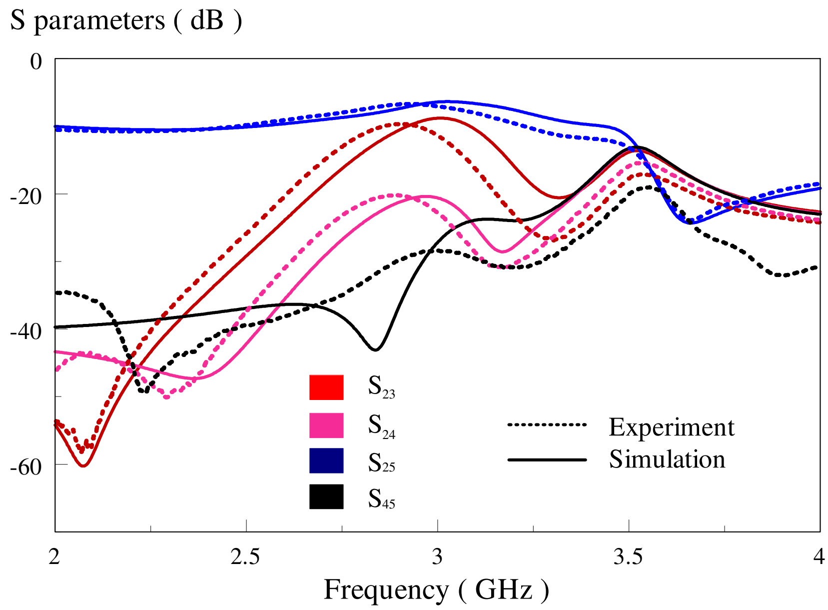

(b)

Figure 3.30: Simulated and measured (a) reflection and transmission coefficients, and (b) isolation levels between the output ports.

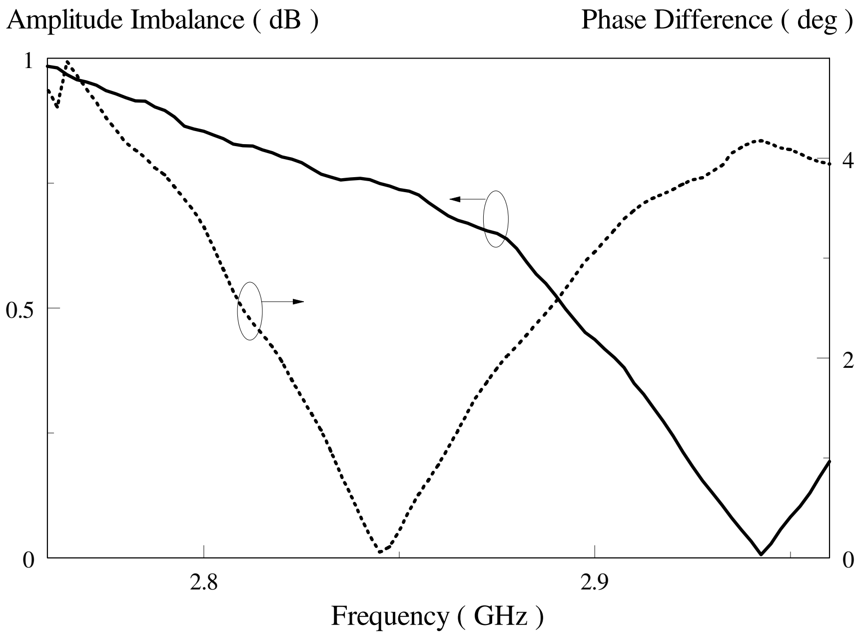

(a)

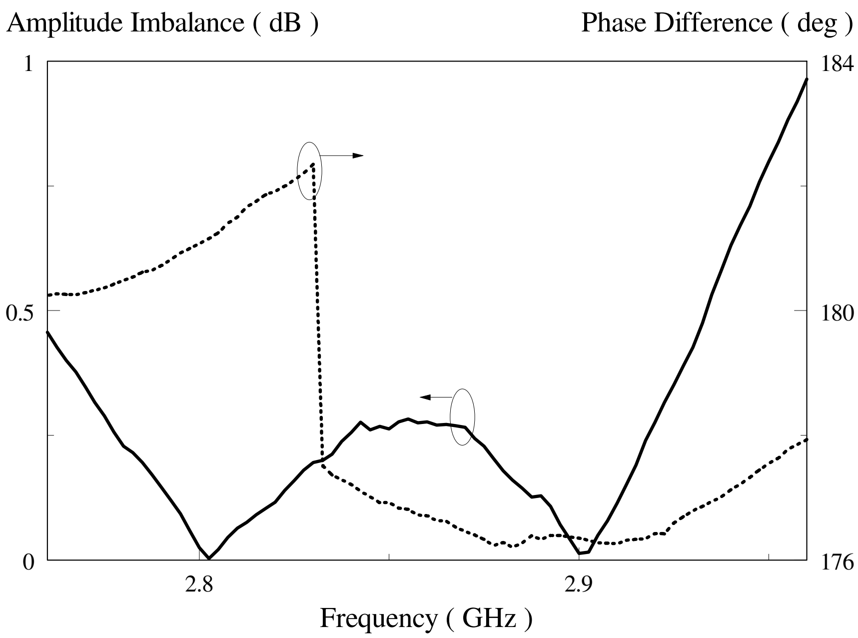

(b)

Figure 3.31: Calculated amplitude imbalance of the (a) half-powered outputs, and (b) 10dB coupled ports.

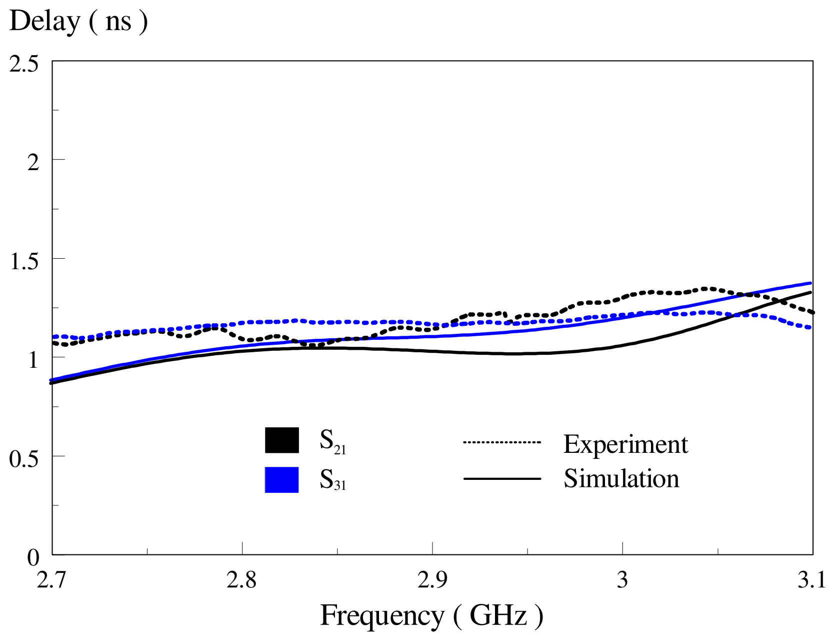

(a)

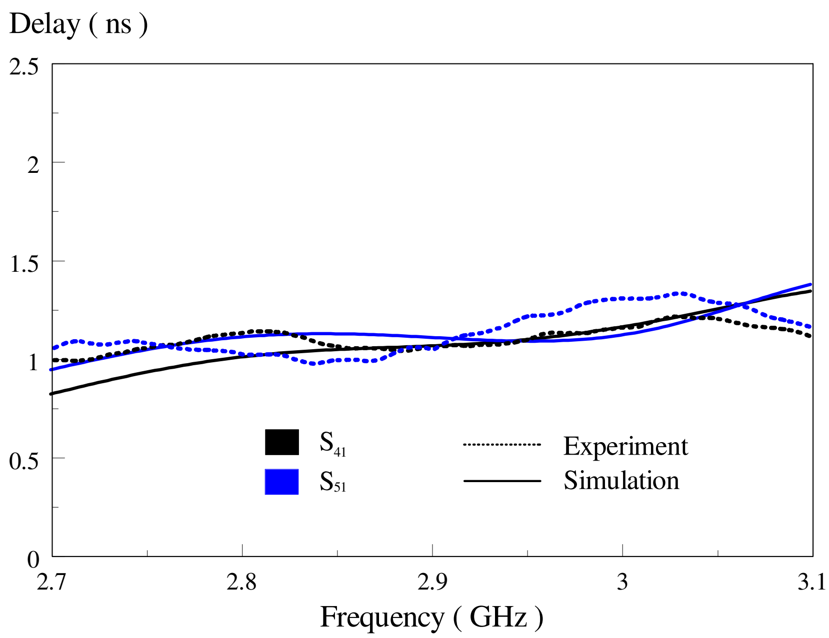

(b)

Figure 3.32: Simulated and measured group delays of the (a) half-powered outputs, and (b) 10dB coupled ports.

3.4.3 20dB Power-dividing Directional Coupler

Another new power-dividing directional coupler is proposed in this section. This time the same configuration is made to generate two in-phase 20dB coupled signals. To do that, the feeding positions for *Port* 4 and *Port* 5 are adjusted along the edges of the side patches. In this case, the half-powered outputs are also made to be in-phase. The feedlines are designed with a characteristic impedance of 50 Ω, with all of the unused ports terminated with 50 Ω loads during measurement. The top-view schematic of the proposed structure is shown in Figure 3.33. Other design parameters are given by: W_1 = 28 mm, W_2 = 5mm, W_3 = 13 mm, L_1 = 20 mm, L_2 = 10 mm, and g_1 = 0.2 mm. Figure 3.34 shows the photograph of the fabricated prototype.

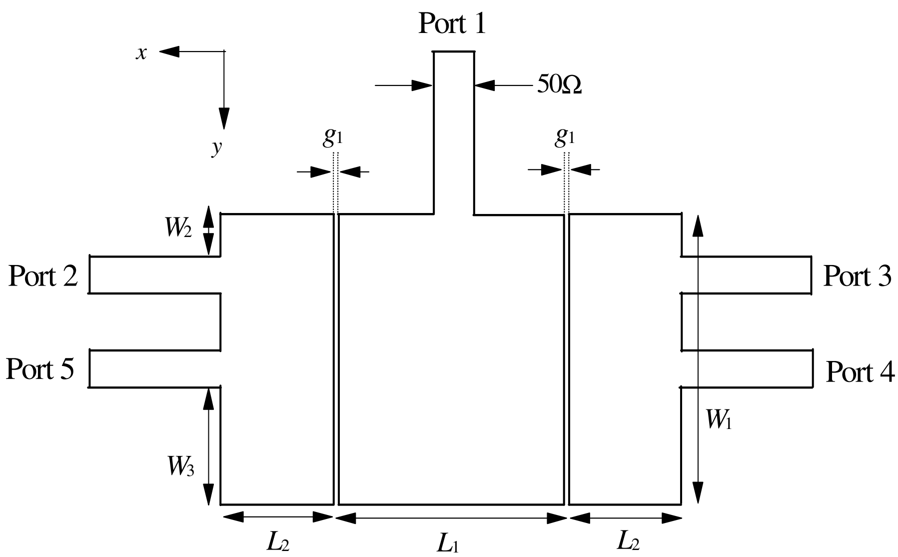

Figure 3.33: Top-view schematic of the proposed 20dB power-dividing directional coupler.

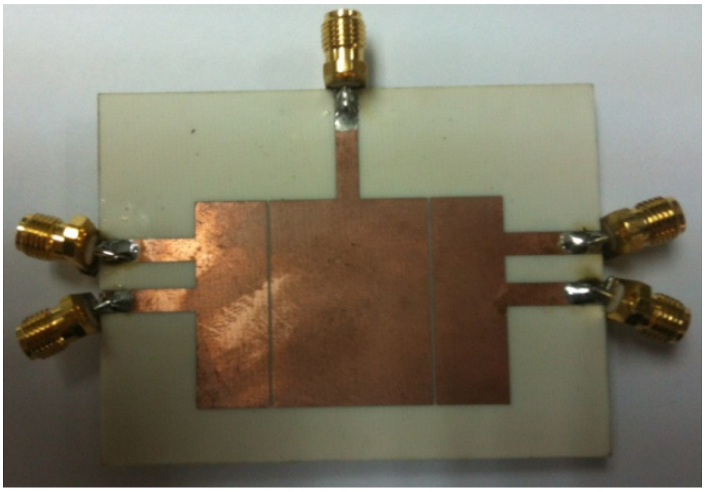

Figure 3.34: Prototype of the proposed 20dB power-dividing directional coupler.

3.4.3.1 Simulation and Experimental Results

The simulated and measured S parameters of the proposed structure are depicted in Figure 3.35(a). It has a measured passband of 2.77 – 2.99 GHz (simulation: 2.85 – 3.08 GHz), with a FBW of 7.9% (simulation: 7.58%). The measured and simulated center frequencies are 2.88 GHz and 2.96 GHz, respectively, with an error of 2.95%. Transmission zeros are observed in both of the power division and coupled signals. For the half-power division, a transmission zero is measured at 3.78 GHz (simulation: 3.74 GHz), very near to the upper cutoff frequency of the passband. For the coupled signals, very interestingly, one transmission zero is found near to the lower cutoff frequency (measurement: 2.43 GHz and simulation: 2.55 GHz) while another is observed in the proximity of the higher one (measurement: 3.27 GHz and simulation: 3.25 GHz). The simulated and measured coupling coefficients between the output and coupled ports are shown in

Figure 3.35(b). Good agreement is observed between simulation and experiment. Figure 3.36 illustrates the calculated amplitude imbalance and phase difference of the proposed configuration. The amplitude imbalance and phase difference are fluctuating within $|S_{21}$ or $S_{31}| - |S_{41}$ or $S_{51}|=20\pm0.7$ dB and $|\angle S_{21}-\angle S_{31}|\leq\pm0.9^{o}$, $|\angle S_{41}-\angle S_{51}|\leq\pm4.9^{o}$, respectively, across the passband. The corresponding group delays of the half-powered outputs and coupled ports are shown in Figure 3.37. Reasonable agreement between measurement and simulation results can be observed.

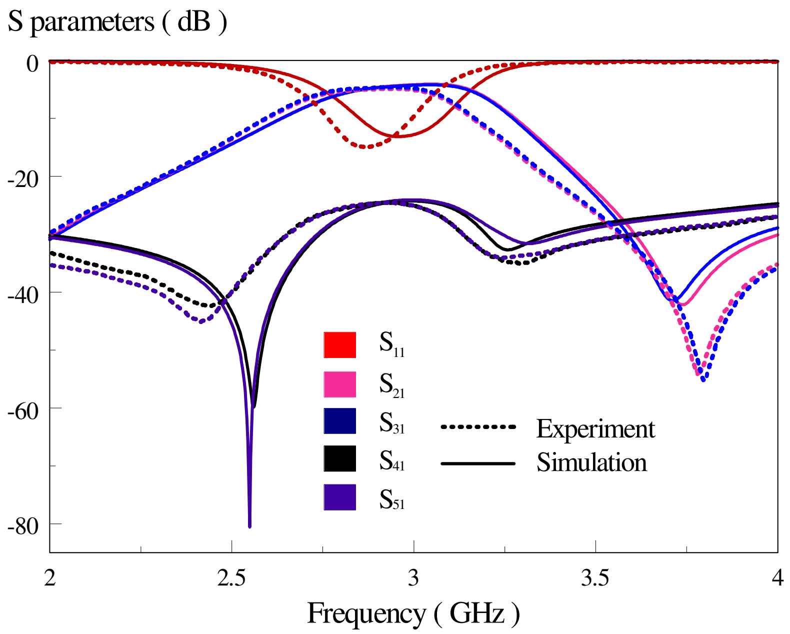

(a)

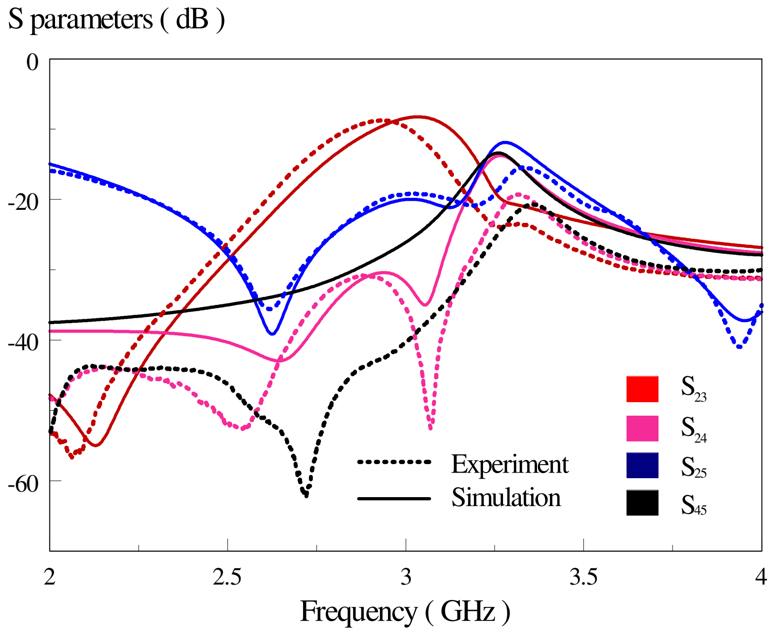

(b)

Figure 3.35: Simulated and measured (a) reflection and transmission coefficients, and (b) isolation levels between the output ports

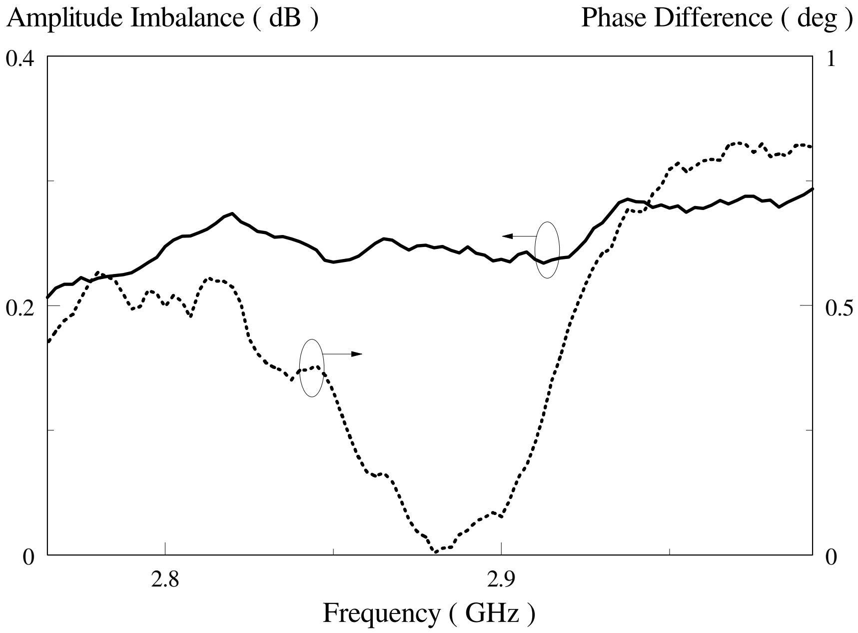

(a)

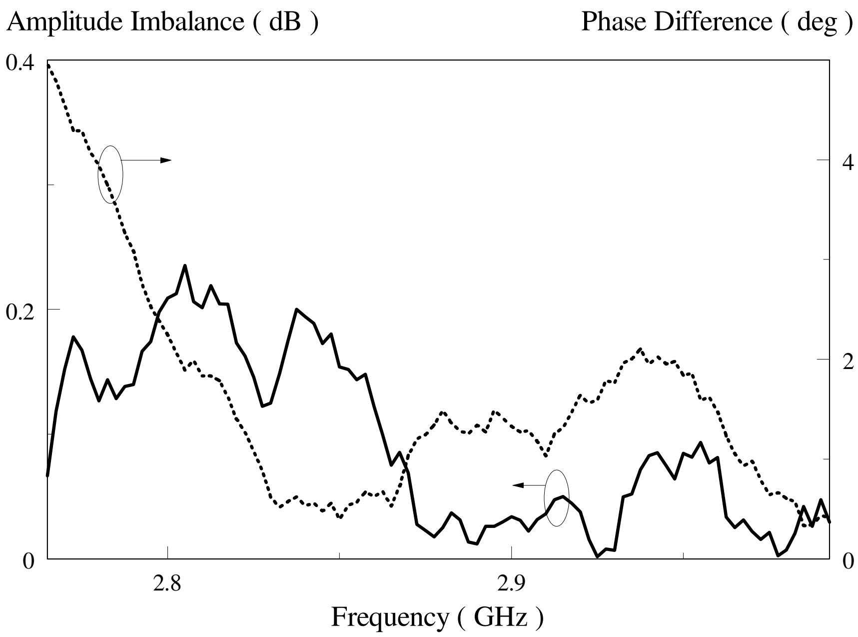

(b)

Figure 3.36: Calculated amplitude imbalance of the (a) half-powered outputs, and (b) 20dB coupled ports.

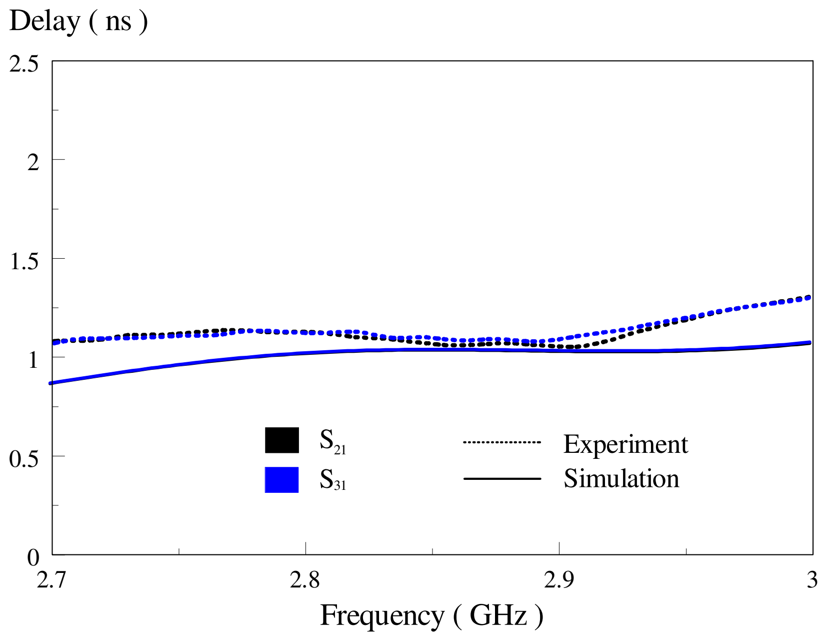

(a)

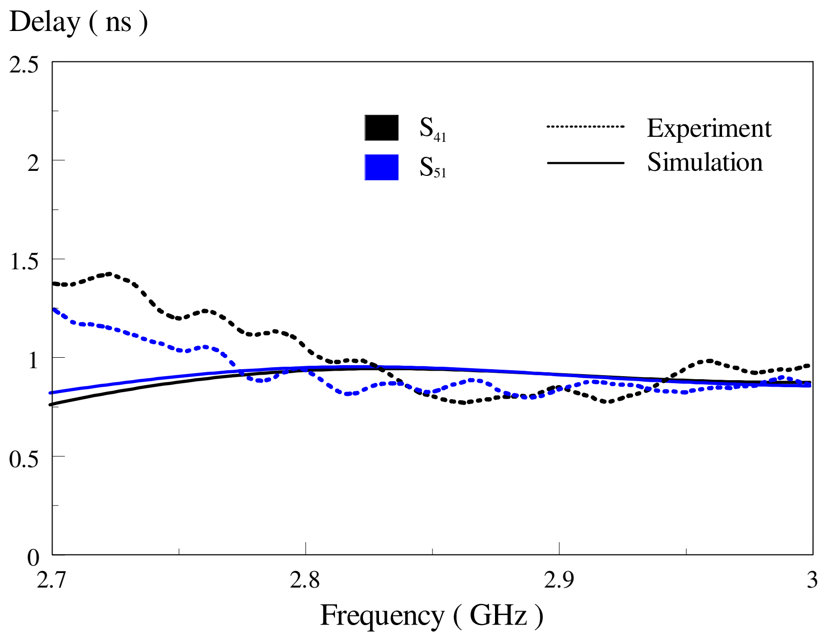

(b)

Figure 3.37: Simulated and measured group delays of the (a) half-powered outputs, and (b) 20dB coupled ports.

3.5 Multifunctional Directional Coupler with Multiple Outputs

In this section, a multifunctional device that can produce half-power, 10 dB, and 20dB output signals is proposed. It is interesting to note that the three features can now be combined into a single module, leading to significant cost saving. The schematic is depicted in Figure 3.38. In this new design, *Port* 4 and *Port* 5 generate 10dB and 20dB coupled output signals, respectively. The detailed design parameters are given by: W_1 = 28 mm, W_2 = 5 mm, W_3 = 12.9 mm, W_4 = 14.7 mm, L_1 = 20 mm, L_2 = 10 mm, and g_1 = 0.2 mm. The prototype of the proposed structure is shown in Figure 3.39.

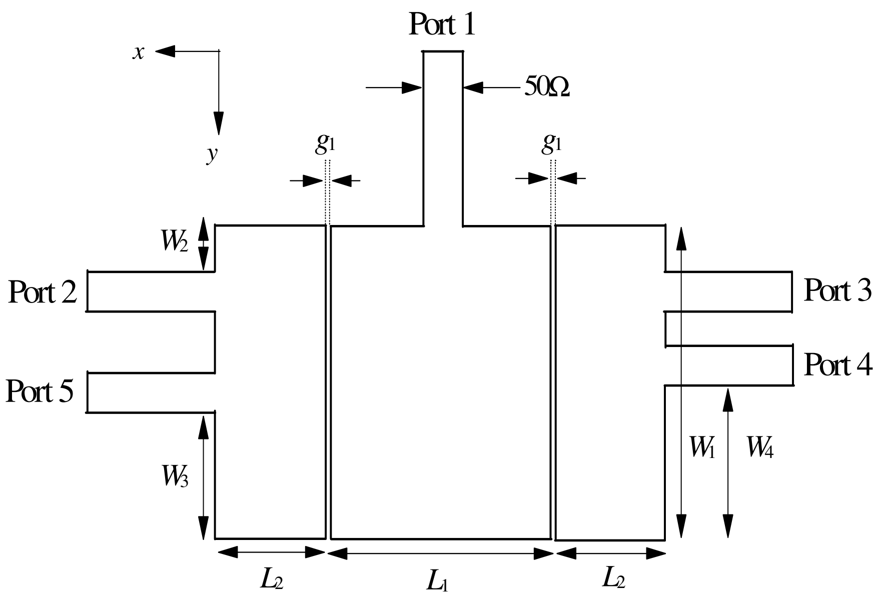

Figure 3.38: Schematic of the proposed multifunctional directional coupler with multiple outputs.

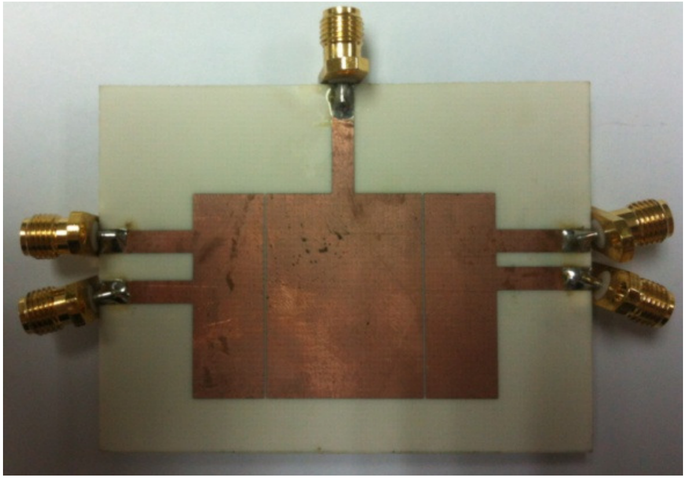

Figure 3.39: Prototype of the proposed multifunctional directional coupler.

3.5.1 Simulation and Experimental Results

In the experiment, all the unused ports were terminated by 50 Ω loads. The simulated and measured S parameters are shown in Figure 3.40. The measured passband is 2.8 – 3.0 GHz (simulation: 2.86 – 3.09 GHz) with a FBW of 7.24% (simulation: 7.72%). The measured center frequency is 2.9 GHz, which is very close to the simulated one of 2.98 GHz, with an error of 2.67%. Transmission zeroes, which are found in the transmission coefficients, have been deployed to sharpen the roll-off of the cutoff skirts of the frequency passbands, as summarized in Table 3.1.

Transmission Zeros	Zeros near to the lower cut-off frequency (GHz)		Zeros near to the higher cut-off frequency (GHz)	
	Measurement	**Simulation**	**Measurement**	**Simulation**
$\mathbf{S_{21}}$	1.81	1.72	3.83	3.72
$\mathbf{S_{31}}$	1.79	1.72	3.80	3.72
$\mathbf{S_{41}}$	2.14	2.20	3.42	3.45
$\mathbf{S_{51}}$	2.41	2.58	3.35	3.23

Table 3.1: Transmission zeros near to the lower and higher cut-off frequencies.

Figure 3.41 shows the isolation performance between the output ports of the proposed structure. Good isolation of ~ -10 dB was observed between the output ports across the passband. The calculated amplitude imbalance and phase difference are depicted in Figure 3.42. It can be observed that the amplitude imbalance and phase difference between two half-powered output ports (*Port* 2 and *Port* 3) fall within ≤ 0.74 dB and ±4.3°, respectively, across the passband. Besides that, the amplitude difference between the half-power output ports and coupled ports (*Port* 4 and *Port* 5) are around 10±0.9 dB and 20±0.9 dB, respectively. Figure 3.43 illustrates the measured and simulated group delays, and again reasonable agreement was observed.

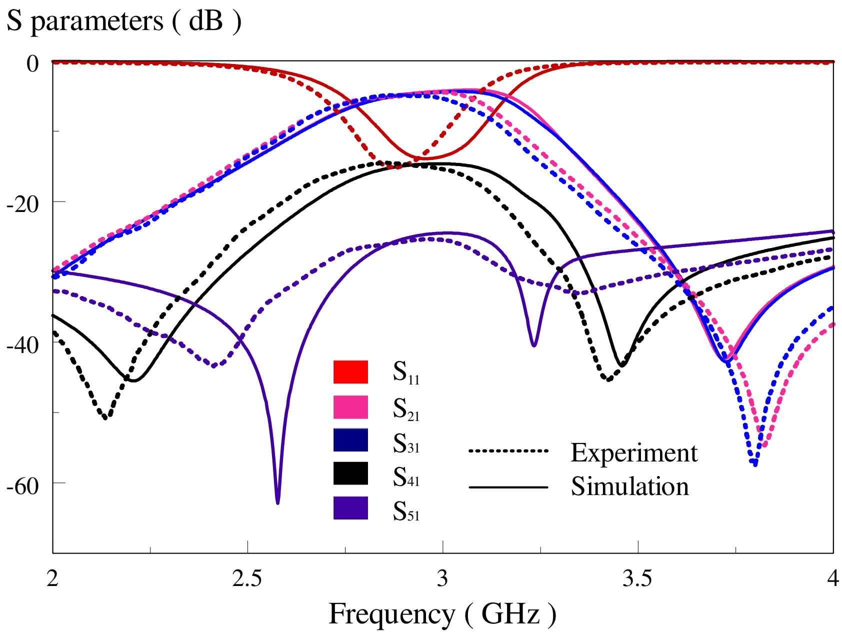

Figure 3.40: Simulated and measured S parameters.

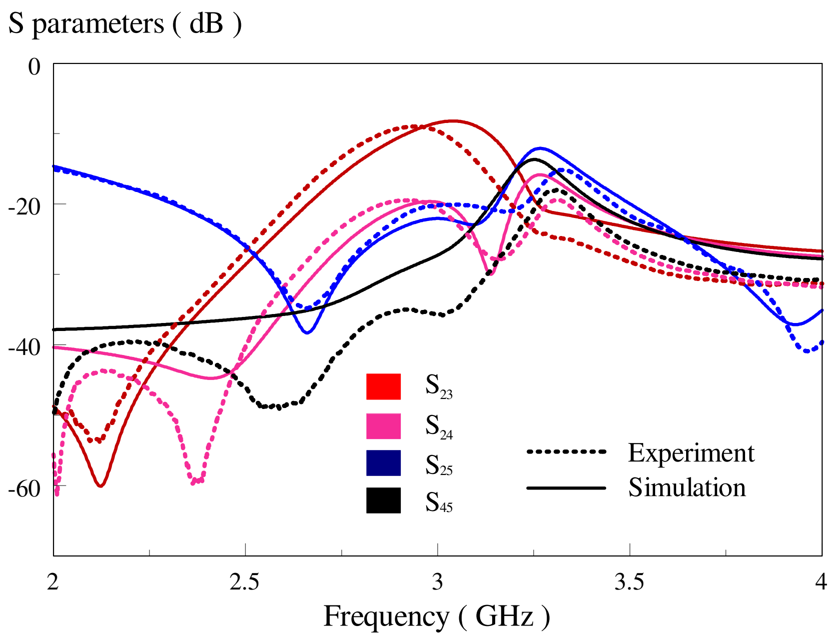

Figure 3.41: Simulated and measured isolation levels between the output ports.

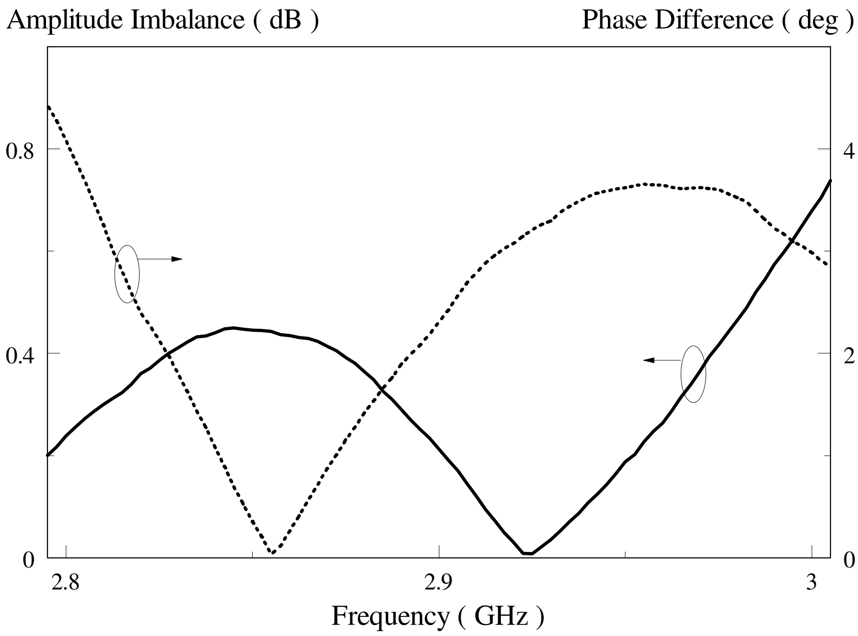

Figure 3.42: Calculated amplitude imbalance and phase difference.

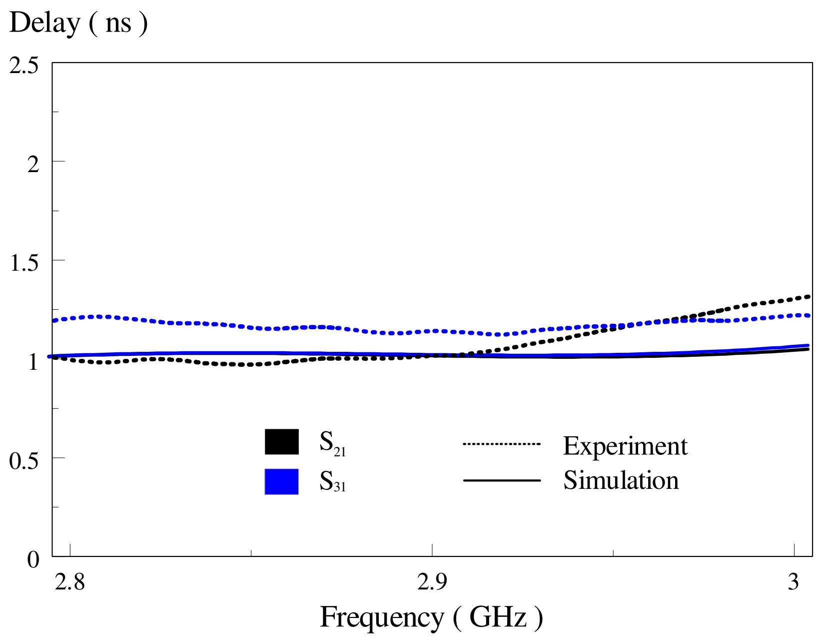

Figure 3.43: Measured and simulated group delays.

3.6 Conclusion

In this chapter, several multifunctional power-dividing couplers havebeen proposed and analyzed. First, the in-phase and out-of-phase power dividers were demonstrated in **Section 3.3.1** and **Section 3.3.2**. The two proposed power dividers are made of the same patch resonator, making them to have the same operating bandwidth. Then, the in-phase one was modified by introducing two additional coupled ports to form different power-dividing directional couplers, as discussed in **Section 3.4**. The multifunctional directional couplers can provide half-powered output signals as well as the 10dB or 20dB coupled signals at the same time without affecting the operating passband. The proposed patch coupler can also accommodate both the10 and 20dB coupled ports simultaneously, which has been demonstrated in **Section 3.5**. It is very encouraging to find that a single piece of resonator can now be used to generate half-powered signals as well as 10dB and 20dB output signals at the same time, making it very versatile. For all the couplers proposed in this chapter, it has been found that the coupling level of a certain output feedline can be tuned by adjusting the feeding position along the edge of the side patch. All the measurement and simulation results show reasonable agreement.

CHAPTER 4

STEPPED-IMPEDANCE SLOTLINE POWER DIVIDERS

4.1 Introduction

Microstrip slotline was first proposed in the 1960s (S. B. Cohn; 1968). It is an alternative to transmission line where a narrow slot or gap is etched on the conductive layer made on dielectric. Later, (S. B. Cohn; 1969) showed that high-permittivity substrate can be used to minimize radiation in the slotline. In this case, the wavelength of the slot mode is much smaller than that for free space, making fields closely confined around the slot. The characteristics of the microstrip slotline were analyzed in (E. A. Mariani, C. P. Heinzman, et al., 1969).

Microstrip slotline has been widely introduced to make microwave components such as antennas (G. Elazar, M. Kisliuk, 1988; H. Iwasaki, K. Kawabata, 1990; K. Itoh, M. Yamamoto; 1997) and couplers (T. N. Tanaka, K. Tsunoda, et al., 1988; C. H. Ho, L. Fan, et al., 1993). In (N. Behdad, K. Sarabandi, 2005), it was found that the a second resonance can be excited by feeding a high-impedance stubline near to the slot edge, combining with the fundamental slot mode to provide broad bandwidth. The slotline with stepped-impedance shape was proposed in (X. D. Huang, C. H. Cheng, et al., 2012) to excite four resonant modes, aiming at achieving ultra-wideband operation. Over the past few years, many analytical methods have been presented to study the characteristics of the slotline antenna. A new and wideband transmission line model (J. E. Ruyle, J. T. Bernhard,

2011) can be established by using an improved approximation of the voltage, conductance, and inductance in the slot resonator. This model is able to calculate the input impedance of the slotline accurately at the higher-order modes. Coupled slotlines were first introduced by (M. Aikawa, H. Ogawa, 1980) for designing magic T, where the authors made use of the two orthogonal modes (odd and even) of this structure to design 180^o hybrid. It was recently found that slotline resonator can also be incorporated with substrate-integrated waveguide (Y. J. Cheng, W. Hong, et al., 2011) for improving its Q factor.

Multifunctional components have been of great recent interest because of their various advantages such as providing compact size and low cost. A myriad of multiple functions have been explored for various couplers. It was shown that a wideband 180^o hybrid, which is able to give in-phase (sigma) and out-of-phase (delta) wideband outputs the same time, can be designed by using the microstrip-slot technology (M. E. Bialkowski, A. M. Abbosh,2007; M. E. Bialkowski, Y. Wang, 2010; M. E. Bialkowski, Y. Wang, 2011). A new 180^o hybrid coupler with dual-bandpass filtering response is proposed in (L. Wu, B. Xia, et al., 2013) by using four properly designed shorted-stub loaded stepped-impedance resonators, which are magnetically or electrically coupled among one another.

In this chapter, two passive power dividers with in-phase and out-of-phase operations have been proposed and investigated. These outputs can be obtained by tapping out signals at different places along the edge of the slotline resonator. Both of them can give two resonance modes, very desirable for wideband performance. Later, the slotline resonator is incorporated with the RF PIN diodes for the design of a multifunctional and reconfigurable power divider. In this case, by switching ON/OFF the diode, the slotline coupler can produce either an in-phase or out-of-phase output. All the proposed power dividers are designed with a stepped-impedance slotline resonator.

Ansoft HFSS is used for conducting all the simulations throughout this research project. Experimental results are measured by using the R&S®ZVB8 Vector Network Analyzer (VNA). In experiment, all the unused ports were terminated by 50Ω loads. The substrate has a dielectric constant of $\varepsilon_r = 3.38$ and a thickness of $h = 1.524$ mm. In this chapter, the frequency responses, parametric analysis, as well as the detailed studies will be performed on the proposed passive in-phase and out-of-phase power dividers and the reconfigurable power divider.

4.2 Design Methodology

The design methodology will be discussed in this section. Figure 4.1(a) shows the configuration of a stepped-impedance slot, which is a simplified version of that in Figure 4.3. It is designed by removing *Slotlines* 2 and 3 along with their feeding ports. Other parameters are given by: $L = 24$ mm, $d = 0.6$ mm, $l_1 = 12$ mm, $l_2 = 15.5$ mm, $a_1 = 9$ mm, and $a_2 = 9.5$ mm. It consists of a hook-shaped microstrip feedline located on the top surface of a grounded substrate along with a stepped-impedance slotline etched on the ground on the reverse. This is done so that the two resonances can be visualized and understood clearer with the use of this simple structure. The corresponding S parameters are shown in Figure 4.1(b) for different W.

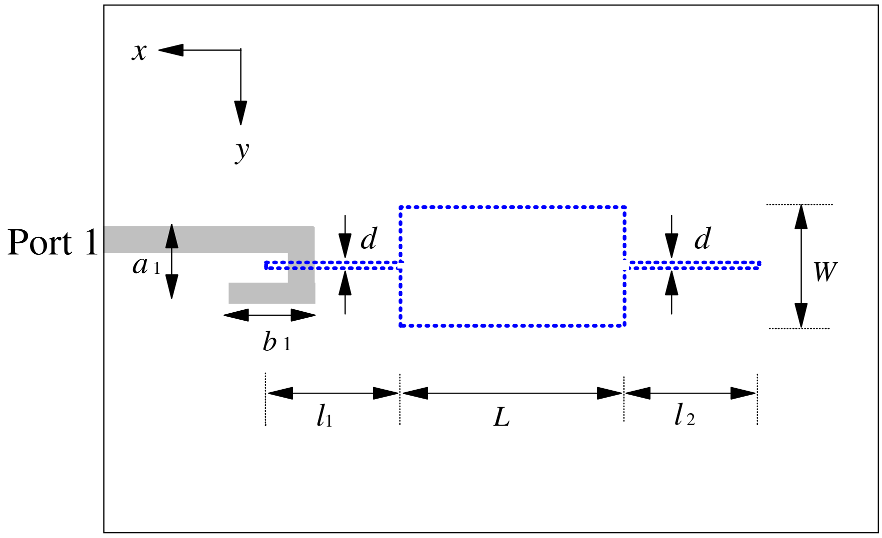

(a)

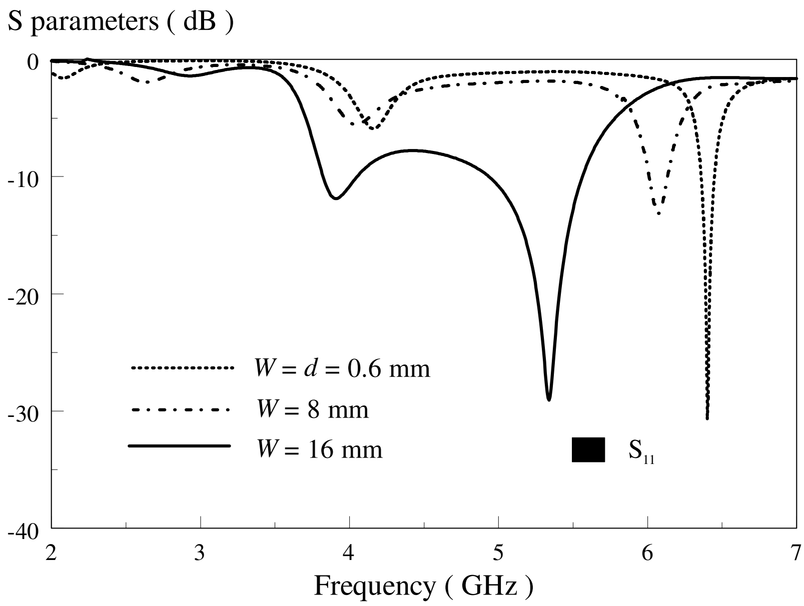

(b)

Figure 4.1: (a) The configuration of the stepped-impedance slot with a hook-shaped feedline, (b) Simulated S parameters of the configuration in Figure 4.1(a) with different width values.

For the case $W = d = 0.6$ mm, two resonances are observed at 4.16 GHz and 6.4 GHz. With W increasing from 0.6 to 16 mm, the second resonance reduces down to 5.35GHz. The same is also observed for the first mode, but with a lesser decrement. Figure 4.2 shows the electric field distribution on the slotline. Regardless of W, it is observed that similar electric field distributions are seen in the first mode. Similar phenomenon is found in the second. The first resonating mode has one null point at the center rolling with two complete cycles of standing waves. This is a higher-order mode. Its resonant frequency can be calculated by using eqn (4.1).Two nulls(or three complete standing waves) are observed along the slotline for second resonance mode, showing that it is a higher-order mode which can be calculated using eqn (4.2).

$$f = \frac{c}{\lambda_o} \tag{4.1}$$

$$f = 1.5\frac{c}{\lambda_o} \tag{4.2}$$

Where c is speed of light, $\lambda_g = \frac{\lambda_0}{\sqrt{\varepsilon_{reff}}}$, and $\varepsilon_{reff} = \frac{\varepsilon_r+1}{2}$. From the equations, the calculated resonant frequencies are 3.93 GHz and 5.9 GHz, which are pretty close to the simulated ones (4.16 GHz and 6.4 GHz).

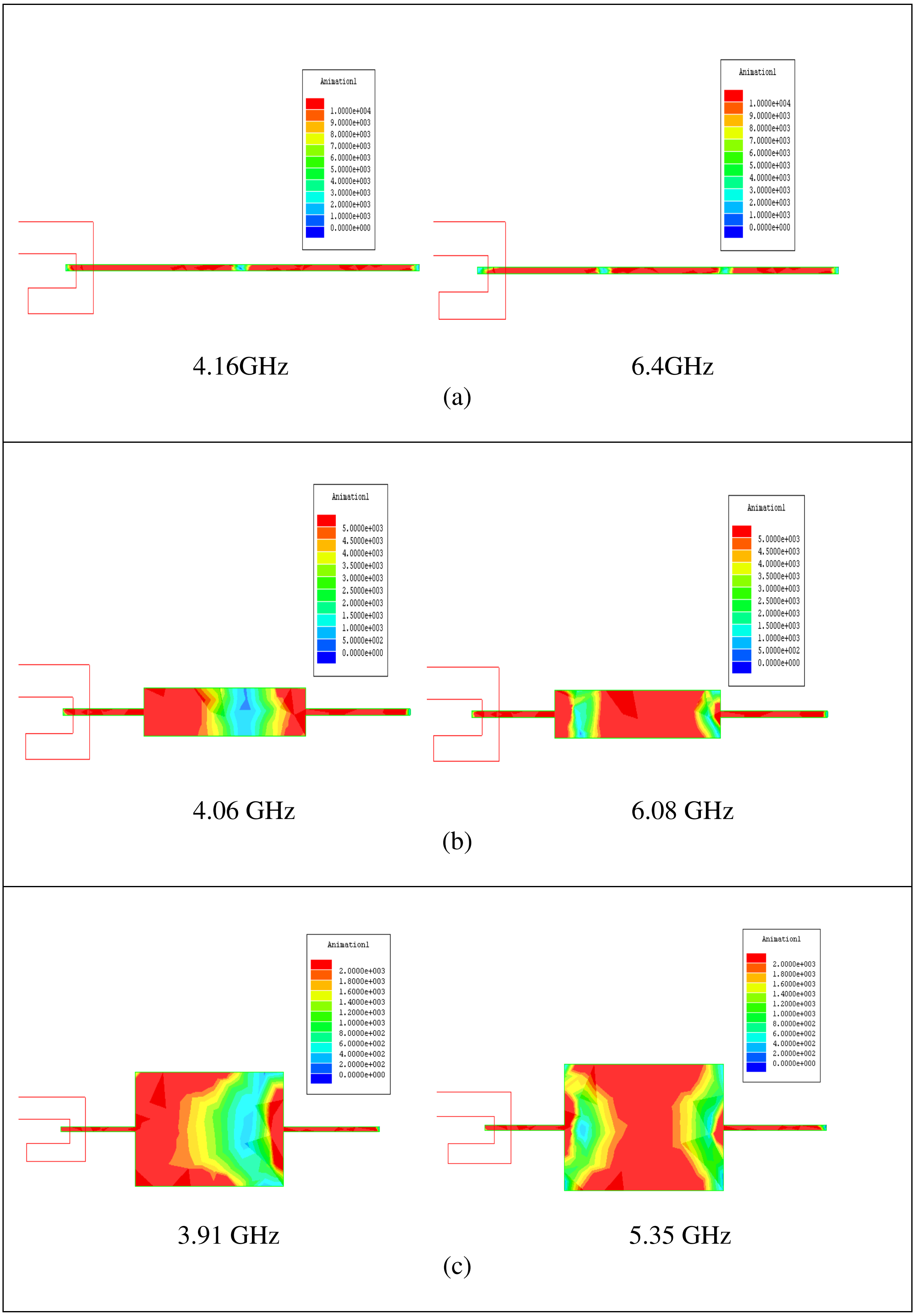

Figure 4.2: The electric field distributions for different W values at the two modes, (a) 0.6 mm, (b) 8 mm, and (c) 16 mm.

4.3 In-phase Power Divider

4.3.1 Configuration

Figure 4.3 shows the top-view schematic of the proposed in-phase power divider. It consists of three hook-shaped microstrip feedlines on one surface of substrate as well as a rectangular slot on the other. The signal coming from the *Slotline* 1 (*Port* 1) excites the slot resonator, and it is later split into two output slotlines (*Port* 2 and *Port* 3). The additional *Slotline* 4 is introduced to the right-hand side of the rectangular slot resonator for tuning impedance matching. All of the microstrip feedlines are designed with a characteristic impedance of 50Ω. Other parameters are given by: W_1 = 16 mm, L_1 = 24 mm, a_1 = 9 mm, a_2 = a_3 = 10 mm, b_1 = 0.6 mm, b_2 = b_3 = 0.7 mm, b_4 = 0.9 mm, c_1 = 7.7 mm, c_2 = 18.05 mm, c_3 = 15.35 mm, c_4 = 8.45 mm, d_1 = 12 mm, d_2 = d_3 = 14.2 mm, d_4 = 15.5 mm, l_1 = l_3= 9.5 mm, and l_2 = 9 mm. Figure 4.4(a) and (b) show the top- and bottom-view photographs of the fabricated prototype.

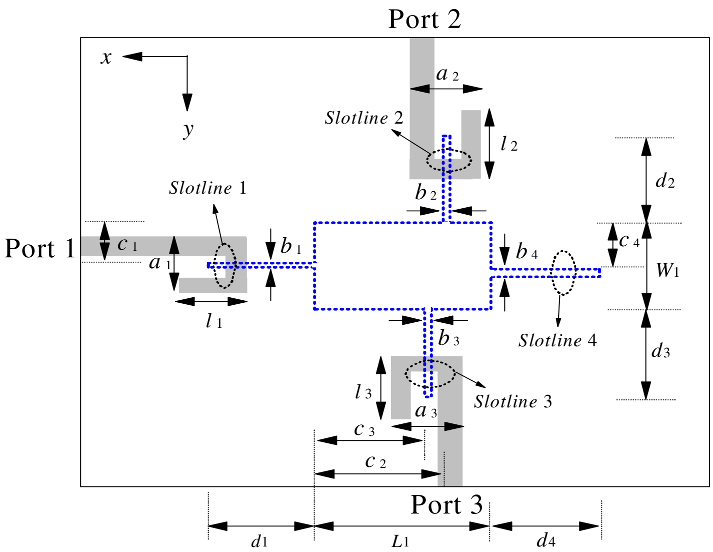

Figure 4.3: Top-view schematic of the proposed in-phase power divider.

(a) (b)

Figure 4.4: Prototype of the proposed in-phase power divider, (a) Top View, (b) Bottom View.

4.3.2 Simulation and Experiment Results

The simulated and measured S parameters are depicted in Figure 4.5(a). The proposed structure has a measured passband of 3.74 GHz- 5.06 GHz (simulation: 3.84 GHz - 5.41 GHz) with a fractional bandwidth (FBW) of 30.11% (simulation: 34.04%). The measured and simulated center frequencies are 4.4 and 4.62 GHz, respectively, with an error of 5.04%.In this case, the measured insertion loss is in the range of 5.6 – 6.2 dB (simulation: 5.2 – 6.1 dB). Higher loss is due to the residual radiation of the microstrip-to-slot transitions (M. E. Bialkowski, Y. Wang; 2010). The insertion loss can be improved by placing the component in a metallic cavity to reduce radiation. Figure 4.5(b) shows the measured and simulated coupling levels between the two output ports, achieving an isolation of less than -10 dB across the passband. Also here, the amplitude imbalance (±0.3 dB) and phase difference (±5^{o}) are calculated from the measured output signals of the proposed structure, as shown in Figure 4.6. The simulated and measured group delays are shown in Figure 4.7. A nearly constant delay (~ 0.8 ns) is observed across the passband.

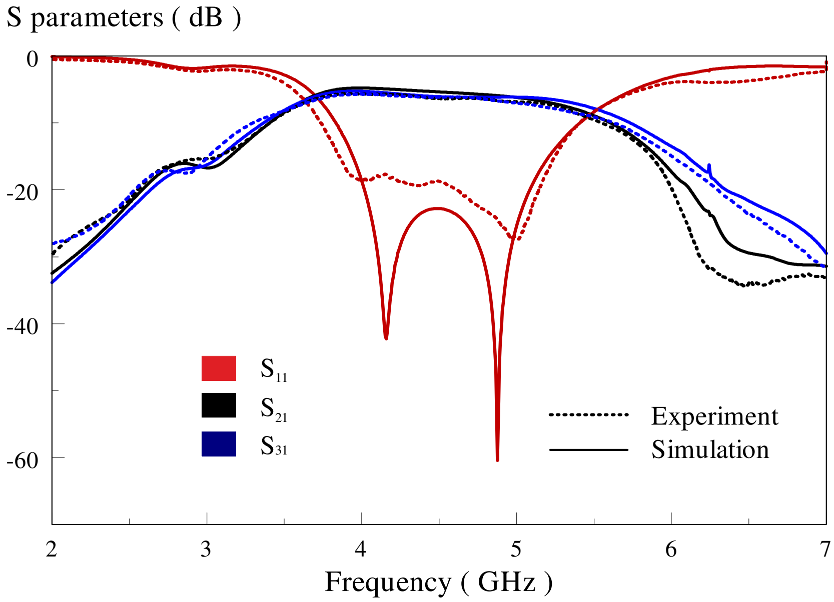

(a)

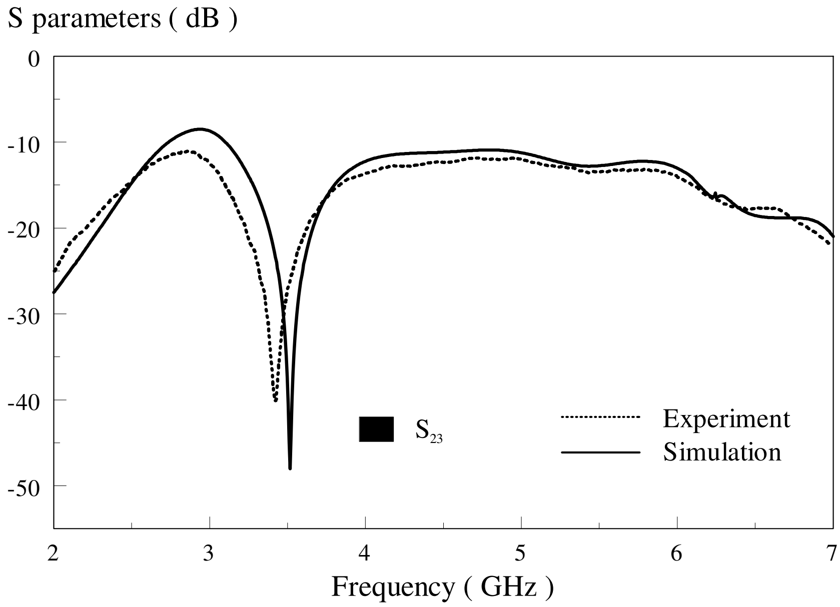

(b)

Figure 4.5: Simulated and measured (a) reflection and transmission coefficients, and (b) isolation level between the output ports.

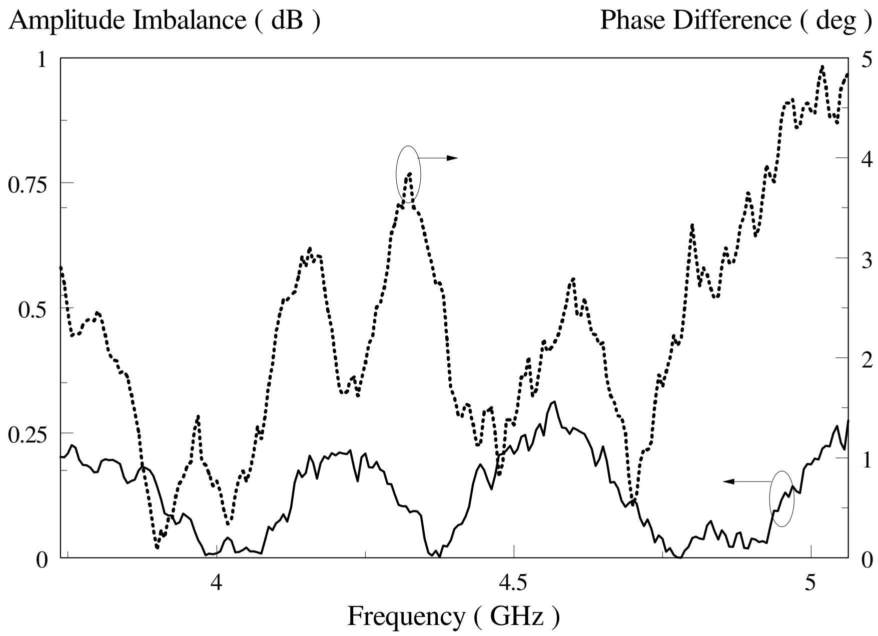

Figure 4.6: Calculated amplitude imbalance and phase difference.

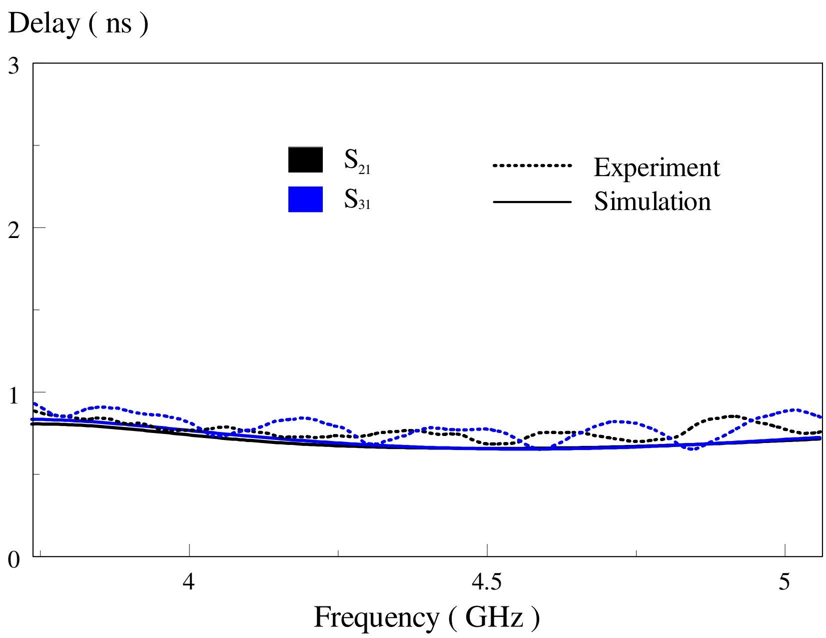

Figure 4.7: Simulated and measured group delays.

4.3.3 Theoretical and Parametric Studies

In this section, electric field distributions will be discussed for the in-phase power divider. Figure 4.8 depicts the electric field distributions in the slot at the two poles (4.16 and 4.88 GHz). For both of the first and second resonance modes, it can be observed that the electric field patterns are similar to those for the stepped-impedance slot in Figure 4.2(c), showing that identical physical resonances have also been excited for the proposed power divider. The inclusion of the output slotlines (*Ports* 2 and 3) are causing the resonant frequencies of the first and second resonance modes to move closer. *Slotline* 4 is made offset for a better impedance matching. To understand the proposed power divider better, all the parameters are varied to study their effects.

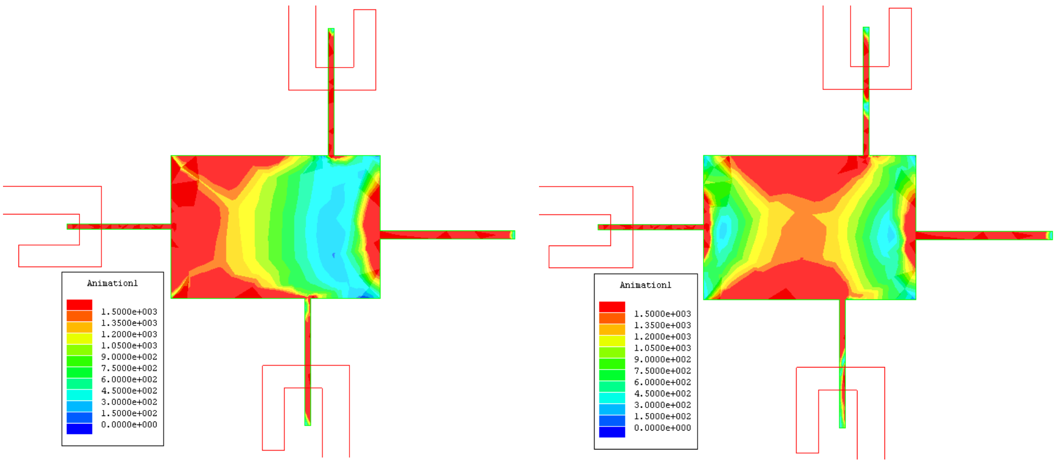

(a) (b)

Figure 4.8: The electric field distributions of the proposed in-phase power divider at (a) the first pole at 4.16 GHz, (b) the second pole at 4.88 GHz.

4.3.3.1 Slot Length L_1

The slot length L_1 is now studied. Figure 4.9 illustrates the simulated S parameters with respect to the change of L_1. With reference to the figure, the coupling and matching levels are greatly affected. When L_1 is decreased to 22 mm, the two resonance modes shift to lower frequencies (4.16 GHz →4.03 GHz and 4.88 GHz → 4.75 GHz). Frequency shifts when L_1 is increased to 26 mm, showing resonances at 4.34 GHz and 5.0 GHz. It is found that the optimal $L_1$is able to give the best reflection coefficient (S_{11}), giving a matching level of below -20dB across the operating frequency band.

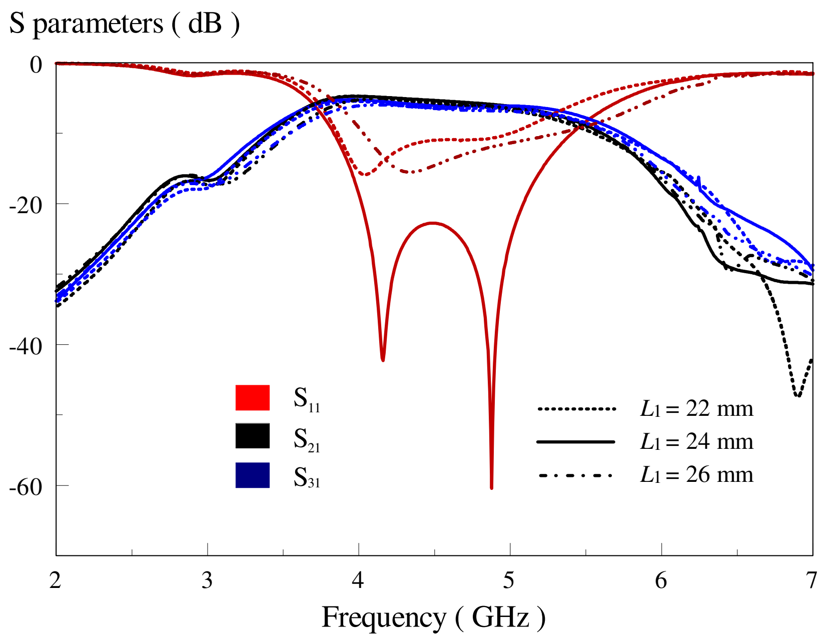

Figure 4.9: Effects of the slot length L_1 on the S parameters.

4.3.3.2 Slot Width W_1

The simulated S parameters are shown in Figure 4.10 with respect to changing W_1. It can be observed that the resonating modes shift when W_1 is varied. When altered from 16 mm to 11 mm, the second mode shifts from 4.88 GHz to 5.3 GHz while the first mode remains at 4.16 GHz. Both of the resonances are found to shift lower (4.16 GHz → 4.05 GHz and 4.88 GHz → 4.52 GHz) when W_1 is increased to 21 mm. Besides that, a flat coupling response is not achievable, which causes the amplitude imbalance between the two output ports to be greater than 1 dB.

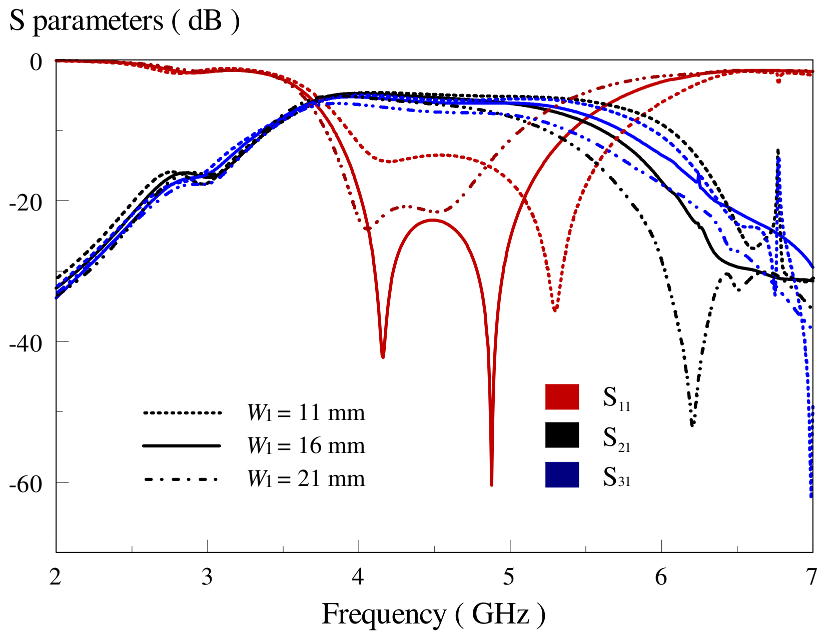

Figure 4.10: Effect of the slot width W_1 on the S parameters.

4.3.3.3 Slotline Length d_1

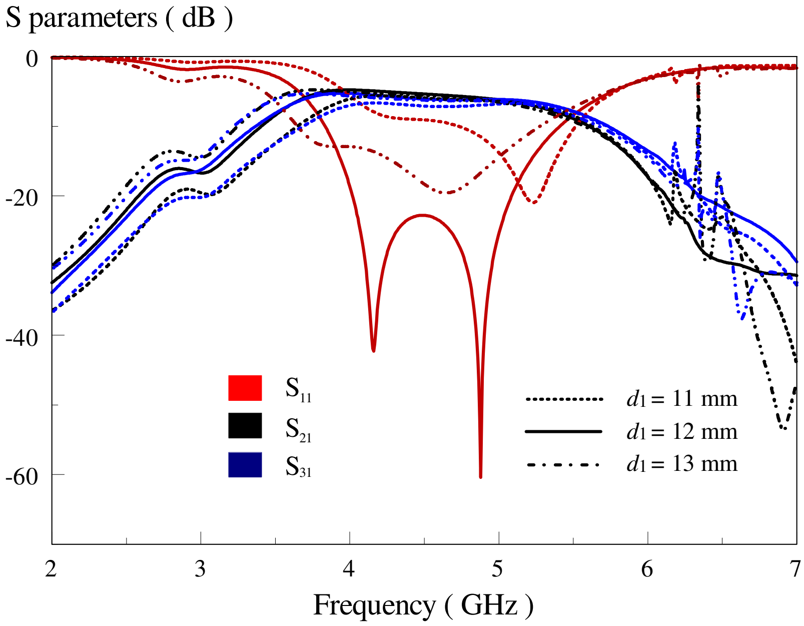

Figure 4.11: Effect of the slotline length d_1 on the S parameters.

With reference to Figure 4.11, the optimal length of slotline 1 is 12mm. For others, both the matching and coupling level deteriorate. Furthermore, the poles are also greatly affected, which can be seen from the displacement of the first and second resonances. When d_1 is decreased to 11mm, both of the poles become higher (4.15 GHz→4.25 GHz, 4.88 GHz→5.24 GHz). They move down (4.15 GHz→3.78 GHz, 4.88 GHz→4.63 GHz) when d_1 is increased to 13mm.

4.3.3.4 Slotline Length d_4

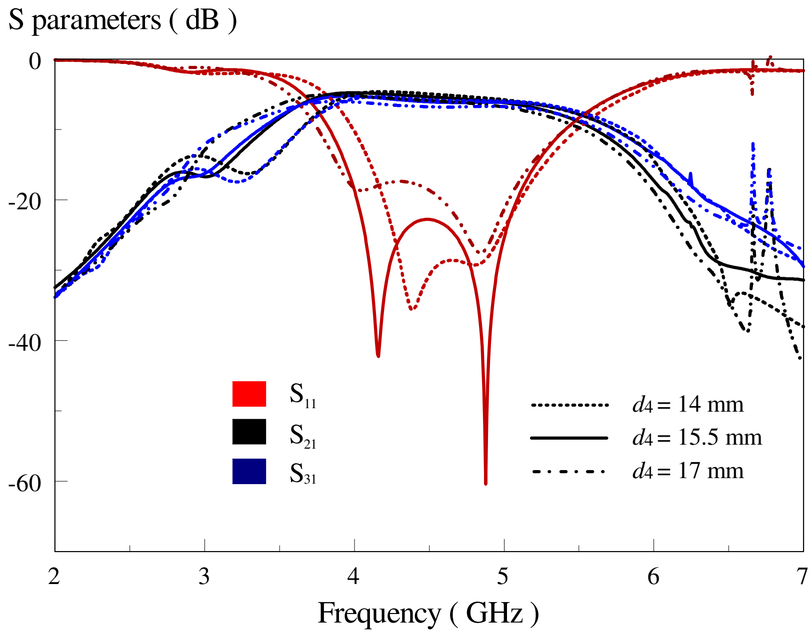

Figure 4.12: Effect of the slotline length d_4 on the S parameters.

Figure 4.12 depicts the simulated S parameters with respect to the change of d_4. It is observed that d_4 only affects the frequency of the first resonance. When d_4 is decreased to 14 mm, the first pole moves to higher frequency (4.15 GHz → 4.4 GHz). On the other hand, it becomes lower (4.15 GHz → 4.02 GHz) when d_4 is increased to 17 mm. Varying d_4 does not affect the second mode but flat coupling responses inside the passband are not obtainable for 14 mm and 17 mm.

4.3.3.5 Slotline Widths b_1 and b_4

Figure 4.13 and 4.14 illustrate the simulated S parameters with changing slotline width. With reference to both of the figures, it is observed that b_1 affects the second resonance while b_4 affects the first one. From Figure 4.13, the first mode shifts lower (4.88 GHz→4.75 GHz) when b_1 is reduced to 0.4 mm. It moves higher (4.88 GHz→5 GHz) when b_1 is equal to 0.8 mm. The first resonance remains unchanged (4.15 GHz) when b_1 is altered. Referring to Figure 4.14, the first pole shifts when b_4 is varied while the second one remains (4.88 GHz). When b_4 is decreased to 0.5 mm, the first mode shifts lower (4.15 GHz→4.08 GHz). But it goes higher (4.15 GHz→4.22 GHz) when b_4 is made 1.5 mm.

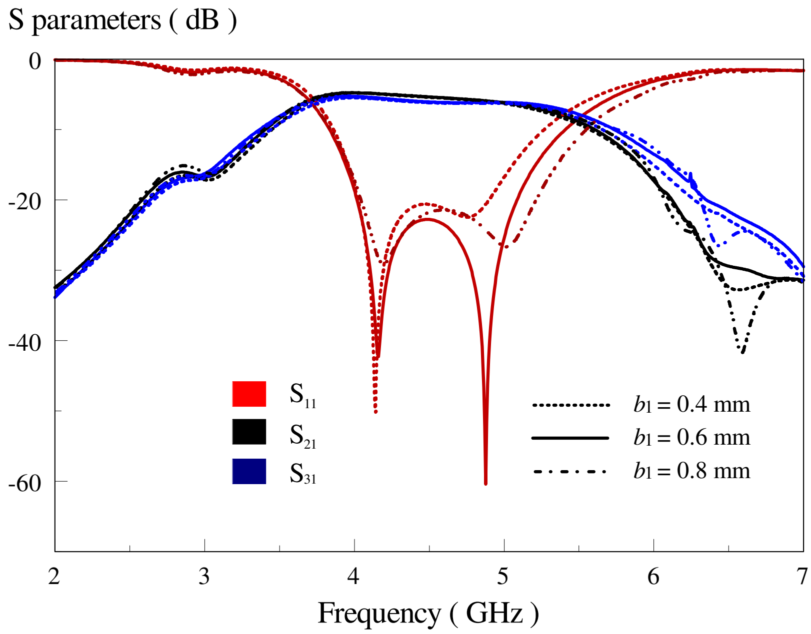

Figure 4.13: Effect of the slotline width b_1 on the S parameters.

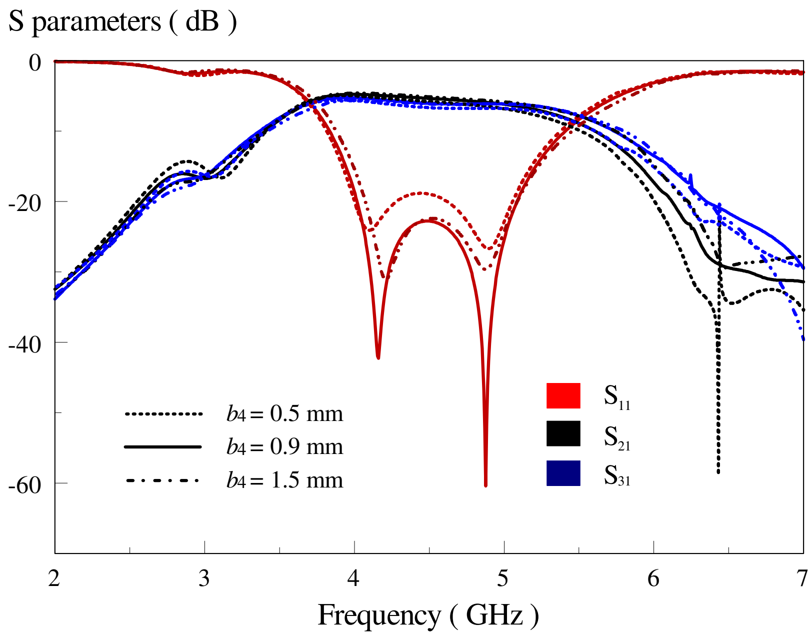

Figure 4.14: Effect of the slotline width b_4 on the S parameters.

4.3.3.6 Stripline Lengths l_2 and l_3

Referring to Figure 4.15, the stripline length l_2 does not affect the S parameters much. This is because it is not in the direction of the standing waves. Varying l_2 slightly affects the operating frequency of the second pole. When l_2 is reduced to 5.5 mm, the second pole shifts higher (4.88 GHz → 5 GHz). It shifts to 4.82 GHz for a longer length of 7.5mm. Here, the optimum value for l_2 is designed to be 6.5mm, giving the best impedance matching. Similar trend has been observed for the stripline l_3 which is shown in Figure 4.16.

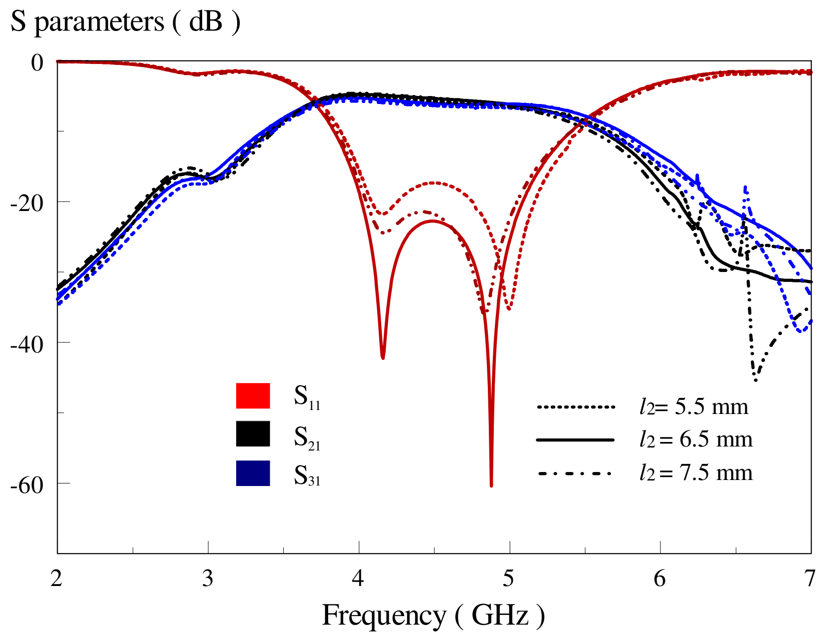

Figure 4.15: Effect of the stripline length l_2 on the S parameters.

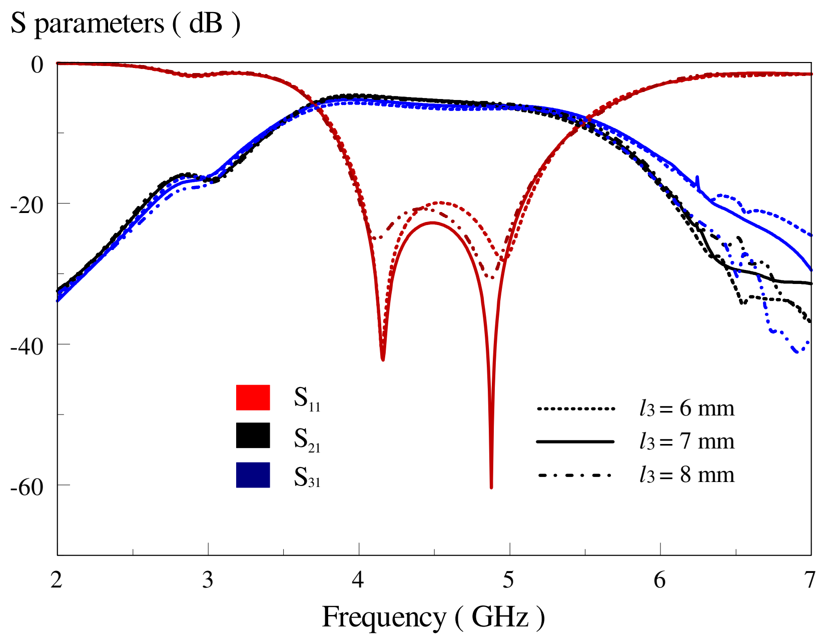

Figure 4.16: Effect of the stripline length l_3 on the S parameters.

4.4 Out-of-Phase Power Divider

4.4.1 Configuration

By changing the direction of the hook-shaped microstrip feedline at *Port* 2, the in-phase power divider can be designed to become an out-of-phase one. The proposed structure also consists of three hook-shaped microstrip lines on the top plane with a stepped-impedance slot on the ground plane, using only a single-layered substrate. Figure 4.17 shows the top view schematic of the proposed configuration. The detailed design parameters are given by: W_1 = 16 mm, L_1 = 24mm, a_1 = 9 mm, a_2 = a_3 = 10 mm, b_1 = 0.2 mm, b_2 = b_3 = 0.7 mm, b_4 = 1 mm, c_1 = 7.2 mm, c_2 = 16 mm, c_3 = 8.3 mm, d_1 = 12.3 mm, d_2 = 13.2 mm, d_3 = 13mm, d_4 = 18 mm, l_1 = l_3 = 9.5 mm, and l_2 = 10 mm. Figure 4.18(a) and (b) show the top- and bottom-view photographs of the fabricated prototype.

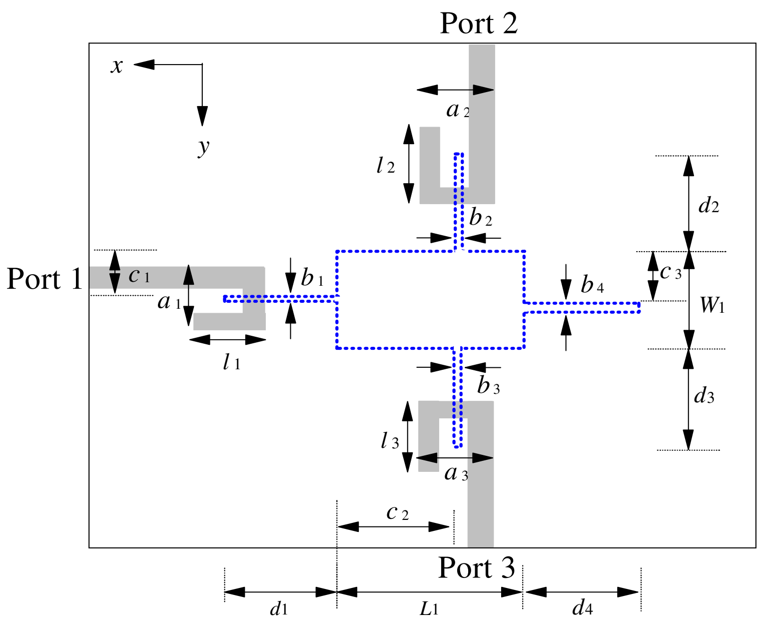

Figure 4.17: Top-view schematic of the proposed out-of-phase power divider.

(a) (b)

Figure 4.18: Prototype of the proposed out-of-phase power divider, (a) Top View, (b) Bottom View.

4.4.2 Simulation and Experiment Results

In this section, the simulation and experiment results of the out-of-phase power divider are illustrated and discussed. The simulated and measured S parameters of the proposed configuration are shown in Figure 4.19(a). It has a measured passband of 3.66 – 4.81 GHz (simulation: 3.84 – 5.0 GHz) with the center frequency of 4.23 GHz (simulation: 4.41 GHz). The measured fractional bandwidth (27.01%) is slightly larger than simulated one (26.21%), with output coupling coefficient of less than 10 dB (in experiment)as illustrated in Figure 4.19(b). Figure 4.20 shows the calculated amplitude imbalance and phase difference, which fall within ± 0.7 dB and180±3° in the passband, respectively. Reasonable agreement is observed between the measurement and simulation resultsfor the group delay in Figure 4.21. This is very positive as it shows that the same piece of resonator can be made either as an in-phase or an out-of-phase power divider. This interesting feature will be used to design the reconfigurable power divider when incorporated with the RF pin diodes, which will be discussed in **Section 4.5**.

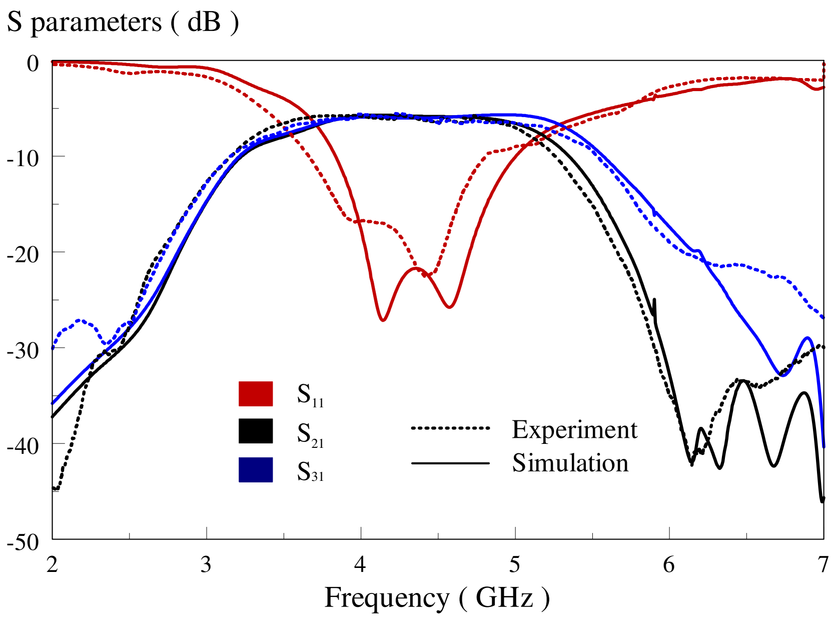

(a)

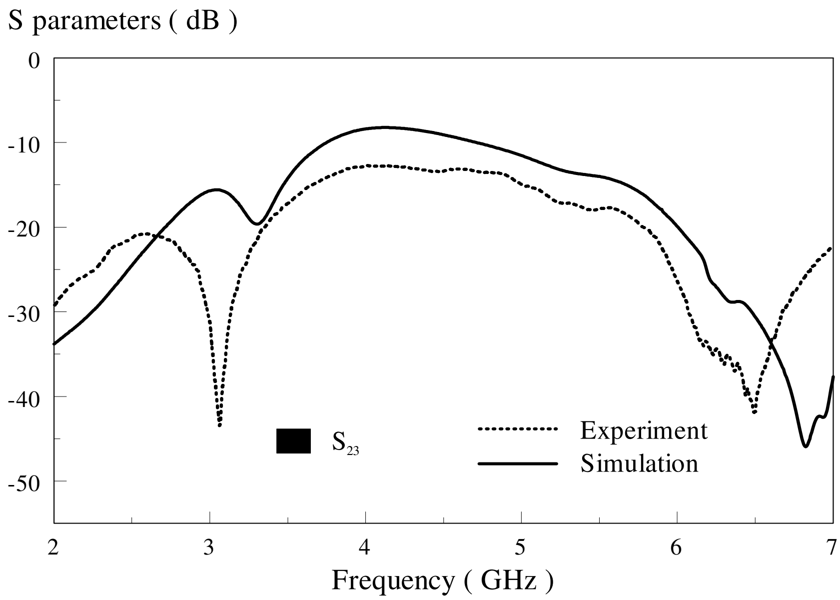

(b)

Figure 4.19: Simulated and measured (a) reflection and transmission coefficients, and (b) isolation level between the output ports.

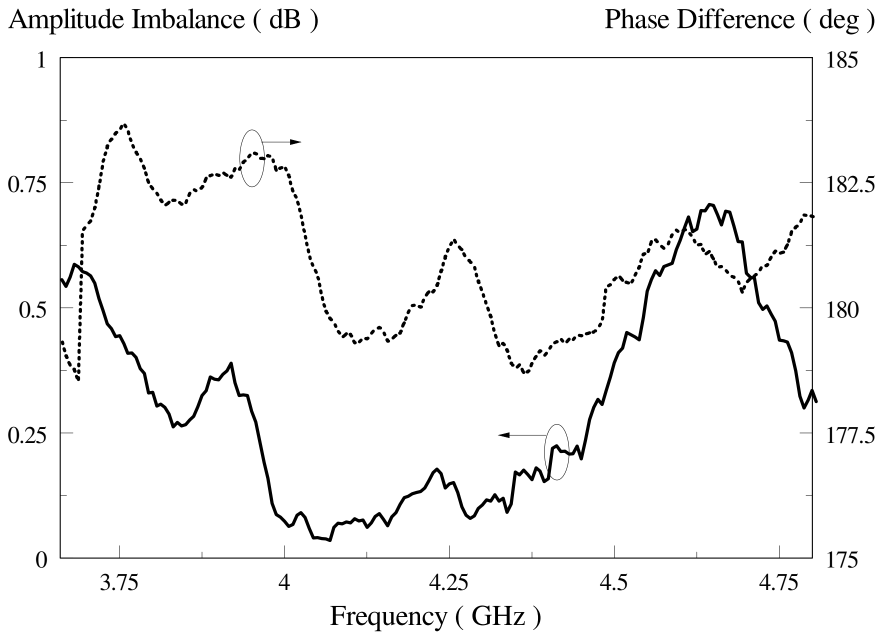

Figure 4.20: Calculated amplitude imbalance and phase difference.

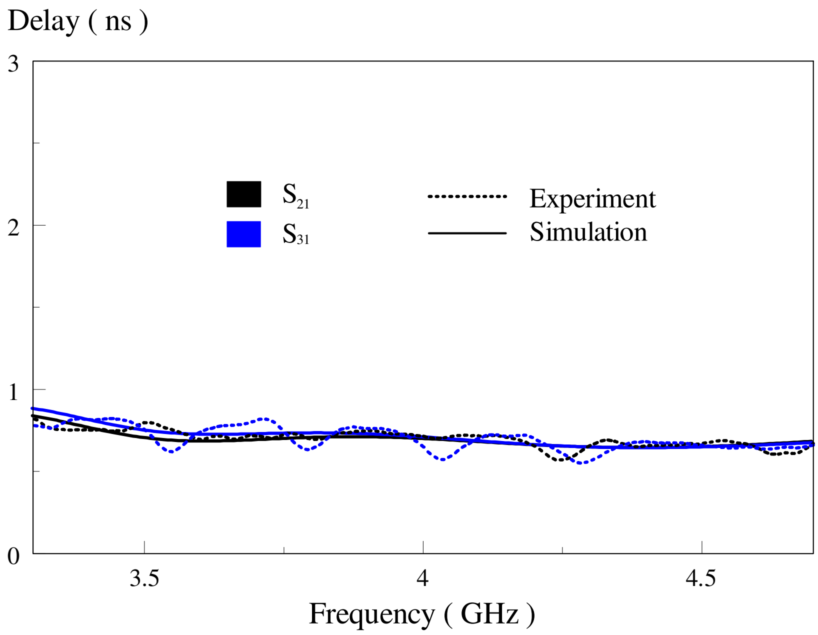

Figure 4.21: Simulated and measured group delays.

4.4.3 Theoretical and Parametric Studies

A theoretical study of the proposed out-of-phase power divider will be made in this section. Figure 4.22 illustrates the simulated electric field distributions of the stepped-impedance slot resonator at the two resonances (4.14 and 4.57 GHz). It can be observed that the electric field patterns in Figure 4.22 are similar with those in Figure 4.2(c) and 4.8 as an identical slot resonator has been used.With respect to Figure 4.22(a), one field null is observed for the first resonance (4.14 GHz), but two for the second (4.57 GHz). Again, this slotline (*Slotline*4) is positioned with a slight offset for a better impedance matching.

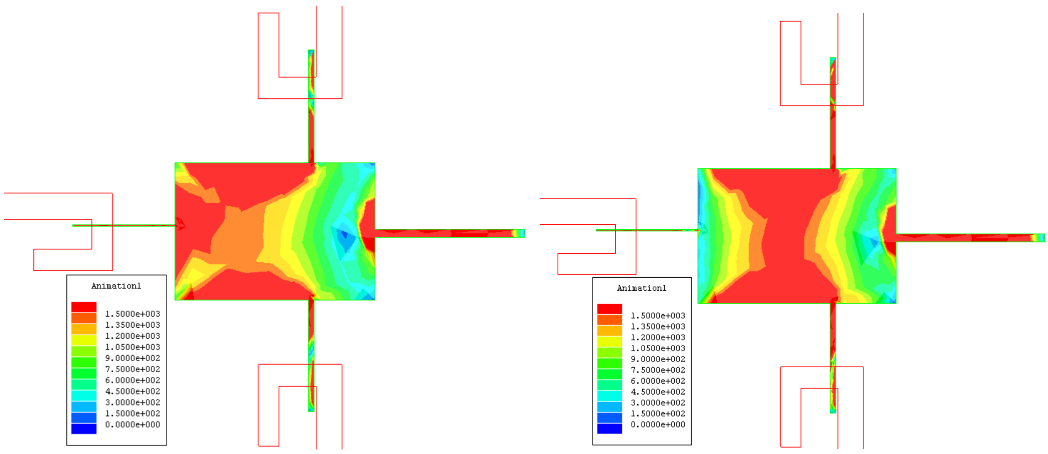

(a) (b)

Figure 4.22: The electric field distributions of the proposed out-of-phase power divider at the poles at (a) 4.14 GHz, and (b) 4.57 GHz.

4.4.3.1 Slot Length L_1

Figure 4.23 illustrates the simulated S parameters with respect to the change of the length of slotline L_1. It is observed that the matching level and operating bandwidth are greatly affected. When L_1 is increased to 26 mm, the two poles are moving closer to each other and, finally, combining at 4.32 GHz. The two resonating modes move further apart (4.14 GHz → 4.11 GHz and 4.57 GHz → 4.83 GHz) when L_1 is set to be 22 mm. Besides that, the amplitude imbalance between the two output ports fluctuates for more than 1 dB across the passband when L_1 is varied.

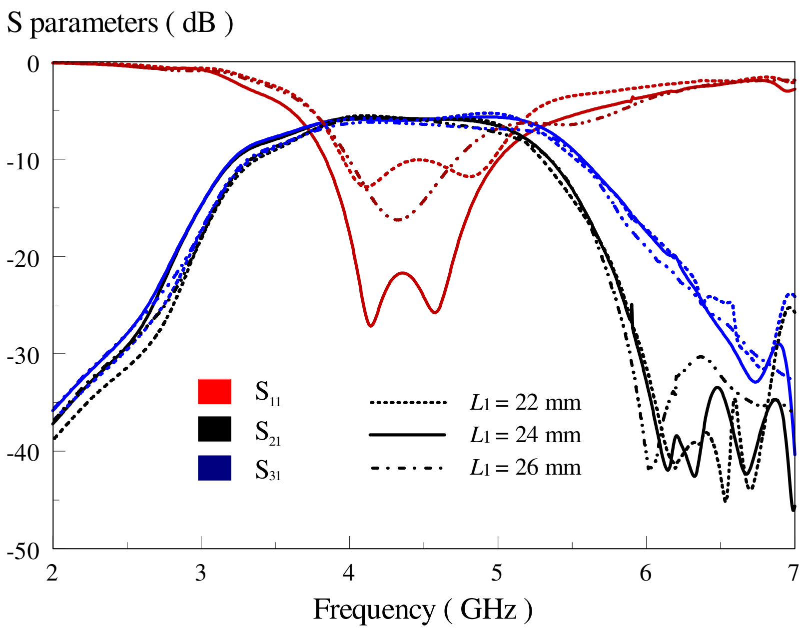

Figure 4.23: Effect of the slot length L_1 on the S parameters.

4.4.3.2 Slot Width W_1

The optimum value for W_1 is found to be 16mm. As can be seen from Figure 4.24, when W_1 is reduced to 14mm, the two poles combine into one at 4.41 GHz, narrowing the operating bandwidth. When increased to 18mm, the two poles move further apart where the first mode is shifting to a lower frequency (4.14 GHz → 3.97 GHz) while the second is moving higher (4.57 GHz → 4.64 GHz). Flat coupling response is not obtainable across the passband when W_1 is altered.

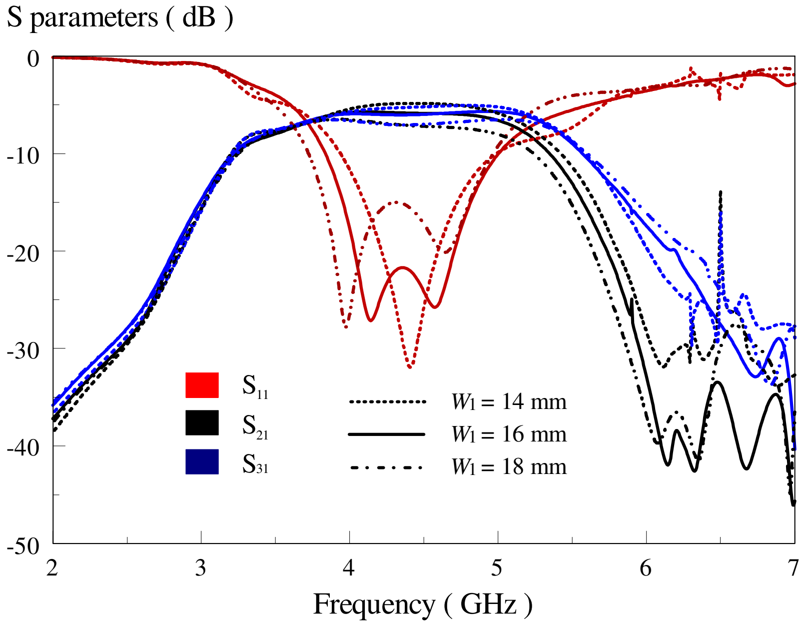

Figure 4.24: Effect of the slot width W_1 on the S parameters.

4.4.3.3 Slotline Length d_1

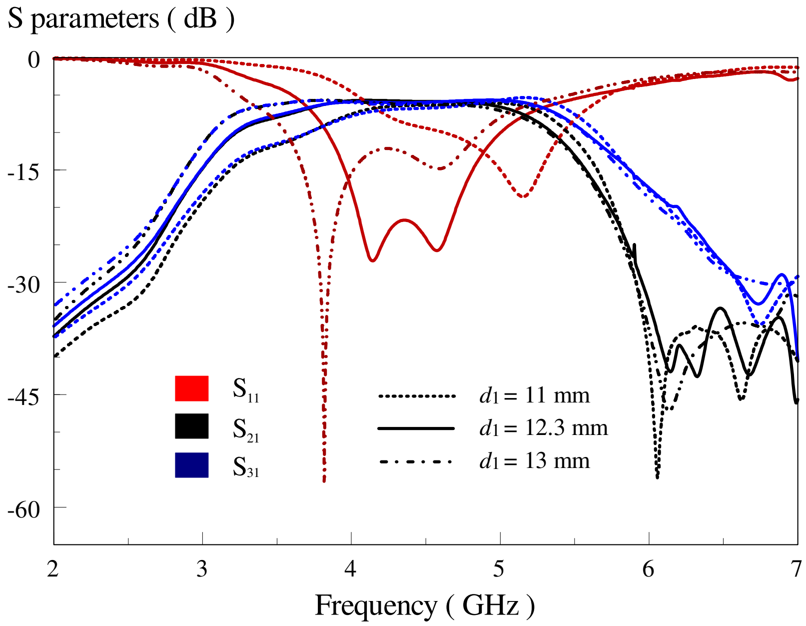

Figure 4.25: Effect of the slotline length d_1 on the S parameters.

With reference to Figure 4.25, the coupling level deteriorates when the length of *Slotline* 1 is varied. It can be observed that both of the poles are moving higher (4.41 GHz and 5.15 GHz) at the same time when d_1 is set to be 11 mm. But for 13 mm, they are in the reverse trend (3.82 GHz and 4.55 GHz).

4.4.3.4 Slotline Length d_4

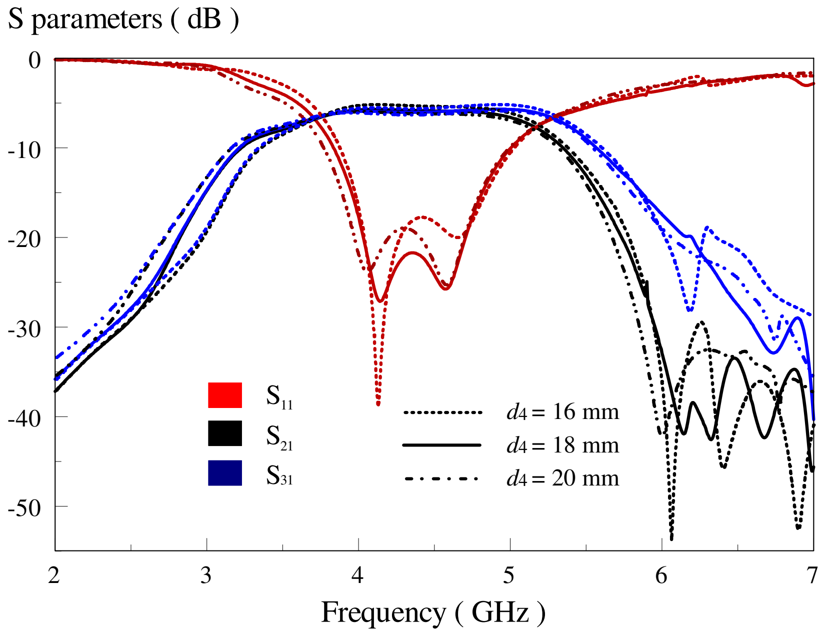

Figure 4.26: Effect of the slotline length d_4 on the S parameters.

The slotline length d_4 is now studied. With reference to Figure 4.26, when d_4 is decreased to 16 mm, the second resonance becomes slightly higher (4.57 GHz→4.66 GHz) while the first one remains unchanged (4.14 GHz). The first pole moves slightly lower (4.14 GHz→4.06 GHz) but the second remains at 4.57 GHz when d_4 is increased to 20 mm. A slotline length of 18 mm gives the best reflection coefficient (S_{11}) which is below -20 dB across the passband.

4.4.3.5 Stripline Lengths l_2 and l_3

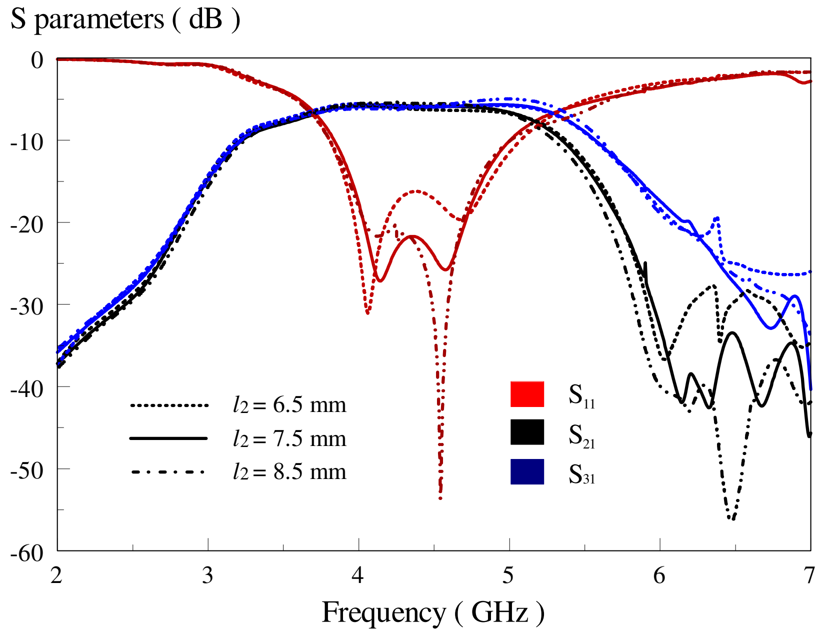

Figure 4.27: Effect of the stripline length l_2 on the S parameters.

With reference to Figure 4.27, the S parameters are not affected much when the stripline length l_2 is altered. When the l_2 value changes, the frequencies of the poles are also varied. At l_2 = 6.5 mm, the first pole shifts to a lower frequency (4.13 GHz→4.05 GHz) while the second one moves higher (4.57 GHz→4.67 GHz). It does not affect the poles significantly when l_2 is increased to 8.5mm. Similar trend is also observed for the stripline l_3, which is shown in Figure 4.28.

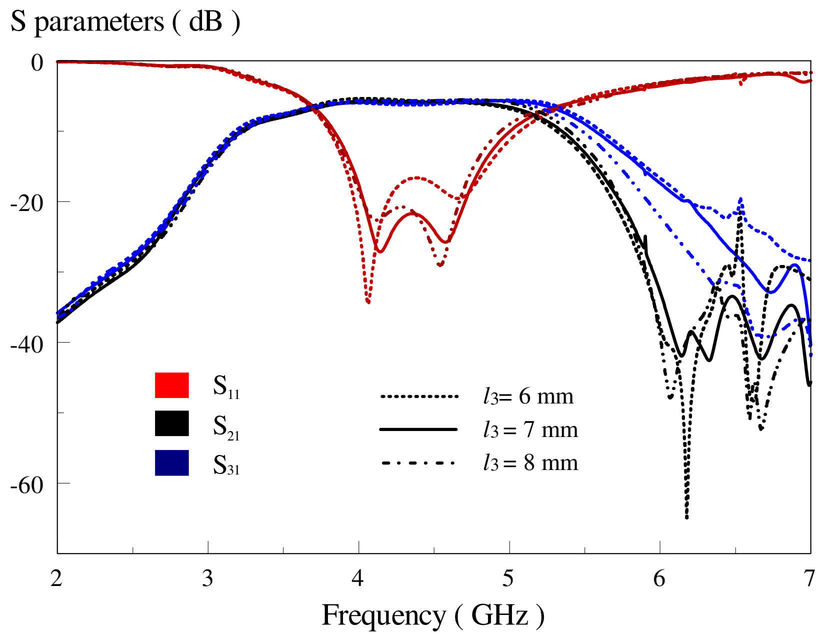

Figure 4.28: Effect of the stripline length l_3 on the S parameters.

4.5 Reconfigurable Power Divider

4.5.1 Configuration

In this section, the previously discussed in-phase and out-of-phase power dividers are combined to form a new multifunctional device that can provide both output phases in one, leading to cost saving. The schematic of the proposed configuration is shown in Figure 4.29. In this new design, each output port is incorporated with the BAR50-02V RF PIN diodes, manufactured by Infineon Technologies. When the RF diode is reverse-biased, it can be used to block the RF signal because of its low capacitance, for a better isolation. A RF diode is a good conductor when it is forward-biased and let the RF signal to pass through. The BAR50-02V RF PIN diode is chosen because of its good performance at high frequency. In this project, two RF PIN diodes are used for each output port in order to achieve isolation level of better than -20dB when it is in the OFF state (reverse-biased).

The detailed design parameters are given by: W_1 = 16 mm, L_1 = 24 mm, a_1 = 9 mm, a_2 = a_3 = 11.5mm, b_1 = 0.2 mm, b_2 = b_3 = 0.7 mm, b_4 = 1 mm, c_1 = 7.9 mm, c_2 = 16.5 mm, c_3 = 9 mm, d_1 = 12.3 mm, d_2 = 12 mm, d_3 = 12 mm, d_4 = 16 mm, l_1 = 9.5 mm, l_2 = 10 mm, and l_3 = 9 mm. The prototype of the proposed structure is shown in Figure 4.30.

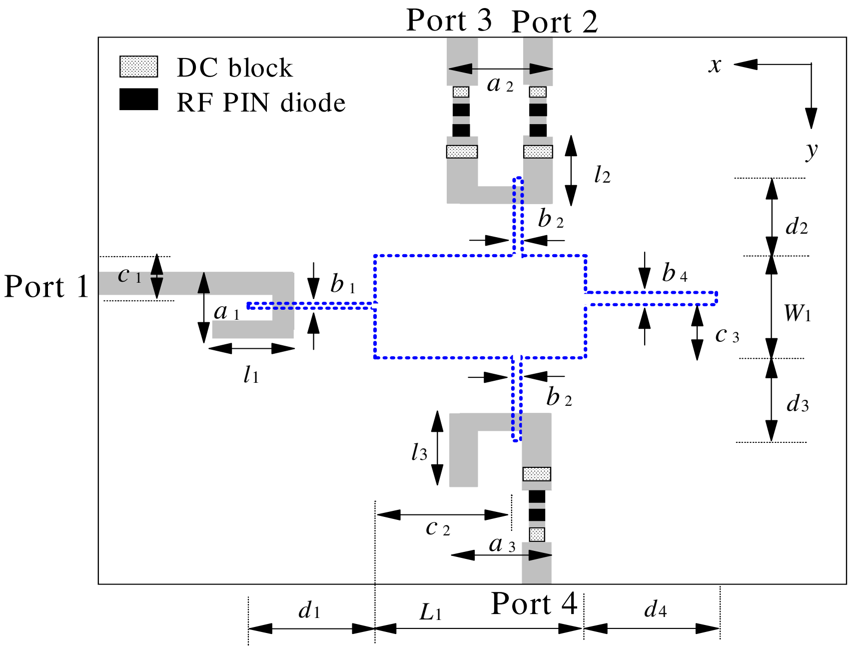

Figure 4.29: Schematic of the proposed reconfigurable power divider.

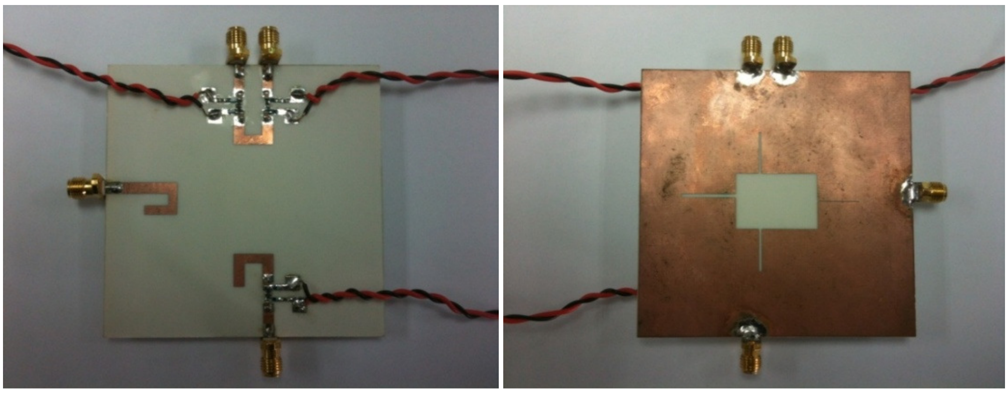

(a) (b)

Figure 4.30: Prototype of the proposed reconfigurable power divider, (a) Top View, (b) Bottom View.

4.5.2 Biasing Circuitry for RF PIN Diode

Figure 4.31 illustrates the biasing circuitry of the RF PIN diode. As can be seen from the figure, the RF and DC signal paths are highlighted with red and blue colors, respectively. In order to switch to ON state (forward-biased), the diodes are biased with a voltage drop of 2 V. The RF choke (inductor) in the biasing circuitry is used to avoid leakage of microwave signal to the DC path while the DC block (capacitor) is used to prevent the DC signal from flowing into the proposed configuration.

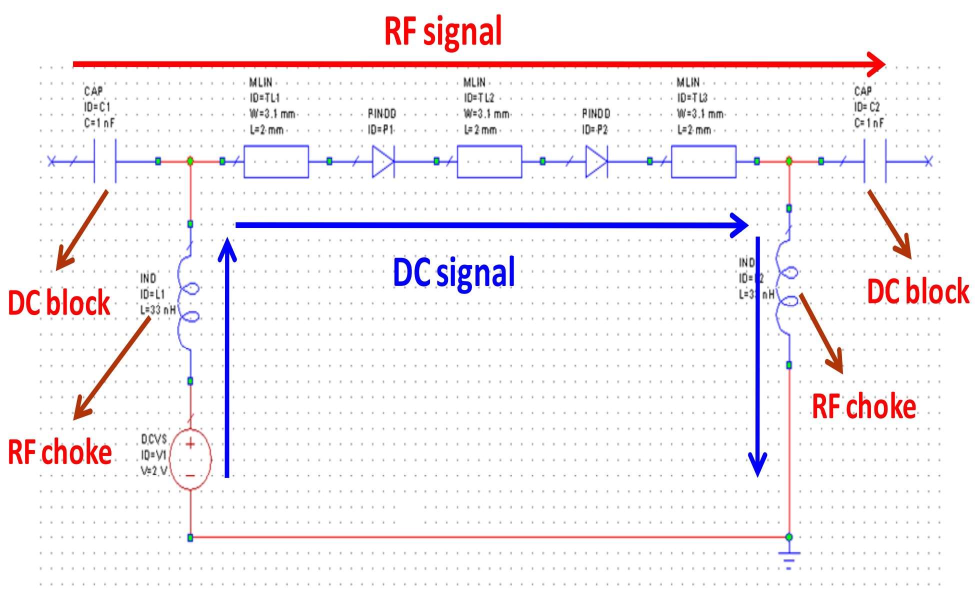

Figure 4.31: Biasing Circuitry for the RF PIN Diode.

Referring to the datasheet, for each RF diode, the insertion loss is approximately 0.3 dB, giving a 10mA forward current at 4 GHz. In OFF state (reverse-biased), each diode is able to provide an isolation level of about -14 dB at 4 GHz. Placing the two diodes at each output port improves the isolation level to be greater than -14 dB, avoiding microwave signals from reaching the unused ports more effectively.

4.5.3 Simulation and Experimental Results

The proposed structure is first configured into the in-phase mode. By reverse-biasing (OFF) the diodes, *Port* 2 can be easily disconnected. *Port* 3 and *Port* 4 are set at ON state by forward-biasing the diodes. Figure 4.32 shows the simulated and measured S parameters. The measured passband is 3.61 – 4.36 GHz (simulation: 3.67 – 4.78 GHz) with a FBW of 19% (simulation:26%). It can be seen from the figure that the measured and simulated center frequencies are 3.98 GHz and 4.23 GHz, respectively, showing reasonable agreement with an error of 6.28%. This result is acceptable for the active case. With the two diodes, the isolated level ($|S_{21}|$) is managed well below -25dB across the entire passband. This proves that the BAR50-02V pin diode can give excellent isolation in the OFF state (reverse-biased). With reference to Figure 4.33, it is observed that the amplitude imbalance and phase difference between the two output ports (*Port* 3 and *Port* 4) fall within ≤ 0.6 dB and ± 4.8°, respectively, both of which are calculated from measurements.

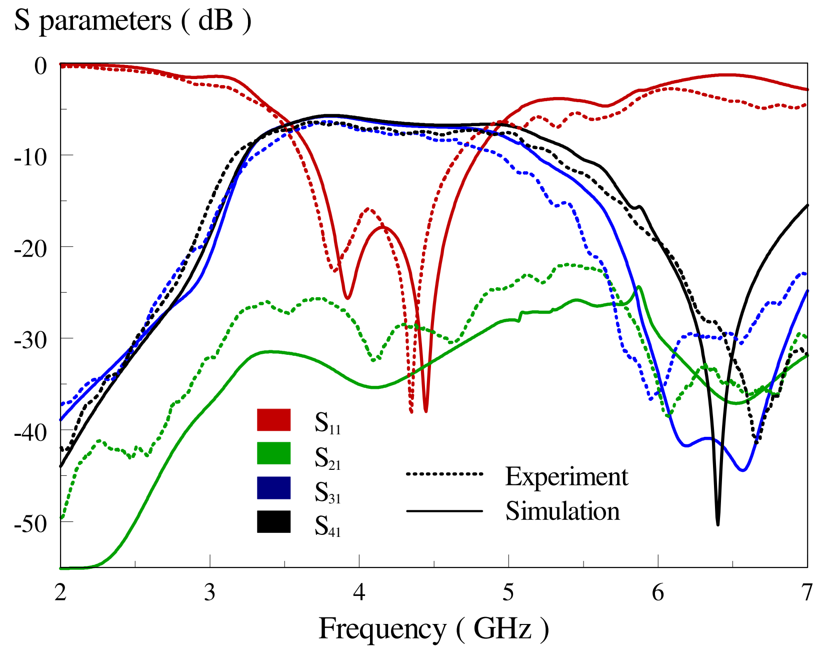

Figure 4.32: Simulated and measured S parameters of the reconfigurable in-phase power divider (with *Port* 2 OFF but others ON).

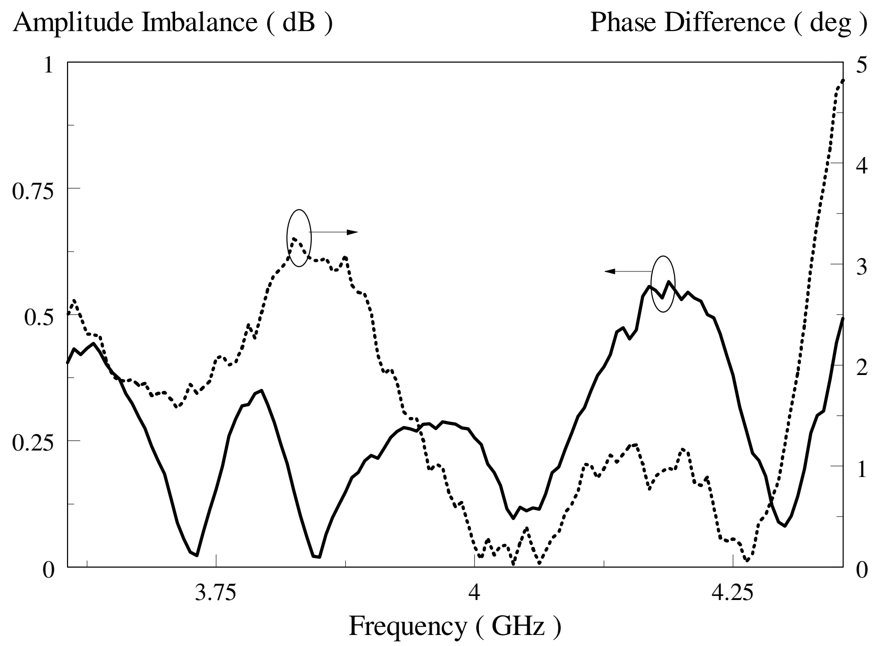

Figure 4.33: Calculated amplitude imbalance and phase difference of the reconfigurable in-phase power divider (with *Port* 2 OFF but others ON).

Next, the configuration is made out-of-phase by turning the diodes into OFF state at *Port* 3. Figure 4.34 shows the simulated and measured S parameters. The measured and simulated center frequencies are 3.98 and 4.14 GHz, respectively, with an error of 4.02%. The measured FBW (18.67%) is lower than the simulated one (23.8%). The isolation level ($|S_{31}|$) is measured ~ -20dB in the passband. The amplitude imbalance and phase difference of the out-of-phase configuration are shown in Figure 4.35, giving ≤0.54 dB and 180± 4.9° across the entire passband.

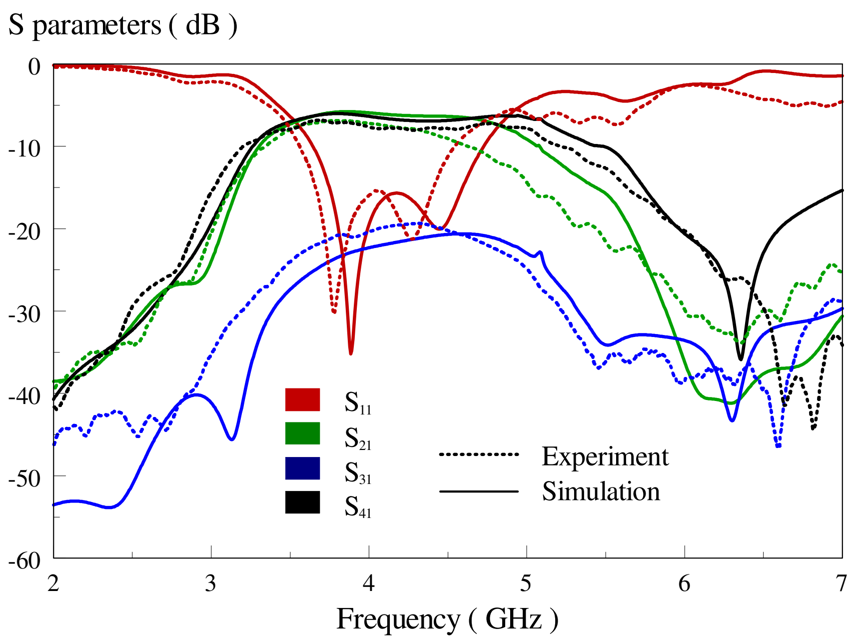

Figure 4.34: Simulated and measured S parameters of the reconfigurable out-of-phase power divider (with *Port* 3 OFF but others ON).

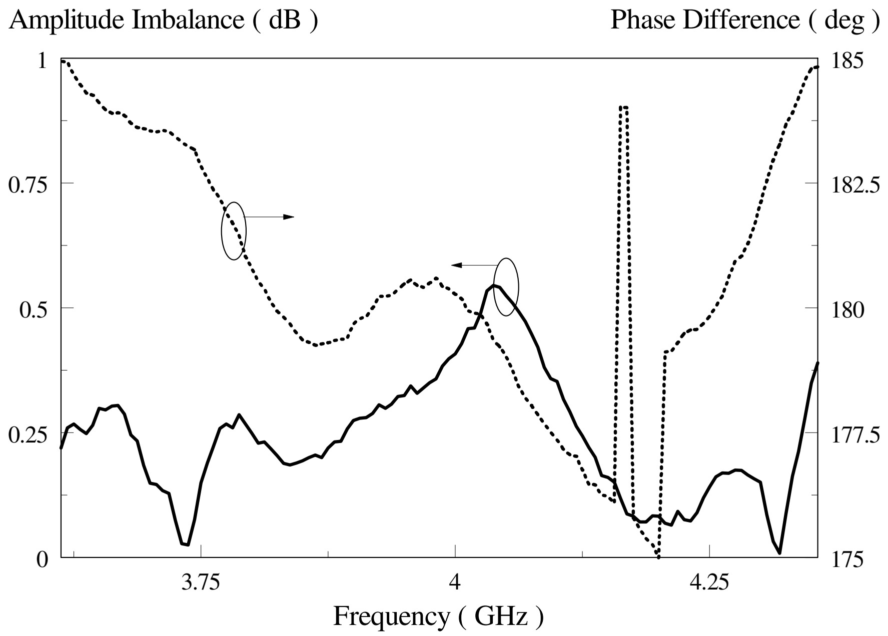

Figure 4.35: Calculated amplitude imbalance and phase difference of the reconfigurable out-of-phase power divider (with *Port* 3 OFF but others ON).

4.6 Conclusion

In this chapter, a passive in-phase, a passive out-of-phase, and a reconfigurable power dividers have been proposed. In the first part, the passive components are designed and optimized. It was found that the phase polarity of the output signal is changeable by inverting the current direction of the hook-shaped microstrip feedline. Next, the in-phase and out-of-phase power dividers are combined to form a reconfigurable power divider. By incorporating several RF PIN diodes into the output feedlines, the proposed active power divider is able to generate the in-phase or out-of-phase outputs. All the measured results show reasonable agreement with the simulated ones.

CHAPTER 5

CONCLUSION

5.1 Conclusion

In this thesis, two different multifunctional couplers have been proposed. In the first part, the multiport power-dividing directional coupler with multiple output levels has been designed by using the microstrip rectangular patch resonator. This multifunctional structure can produce half-powered division as well as coupled signals (10 dB and 20 dB) at the same time. In the second, the stepped-impedance slotline resonator has been explored for designing in-phase and out-of-phase passive power dividers. By incorporating RF PIN diodes, the two passive components can be combined, resulting in a reconfigurable component that can provide either in-phase or out-of-phase operation at any one time. Experiments have been conducted, showing reasonable agreement to simulations.

5.2 Future Work

The proposed structure in the first part of the project can be made even more compact with the use of new technologies. Additional modes can also be added to increase the fractional bandwidth. For the second part of the project, the stepped-impedance slotline reconfigurable power divider may be made even more versatile by including output ports to provide 45˚ and 90˚ phase differences. Furthermore, the bandwidth of the proposed structure can be increased by adding more resonances into the operating frequency passband.

Bibliography

1. S. L. Lim, E. H. Lim, and F. L. Lo, 'Multifunctional Power-dividing Directional Couplers with Multiple Output Levels', *IET Microwaves, Antennas & Propagation.* (Submitted)

2. S. L. Lim, E. H. Lim, and F. L. Lo, 'Reconfigurable Stepped-impedance Slotline Power Dividers', *IET Microwaves, Antennas & Propagation.* (Submitted)

References

A. A. Kishk and W. Huang, 2011 Size Reduction Method for Dielectric Resonator Antenna, *IEEE Antennas and Propag. Magazine*, 53(2), pp. 26-38

A. A. Semenov, P. Yu. Beljavski, A. A. Nikitin, S. F. Karmanenko, B. A. Kalinikos and G. Srinivasan, 2008 Dual Tunable Thin-film Ferrite-ferroelectric Slotline Resonator, *Electron. Lett.*, 44(24), pp. 1406-1407.

A. Bhardwaj and V. D. Kumar, 2012 Optical Dielectric Resonator Antenna, *International Conference Communications*, pp. 159-162.

A. Dadgarpour, G. Dadashzadeh, M. Naser-Moghadasi, F. Jolani and B. S. Virdee, 2010 PSO/FDTD Optimization Technique for Designing UWB In-phase Power Divider for Linear Array Antenna Application, *IEEE Antennas and Wireless Propag.Lett.*, 9, pp. 424-427.

A. S. S. Mohra, 2008 Compact Dual Band Wilkinson Power Divider, *Radio Science Conference*, pp. 1-7.

Ansoft Corporation, High Frequency Structure Simulator (HFSS) v. 11 [Online]. Available: http://www.ansoft.com/products/hf/hfss/. [11 July 2010]

B. Li, X. Wu, Y. Li, J. Zhang and W. Wu, 2010 A Dual-Band Wilkinson Power Divider with 6:1 Power Dividing Ratio Using Coupled Lines, *IEEE Antennas and Propag. Society International Symposium*, pp. 1-4.

B. Li, X. Wu, C. Hua, N. Yang, D. Zhu and W. Wu, 2011 A Tri-band Wilkinson Power Divider using Extended T-shaped Stubs, *Microwave Conference Proceedings*, pp. 1-4.

C. H. Ho, L. Fan and K. Chang, 1993 Slot-Coupled Double-Sided Microstrip Interconnects and Couplers, *International Microw. Symp. Dig.*, 3, pp. 1321-1324.

C. H. Ng, E. H. Lim and K. W. Leung, 2011 Compact Microstrip Patch Balun Filter, *Cross Strait Quad-Regional Radiao Science and Wireless Tech. Conference*, 1, pp. 1749-1751.

C. Lee, C. G. Hsu and C. Chen, 2012 Band-notched Balanced UWB BPF with Stepped-Impedance Slotline Multi-mode Resonator, *IEEE Microw. Wireless Compon. Lett.*, 22(4), pp. 182-184.

C. Lin and S. Chung, 2011 A Compact Filtering 180^{o} Hybrid, *IEEE Trans. Microw. Theory Tech.*, 59(12), pp. 3030-3036.

C. Wang and K. Chang, 2002 A 3-D Broadband Dual-layer MultiapertureMicrostrip Directional Coupler, *IEEE Microw. Wireless Compon.Lett.*, 12(5), pp. 160-162.

D. Hawatmeh, N. Dib and K. A. Shamaileh, 2012 Design and Analysis of a 3-way Unequal Split Ultra Wideband Wilkinson Power Divider, *IEEE Antennas and Propag. Society International Symp.*, pp. 1-2.

D. M. Pozar, 2011 Microwave Engineering, John Wiley & Sons, Inc., Fourth Edition.

D. Woo and T. Lee, 2005 Suppression of Harmonics in Wilkinson Power Divider using Dual-Band Rejection by Asymmetric DGS, *IEEE Trans. Microw. Theory Tech.*, 53(6), pp. 2139-2144.

E. A. Mariani, C. P. Heinzman, J. P. Agrios and S. B. Cohn, 1969 Slot Line Characteristics, *IEEE Trans. Microw. Theory Tech.*, 17(12), pp. 1091-1096.

E. H. Lim and K. W. Leung, 2012 Compact Multifunctional Antennas for Wireless Systems, John Wiley & Sons, Inc.

E. J. Wilkinson, 1960 An N-way Hybrid Power Divider, *IRE Trans. Microw. Theory Tech.*, 8 (1), pp. 116-118.

F. Xu, G. Guo, E. Li and J. Wu, 2012 An Ultra-broadband 3-dB Power Divider, *Global Symp.on Millimeter Waves*, pp. 347-350.

G. Elazar and M. Kisliuk, 1988 Microstrip Linear Slot Array Antenna for X-band, *IEEE Trans. Antennas Propag.*, 36(8), pp. 1144-1147.

H. Chen and Y. Pang, 2011 A Tri-band Wilkinson Power Divider utilizing Coupled Lines, *IEEE Antennas and Propag. Society International Symp.*, pp. 25-28.

H. Iwasaki, K. Kawabata and K. Yasukawa, 1990 A Circularly Polarized Microstrip Antenna using a Crossed-Slot Feed, *International Symp. Antennas Propag. Society*, 2, pp. 807-810.

H. Ma, Q. Chu and L. Ye, 2008 Wideband Uniplanar 180^{o} Out-of-phase Power Divider, *Asia-Pacific Microw. Conference*, pp. 1-4.

I. Wolff, 1972 MicrostripBandpass Filter using Degenerate Modes of a Microstrip Ring Resonator, *Electron. Lett.*, 8(12), pp. 302-303.

J. E. Ruyle and J. T. Bernhard, 2013 A Wideband Transmission Line Model for a Slot Antenna, *IEEE Trans. Antennas Propag.*, 61(3), pp. 1407-1410.

J. Kao, Z. Tsai, K. Lin and H. Wang, 2012 A Modified Wilkinson Power Divider with Isolation Bandwidth Improvement, *IEEE Trans. Microw. Theory Tech.*, 60(9), pp. 2768-2780.

J. Lee, I. Jeon, Y. Cho, X. Wang and S. Yun, 2012 Design of Dual-band Power Divider using Shunt Open-stubs with Enhanced Attenuation Characteristics, *Asia-Pacific Microw. Conference Proceedings*, pp. 1199-1201.

J. Li and B. Wang, 2011 Novel Design of Wilkinson Power Dividers with Arbitary Power Division Ratios, *IEEE Trans. Industrial Electron.*, 58 (6), pp 2541-2546.

J. Li, J. Wang, X. Yang and B. Wang, 2010 A Study of Dual-mode Patch Resonator-based Microwave Filter, *International Conference on Microw. and Millimeter Wave Tech.*, pp. 48-51.

J. Reed and G. J. Wheeler, 1956 A Method of Analysis of Symmetrical Four-Port Networks, *IRE Trans. Microw. Theory Tech.*, 4(4), pp. 246-252.

J. W. Burns, 1985 Planar, Quadrature Microwave Coupler, *U. S. Patent*, no. 4,492,939.

J. Wang, J. Ni, Y. Guo and D. Fang, 2009 Miniaturized Microstrip Wilkinson Power Divider with Harmonic Suppression, *IEEE Microw. Wireless Compon.Lett.*, 19(7), pp. 440-442.

J. X. Chen, C. Y. Cheung and Q. Xue, 2007 Integrated Bandpass Filter Balun based on Double-sided Parallel-strip Line with an Inserted Conductor Plane, *Asia-Pacific Microw. Conference*, pp. 1-4.

J. Xiao, Q. Chu and Y. Wang, 2008 New Patch Resonator Bandpass Filter with Wideband and Tunable Operation, *Asia-Pacific Microw. Conference*, pp. 1-3.

J. Yen, S. Hsu and T. Wu, 2011 A Novel Compact Backward-wave Directional Coupler Design with Defected Ground Structure, *Asia-Pacific Microw. Conference Proceedings*, pp. 1150-1153.

J. Yen, S. Hsu and T. Wu, 2011 A Novel Miniaturized Forward-wave Directional Coupler Loaded with Periodic Shunt Inductors, *European Microw. Conference*, pp. 782-785.

K. A. O'Connor and R. D. Curry, 2012 A Dielectric Resonator Antenna based on High Dielectric Constant Composites for High Power UHF Antenna Applications, *IEEE Power Modulator and High Voltage Conference*, pp. 245-249.

K. C. Gupta and M. D. Abouzahra, 1985 Analysis and Design of Four-Port and Five-Port Microstrip Disc Circuits, *IEEE Trans. Microw. Theory Tech.*, 33(12), pp. 1422-1428.

K. Itoh and M. Yamamoto, 1997 A Slot-Coupled Microstrip Array Antenna with a Triplate Line Feed where Parallel-Plate Mode is Suppressed Efficiently, *International Symp. Antennas Propag. Society*, 4, pp. 2135-2138.

K. L. Chan, F. A. Alhargan and S. R. Judah, 1997 A Quadrature-hybrid Design using a Four-port Elliptic Patch, *IEEE Trans. Microw. Theory Tech.*, 45(2), pp. 307-310.

K.Song and Q. Xue, 2010 Novel Ultra-wideband (UWB) Multilayer Slotline Power Divider with Bandpass Response, *IEEE Microw. Wireless Compon.Lett.*, 20(1), pp. 13-15.

K. Song, Y. Fan and X. Zhou, 2008 Broadband Multilayer In-phase Power Divider, *Electron. Lett.*, 44(6), pp. 417-418.

K. Yi and B. Kang, 2003 Modified Wilkinson Power Divider for *n*th Harmonic Suppression, *IEEE Microw. Wireless Compon.Lett.*, 13(5), pp. 178-180.

L. Wu, B. Xia, W. Yin and J. Mao, 2013 Collaborative Design of a New Dual-Bandpass 180 Hybrid Coupler, *IEEE Trans. Microw. Theory Tech.*, 61(3), pp. 1053-1066.

M. A. Beldi, F. Boone and D. Deslandes, 2012 Design of Microstrip Power Dividers with Filtering Functions, *European Microw. Conference*, pp. 384-387.

M. Aikawa and H. Ogawa, 1980 A New MIC Magic-T using Coupled Slotlines, *IEEE Trans. Microw. Theory Tech.*, 28(6), pp. 523-528.

M. D. Abouzahra and K. C. Gupta, 1988 Multiport Power Divider-Combiner Circuits using Circular-Sector-Shaped Planar Components, *IEEE Trans. Microw. Theory Tech.*, 36(12), pp. 1747-1751.

M. Dydyk, 1999 Microstrip Directional Couplers with Ideal Performance via Single-element Compensation, *IEEE Trans. Microw. Theory Tech.*, 47(6), pp. 956-964.

M. E. Bialkowski and A. M. Abbosh, 2007 Design of a Compact UWB Out-of-phase Power Divider, *IEEE Microw. Wireless Compon.Lett.*, 17(4), pp. 289-291.

M. E. Bialkowski and S. T. Jellett, 1994 A 3 dB Planar Coupler in the form of an Elliptically Shaped Disc, *IEEE Microw. Symp. Dig.*, 1, pp. 209-212.

M. E. Bialkowski and S. T. Jellett, 1994 Analysis and Design of a Circular Disc 3 dB Coupler, *IEEE Trans. Microw. Theory Tech.*, 42(8), pp. 1437-1442.

M. E. Bialkowski, N. Seman and M. S. Leong, 2009 Design of a Compact Ultra Wideband 3 dB Microstrip Slot Coupler with High Return Losses and Isolation, *Asia-Pacific Microw. Conference*, pp. 1334-1337.

M. E. Bialkowski and Y. Wang, 2010 Wideband Microstrip 180^o Hybrid utilizing Ground Slots, *IEEE Microw. Wireless Compon.Lett.*, 20(9), pp. 495-497.

M. E. Bialkowski and Y. Wang, 2011 UWB Planar Out-of-phase Wilkinson Power Divider utilizing UWB ±90^o Phase Shifters in Microstrip-slot Technology, *Asia-Pacific Microw. Conference Proceedings*, pp. 1138-1141.

M. E. Goldfarb, 1991 A Recombinant, In-Phase Power Divider, *IEEE Trans. Microw. Theory Tech.*, 39 (8), pp 1438-1440.

M. Nakatsugawa and K. Nishikawa, 2001 A Novel Configuration for 1:N Multiport Power Dividers using Series/Parallel Transmissin-line Division and a Polyimide/Alumina-Ceramic Structure for HPA Module Implementation, *IEEE Trans. Microw. Theory Tech.*, 49(6), pp. 1187-1193.

M. Ohira, Z. Ma and M. Kato, 2011 Resonant-mode Behavior of a New Slotline Embedded Three-mode Microstrip line Resonator and its Filter Application, *Microw. Conference Proceedings*, pp. 1-4.

N. Behdad and K. Sarabandi, 2005 A Wide-band Slot Antenna Design Employing a Fictitious Short Circuit Concept, *IEEE Trans. Antennas Propag.*, 53(1), pp. 475-482.

N. Yang, C. Caloz and K. Wu, 2010 Broadband Compact 180^o Hybrid derived from the Wilkinson Divider, *IEEE Trans. Microw. Theory Tech.*, 58(4), pp. 1030-1037.

P. Cheong, T. Lv, W. Choi and K. Tam, 2011 A Compact Microstrip Square-Loop Dual-mode Balun-Bandpass Filter with Simultaneous Spurious Response Suppression and Differential Performance Improvement, *IEEE Microw. Wireless Compon.Lett.*, 21(2), pp. 77-79.

P. Chi and T. Itoh, 2009 Miniaturized Dual-Band Directional Couplers Using Composite Right/Left-Handed Transmission Structures and Their Applications in Beam Pattern Diversity Systems, *IEEE Trans. Microw. Theory Tech.*, 57(5), pp. 1207-1215.

P. K. Singh, S. Basu and Y. H. Wang, 2009 Coupled Line Power Divider with Compact Size and Bandpass Response, *Electron. Lett.*, 45(17), pp. 892-894.

Q. Li, J. Gong, X. Shi, X. Wang and F. Wei, 2010 A Compact Broadband Multilayer In-phase Power Divider, *International Conference on Microwav. And Millimeter Wave Tech.*, pp. 756-758.

R. Zhang, L. Zhu and S. Luo, 2012 Dual-mode Dual-band Bandpass Filter using A Single Slotted Circular Patch Resonator, *IEEE Microw. Wireless Compon.Lett.*, 22(5), pp. 233-235.

R. Zhang and R. R. Mansour, 2007 Low-cost Dielectric Resonator Filter with Improved Spurious Performance, *IEEE Trans. Microw. Theory Tech.*, 55(10), pp. 2168-2175.

S. B. Cohn, 1968 Slot Line - An Alternative Transmission Medium for Integrated Circuits, *International Microw. Symp.*, pp. 104-109.

S. B. Cohn, 1969 Slot Line on a Dielectric Substrate, *IEEE Trans. Microw. Theory Tech.*, 17(10), pp. 768-778.

S. Gruszcynski and K. Wincza, 2007 Broadband Multisection Asymmetric 8.34-dB Directional Coupler with Improved Directivity, *Asia-Pacific Microw. Conference*, pp. 1-4.

S. Hsu, C. Tsai and T. Wu, 2010 A Novel Miniaturized Forward-wave Directional Coupler with Periodical Mushroom-shaped Ground Plane, *IEEE Trans. Microw. Theory Tech.*, 58(8), pp. 2277-2283.

S. Lin, M. Eron, S. Turner and J. Sepúlveda, 2011 Development of Wideband Low-loss Directional Coupler with Suspended Stripline and Microstrip Line, *Electron. Lett.*, 47 (25), pp. 1377-1379.

S. Mao and M. Wu, 2007 A Novel 3-dB Directional Coupler with Broad Bandwidth and Compact Size using Composite Right/Left-handed Coplanar Waveguides, *IEEE Microw. Wireless Compon.Lett.*, 17(5), pp. 331-333.

S. R. Zinka, A. Mohan and A. Biswas, 2007 Bandpass Filter Realization using Degenerate Dual-modes of a New Type of Patch Resonator for Significant Size Reduction, *Asia-Pacific Microw. Conference*, pp. 1-4.

S. Sun and L. Zhu, 2010 Miniaturized Patch Hybrid Couplers using Asymmetrically Loaded Cross Slots, *IET Microw. Antennas and Propag.*, 4(9), pp. 1427-1433.

S. Sun and W. Menzel, 2011 Novel Dual-mode BalunBandpass Filters using Single Cross-Slotted Patch Resonator, *IEEE Microw. Wireless Compon.Lett.*, 21(8), pp. 415-417.

S. W. Wong and L. Zhu, 2008 Ultra-wideband Power Divider with Good In-band Splitting and Isolation Performance, *IEEE Microw. Wireless Compon.Lett.*, 18(8), pp. 518-520.

S. Y. Zheng, S. H. Yeung, W. S. Chan, K. F. Man and S. H. Leung, 2009 Size-Reduced Rectangular Patch Hybrid Coupler using Patterned Ground Plane, *IEEE Trans. Microw. Theory Tech.*, 57(1), pp. 180-188.

T. Kawai, I. Ohta, M. Nishimura and T. Kaneko, 1992 A Rectangular Disk 3 dB Quadrature Hybrid with Flat Coupling, *Asia-Pacific Microw. Conference*, 2, pp. 673-676.

T. Tanaka, K. Tsunoda and M. Aikawa, 1988 New Slot-Coupled Directional Couplers between Double-Sided Substrate Microstrip Lines, and Their Applications, *International Microw. Symp. Dig.*, 2, pp. 579-582.

V. F. Fusco and J. A. C. Stewart, 1986 Design and Synthesis of Patch Microwave Couplers, *European Microw. Conference*, pp. 401-406.

V. F. Fusco and L. N. Merugu, 1990 Full Wave Analysis of 94 GHz Patch Coupler, *International Microw. Symp. Dig.*, 2, pp. 649-652.

W. Liu, F. Wei, C. Pang and X. Shi, 2012 Design of A Compact Ultra-wideband Power Divider, *International Conference on Microw. and Millimeter Wave Tech.*, 2, pp. 1-3.

X. D. Huang, C. H. Cheng and L. Zhu, 2012 An Ultrawideband (UWB) Slotline Antenna under Multiple-Mode Resonance, *IEEE Trans. Antennas Propag.*, 60(1), pp. 385-389.

X. Li, Y. Yang, L. Yang, S. Gong, T. Hong, X. Chen and Y. Zhang, 2009 Design of Unequal Wilkinson Power Divider for Dual-band Operation with Isolation Stubs, *Electron. Lett.*, 45(24), pp. 1245-1247.

X. Ou and Q. Chu, 2008 A Modified Two-section UWB Wilkinson Power Divider, *International Conference Microw, and Millimeter Wave Tech.*, 3, pp. 1258-1260.

X. Wang, Y. Bai, H. Xu, W. Cheng and X. Shi, 2011 A Tri-band Wilkinson Power Divider using Step-impedance Resonator, *IEEE Electrical Design of Advanced Packaging and Systems Symp.*, pp. 1-4.

Y. J. Cheng, W. Hong, K. Wu and Y. Fan, 2011 A Hybrid Guided-Wave Structure of Half Mode Substrate Integrated Waveguide and Conductor-Backed Slotline and its Application in Directional Couplers, *IEEE Microw. Wireless Compon.Lett.*, 21(2), pp. 65-67.

Y. Lu, S. Chen and P. Hsu, 2012 A Differential-mode Wideband Bandpass Filter with Enhanced Common-mode Suppression using Slotline Resonator, *IEEE Microw. Wireless Compon.Lett.*, 22(10), pp. 503-505.

Y. Wu, X. Xie, R. Xu, X. Zhao and S. Xie, 2012 Analysis and Design of A Novel Coupled-line Wideband Wilkinson Power Divider, *International Conference Microw, and Millimeter Wave Tech.*, 3, pp. 1-4.

Y. Wu, Y. Liu and Q. Xue, 2011 An Analytical Approach for a Novel Coupled-line Dual-band Wilkinson Power Divider, *IEEE Trans. Microw. Theory Tech.*, 59(2), pp. 286-294.